Ablative Pyrolysis of Beetle-killed Trees

Guanqun Luo

A dissertation

submitted in partial fulfillment of the

requirements for the degree of

Doctor of Philosophy

University of Washington

2016

Reading Committee:

Fernando L. P. Resende, Chair

Renata Bura

Richard R. Gustafson

Program Authorized to Offer Degree:

Environmental and Forest Sciences

University of Washington

Abstract

Ablative pyrolysis of beetle-killed trees

Guanqun Luo

Chair of the Supervisory Committee:
Dr. Fernando L.P. Resende
School of Environmental and Forest Sciences

The bark beetle outbreak has severely affected the forests across the western U.S., and the infested trees need to be disposed of to avoid falling and minimize wildfire hazards. Thus, we propose to use ablative pyrolysis to convert beetle-killed wood chips into bio-oil near the harvesting point, greatly reducing the costs of drying, grinding, and transportation. Firstly, we evaluated the effect of degradation stages of beetle-killed trees on the performance of fast pyrolysis using Py-GC/MS, which has not been reported previously. Our results revealed that bio-oil produced from trees that have been attacked and dead for 4 years had similar yield and selectivity to that from the healthy trees. Moreover, oxygenated pyrolysis vapors from beetle-killed trees were upgraded into value-added aromatic hydrocarbons in the presence of HZSM-5 catalyst. According to the contact method between the catalyst and pyrolysis vapors, the catalytic upgrading can be classified into *in-situ* and *ex-situ* configurations. In this research, a direct comparison between these methods was

made using Py-GC/MS under identical conditions. The *in-situ* and *ex-situ* upgrading showed largely similar yields of aromatic volatiles (21-25%) and carbonaceous residues (34-40%), with differences primarily on species selectivity. As a result of the alkylation/dealkylation reactions, the *in-situ* upgrading showed higher selectivity to xylenes and aromatics with nine carbons, and the *ex-situ* upgrading exhibited higher selectivity to benzene and toluene.

A semi-batch lab-scale ablative pyrolysis reactor was designed and constructed to simulate the conditions that would be used in the mobile pyrolysis unit in the field. Prior to the ablative pyrolysis experiments, the wood temperature profile during reactor pre-heating was evaluated, and the modeling results suggested that the extent of slow pyrolysis of wood was insignificant, which is in good agreement with experimental measurements. In the ablative reactor, entire wood chips (up to 10 × 20 mm) were successfully pyrolyzed into bio-oil, of which yield was as high as 60 wt. % with a water content of 34%. The yield and composition of bio-oil from ablative pyrolysis were in the same range with those from fast pyrolysis of < 1 mm particles using a fluidized bed reactor, with the small differences (4 wt. % lower yield and HHV, and higher water content) attributed to the longer vapor residence times in ablative reactor. The effects of operating conditions on the ablative pyrolysis results were also investigated. The yield of bio-oil was favored at moderate pyrolysis temperature of 500 °C, thin layer of wood chips (≤ 5 mm), low applied pressure (≤ 0.5 bar), and high rotation speed (≥ 100 rpm). The elemental composition of bio-oil was highly affected by its water content, and the elemental composition of char was primarily affected by the temperature. At higher temperature, char became more carbonaceous in nature. Depending on the operating conditions, bio-oil and char had HHV of 11-15 MJ/kg and 28 MJ/kg, respectively.

TABLE OF CONTENTS

LIST OF FIGURES

LIST OF TABLES

ACKNOWLEDGEMENTS

First and foremost, I would like to take this special opportunity to thank my supervisor, Dr. Fernando Resende, for giving me the opportunity to study at UW under his mentorship. I am grateful for his patience, understanding, guidance, and helpful advice throughout my PhD program. His knowledge, and enthusiastic attitude for research has encouraged me to work to the best of my capability.

I would also like to express my gratitude to my committee members, Dr. Rick Gustafson, Dr. Renata Bura, Dr. Bill Mckean, and Dr. Jim Pfaendtner for their helpful discussion and feedback during my committee meeting, qualify exam, and general exam.

Ablative reactor construction and operation allowed me to work with the Alaskan Copper who provided reactor manufacturing and maintenance. I am grateful for their knowledge and professional experience which have helped me tremendously throughout my PhD project. Special thanks are given to the Engineering Manager- Donald Rosen, and the Electrician-Sheung Gee.

I would also like to thank the labmates in Resende's group: Oliver Jan, Kayla Sprenger, Devin Chandler, Luiz Anjos, and Fernando Camargo. I have really enjoyed working with these friendly, supportive, and helpful colleagues. It was also a pleasure to work with the undergraduate students: Matias Gonzalez, Vinh Tran, Daniel Suss Riter, Ryan Eng, and Pei Jia. Special thanks to Pei Jia and Ryan Eng who offered assistance in ablative reactor modification and operation and special thanks to Neethi Nagarajan for assistance in Klason lignin analysis, which was conducted in Dr. Renata Bura's lab. I also appreciate the opportunity to work alongside many other talented and helpful graduates in the BBL group.

I would also like to extend my gratitude to the friends I made at UW, including but not limited to Yuting Lin, Jingda Wu, Jiayi Dou, Chang Dou, Cindy Chen, and Si Gao. I deeply appreciate their friendship, care, and support, which made my lifetime at UW enjoyable and meaningful. A huge thanks to Jingda Wu for providing assistance and training with Matlab coding.

Finally, I would like to thank my parents and family for their continuous support and unconditional love. I am above all grateful to my husband, Kaige Wang, who is my best friend and biggest supporter for both my research work and personal life. I am so glad that I went through the PhD journey with him. His endless love, trust, encouragement, and inspiration have bettered myself regardless the long long distances between us.

To my husband, Kaige Wang, whose love I can always rely on

CHAPTER 1. INTRODUCTION AND LITERATURE REVIEW

1.1 THE BARK BEETLE OUTBREAK

In recent years, drought, warmer winters, and aging forests have led to a large bark beetle outbreak in the western United States. Across the landscape from the West Coast through the Rocky Mountains, more than 41.7 million acres of conifer forests have been infested by bark beetles since 1996 and this number is expected to increase in the near future (5-10 years) [1]. Although bark beetles are natural components of western forest ecosystems; recent bark beetle epidemic with high levels of tree mortality has negatively impacted public benefits from forests [2]. Beetle-killed trees easily fall to the ground, posing significant safety threats to the community infrastructures (e.g. road, trail, power line, and water pipe, etc.), and the people who recreate or live nearby. Mitchell and Preisler [3] found that lodgepole pines killed by mountain pine beetles in the central Oregon started falling 3 years after death in the thinned stands, and 5 years after death in the unthinned stands. 90% of beetle-killed trees had fallen within 12 and 14 years in the thinned and unthinned stands, respectively. Waterhouse and Armleder [4] found that the fall rates for beetle-killed trees was higher than heathy trees. The fall rates of dead trees was 1.43%/ha/year, whereas it was only 0.04%/ha/year for live healthy trees. The U.S. Forest Service estimates that as much as 100,000 beetle-killed trees can fall to the ground every day in the southern Wyoming and northern Colorado [1]. Bark beetle-caused tree mortality may also change forest fuel distributions and therefore wildfire characteristics [5]. As bark beetle-killed trees decay and fall to the ground, surface fuel loads start to accumulate. Heavy surface fuel loads not only act as ladders to carry a surface fire into tree crowns but also increase the heat intensity and duration of the fire on the forest floor [2]. Thus, the potential for high-severity wildfire increases without changing the

probability of fire occurrence. What is worse, wildfires increase the susceptibility of trees to the bark beetle attack [2].

After a successful attack by the bark beetles, foliage color changes from green to red, then to grey. In general, green foliage indicates up to one year after attack, red phase describes trees about 2 years after attack, and grey phase applies to trees approximately 3 years after attack [6, 7]. However, the time foliage color changes highly depend on the weather and the physiological condition of a tree [6]. Bark beetle attack is usually associated with a fungi attack. The mountain pine beetles carry a diversity of fungi on the surface of their bodies when attacking. The introduction and propagation of these fungi, mainly staining fungi, cause blue to black stains in the sapwood [6]. Bluish discoloration significantly reduces the commercial value of infested trees for wood products manufacturing and also creates bleaching challenges for pulp and paper industry [8, 9]. Another characteristic of bark beetle-attacked trees is dryness. Reid [10] found that the sapwood moisture content of beetle-killed trees decreased sharply from 85-165% of oven dry weight to around 16% after one-year of attack. This is lower than the fiber saturation point (30%, dry basis), beyond which wood structure starts to collapse as it dries further, leading to the checking and splitting in the wood [11, 12]. Dryness and checking of wood bring difficulties to solid wood processing stages, resulting in fiber losses and low timber recovery. For the thermochemical conversion of beetle-killed trees to produce bioenergy and biofuels, low moisture content is beneficial, as it could save the biomass drying costs. Chemical composition of trees have also been affected by the bark beetle attack. After beetle attack, small amounts of soluble carbohydrates of trees are lost along with moisture [13]. Compared to the healthy trees, beetle-killed trees sometimes showed relative high lignin content, which was likely due to the presence of some decay fungi [13]. Extractive level in the wood increased at the time of attack and shortly

thereafter due to the resinous response to the beetle infestation [14]. However, extractive content decreased with increasing time-since-death, likely due to the utilization of compounds by the fungi. Consequently, beetle-killed trees that have been dead for a number of years have similar extractive contents compared to the healthy trees [15].

1.2 FAST PYROLYSIS OF BIOMASS

1.2.1 Fast pyrolysis principles

Fast pyrolysis has been extensively studied for different types of biomass, ranging from woody biomass, agricultural wastes such as corn stover and wheat straw, energy crops such as sorghum and switchgrass to algae and solid wastes like sewage sludge, to produce liquid fuel that is usually called bio-oil [16-21]. Those biomass are primarily composed of cellulose, hemicelluloses, lignin, and minor amounts of other organics. The behavior of these components in fast pyrolysis has also been investigated. Hemicelluloses and cellulose can degrade rapidly over narrow temperature ranges. The decompositions of hemicelluloses and cellulose happen at temperature ranges of 220-315 °C and 315-400 °C, respectively [22]. However, lignin is more resistant to heat, as it degrades slowly over a wide temperature range of 200-900 °C and produces high yield of solid residues (around 40 wt. %) [22]. In fast pyrolysis, a rapid thermal decomposition process which occurs in the absence of oxygen, biomass decomposes to generate mostly vapors, permanent gases, and char.

The pyrolysis vapors are usually diluted by the inert carrier gas and escape from the reactor system quickly. After cooling and condensation, liquid bio-oil is recovered. The essential features of a fast pyrolysis process of biomass to produce high yield of bio-oil are summarized as follows: i) carefully controlled pyrolysis temperature, 400-600 °C; ii) very high heating rates, > 500 °C/s,

and heat transfer rates; iii) very short vapor residence time, typically less than 2 s; and iv) rapid cooling of pyrolysis vapors [23, 24].

1.2.2 Fast pyrolysis products

The major product from fast pyrolysis of biomass is bio-oil, which typically has a yield of 60-75 wt. %. 10-20 wt. % non-condensable gases and 15-25 wt. % bio-char are also produced in the fast pyrolysis as byproducts [25]. Fast pyrolysis product yields and distributions are highly affected by the composition of biomass as well as the process operating conditions.

Patwardhan et al. [26-28] studied the fast pyrolysis of individual components of biomass (e.g. hemicelluloses, cellulose, and lignin) using a micro-pyrolyzer coupled with a GC-MS/FID. Fast pyrolysis of cellulose and hemicelluloses mainly produced small acids, glycoaldehyde, acetol, furans, and some anhydrosugars [26, 27]. Levoglucosan was the most abundant product from cellulose pyrolysis, and the yield was up to 60 wt. % [26]. Low char yields of 6 wt. % and 10 wt. % were observed respectively for the fast pyrolysis of cellulose and hemicelluloses [26, 27]. Unlike cellulose and hemicelluloses, fast pyrolysis of lignin produced mainly acetic acids, different phenolic compounds, and high yield of char, around 40 wt. % [28]. 15-18 wt. % of CO_2 was also generated in the fast pyrolysis of hemicelluloses and lignin [27, 28]. The presence of minerals in biomass also significantly affected the pyrolysis product distributions. Minerals were found to promote secondary reactions, leading to the formation of CO_2, low molecular weight species, and char in the pyrolysis of hemicelluloses and cellulose [26, 27, 29]. However, inorganic salts did not significantly affect lignin pyrolysis products [28]. Biomass with low ash content such as woody biomass usually produced more bio-oil than herbaceous biomass that has relatively high ash content, under the same pyrolysis conditions [17, 30].

Temperature is one of the most important operating parameters to affect the pyrolysis product yield and distribution. Influence of temperature on pyrolysis product yield and distribution has been widely studied by researchers using various biomass and its individual components. Generally, as pyrolysis temperature increases, the thermal decomposition of biomass, in particular the lignin component, can be promoted to increase bio-oil yield and lower the char yield. However, higher pyrolysis temperature can also enhance the cracking reactions, which favor the formation of non-condensable gases by consuming the bio-oil. Luo et al. [31] investigated the effect of temperature on the pyrolysis product yield from rosewood in a fluidized bed reactor. As temperature increased from 450 °C to 700 °C, bio-oil yield slightly increased first and then decreased. The maximum yield of bio-oil was obtained at 500 °C. The char yield decreased and the gas yield increased with increasing pyrolysis temperature. Garcia-Perez et al. [32] studied the pyrolysis of oil mallee woody biomass in a lab-scale fluidized bed reactor. Increasing pyrolysis temperature from 350 °C to 600 °C lowered the char yield but promoted the non-condensable gases production. The highest yield of bio-oil was achieved at 475 °C. Similar results were also observed by Thangalazhy-Gopakumar et al. [33], when they performed fast pyrolysis of pine wood in an auger reactor. Pyrolysis temperature also has an impact on the product composition. Garcia-Perez et al. [32] found bio-oil produced at higher temperature contained more water-insoluble lignin-derived oligomers and the char produced at higher pyrolysis temperature had less volatile matters. Patwardhan et al. [27-29] studied the effect of temperature on the composition of pyrolysis vapors using cellulose, hemicellulose, and lignin as feedstock in a micro-pyrolyzer. Formation of low molecular weight compounds like formic acid and acetol was favored at higher temperature by consuming the larger oxygenates such as cellulose and hemicelluloses-derived anhydrosugars and large lignin-derived phenolic compounds.

1.2.3 Bio-oil characteristics and applications

Bio-oil from fast pyrolysis of biomass is a dark-brown, free-flowing liquid with an acrid or a smoky odor [34]. It is a mixture of hundreds of oxygenated compounds including acids, ketones, aldehydes, furans, phenols, anhydrosugars, and some oligomers. Bio-oil also has a high water content of 15-30 wt. %, which comes from both original moisture in feedstocks and the products of dehydration reactions during the pyrolysis process [34]. The elemental composition of bio-oil is similar to that of biomass, since it is a direct product from its thermal decomposition. Compared to the heavy fuel oil, bio-oil has much higher oxygen content, lower sulfur, and nitrogen contents (Table 1.1) [35].

Table 1.1 Elemental compositions (wt. %) of typical bio-oil and heavy fuel oil [35]

	Elemental percentage (%)				
	C	H	O	N	S
Bio-oil	54-58	5.5-5.7	35-40	0-0.2	0-0.2
Heavy fuel oil	85	11	1.0	0.3	1.0

As a result of the high water content and high oxygen content, bio-oil has a lower energy content than fossil-based fuels. The higher heating value (HHV) of bio-oil is in a range of 14-18 MJ/kg, which is only half of that for fossil-based fuels, 41-43 MJ/kg [34, 35]. The presence of acids, typically 7-12 wt. %, also leads to a high acidity and a low pH of 2-3 for bio-oil.

Viscosity is an important parameter for fuels, which represents their resistance to a shearing force or angular deformation during motion. The viscosities of bio-oils vary in a wide range (10-100 cP at 40 °C) with the biomass feedstock and pyrolysis conditions [35]. He et al. [36] investigated the effect of reacting conditions on the yield and physiochemical properties of switchgrass pyrolysis oils, and found that lower viscosities can be obtained in the presence of higher content of water in the bio-oils and at higher pyrolysis temperature that would further

decompose biomass into smaller molecules. Instability is also a well known property of bio-oil. Bio-oil is not the product of thermodynamic equilibrium and thereby substantial components in the bio-oils can carry on a variety of reactions such as esterification and polymerization to change the compositions toward thermodynamic equilibrium during the storage [37]. These aging reactions can be accelerated by elevated temperature.

Bio-oil can be combusted in boilers, engines, or turbines to produce heat and power. Compared to the combustion of fossil fuels, bio-oil combustion can be considered as a carbon neutral process with very low sulfur emissions [30]. However, the high acidity of bio-oil may cause corrosion of the facilities. The elevated temperature can also accelerate the corrosion rates [38]. Thus, some minor modifications may be required before the application. Bio-oil is a mixture of oxygenated chemicals, and it can be simply fractionated by adding water into water-soluble phase and water-insoluble phase [39]. Water-soluble fraction is mainly composed of aldehydes and phenols. Red Arrow Products in Wisconsin has been reported to produce liquid smoke from those compounds derived from bio-oil [39]. The water-insoluble fraction is basically composed of lignin-derived oligomers, which has potential to be applied as resins or adhesives [30]. Transportation fuels can also be produced from bio-oil; however, catalytic upgrading processes such as hydrotreating and cracking are needed due to the undesirable properties of bio-oil mentioned above, as well as its immiscibility with fossil fuels.

1.3 CATALYTIC UPGRADING OF PYROLYSIS VAPORS

As discussed in Section 1.2.3, bio-oil suffers from a high oxygen content, rendering it highly viscous, acidic, instable, and immiscible with conventional oils; therefore, its utilization as transportation fuels requires further catalytic upgrading processes. Instead of catalytic upgrading of liquid bio-oil, treating the hot pyrolysis vapors with proper catalysts can simplify the process

by eliminating the steps of condensation and re-evaporation of bio-oil and thereby the energy consumption in the whole process can be reduced. In addition, catalytic upgrading of pyrolysis vapors shows higher overall liquid yield than catalytic upgrading of bio-oil. Park et al. [40] studied the catalytic upgrading of biomass pyrolysis vapors over HZSM-5 and HY catalysts in a fixed bed reactor and compared their results with the data from Vitolo et al. [41]. They found that using biomass instead of bio-oil as feedstock increased the yield of upgraded bio-oil by 10 wt. %.

Various types of catalysts including metal-based and porous materials have been explored to improve the quality of bio-oil [42,43]. Among those tested catalysts, zeolites are the most known used in the catalytic upgrading of bio-oil or pyrolysis vapors due to their ability to produce gasoline-range hydrocarbons. Aho et al. [44] carried out catalytic pyrolysis of pine biomass using Hβ as a catalyst in a fluidized bed reactor at 450 °C. Polyaromatics were formed in the presence of Hβ. Mihalcik et al. [45] investigated the performance of Hβ and calcium exchanged Y-zeolite in the catalytic upgrading of oak-derived pyrolysis vapors in a packed bed column. Both catalysts successfully deoxygenated a considerable fraction of pyrolysis vapors into aromatic hydrocarbons. Up to 22 wt. % of aromatic hydrocarbons was obtained by calcium exchanged Y-zeolite, which is higher than that from Hβ (15.5 wt. %). Recently, micro-pyroprobe equipped with analytical equipment GC/MS (Py-GC/MS) has been widely used to investigate pyrolysis and catalytic upgrading of pyrolysis vapors. Carlson et al. [46] reported catalytic upgrading of cellulose-derived pyrolysis vapors in a CDS pyroprobe. Five types of catalysts were tested including HZSM-5, silicalite, β-zeolite, silica-alumina, and Y-zeolite, among which HZSM-5 was the most effective catalyst to produce aromatic hydrocarbons (30% carbon yield). Similar result was also obtained by Mihalcik et al. [47], who catalytically upgraded pyrolysis vapors derived from eight

lignocellulosic biomass using five types of zeolites including H-Mordenite, HZSM-5, HY, Hβ, and H-Ferrierite.

The Lewis and Brønsted acid sites contained in zeolites act as active sites in the catalytic upgrading process, and the porous nature of zeolites provides shape-selectivity to the final hydrocarbon products [42]. Thus, the yield and selectivity of desirable products highly depends on the acidity and the pore size of the zeolite catalysts. A previous study on catalytic fast pyrolysis of glucose by Foster et al. [48] indicated the silica-to-alumina ratio, namely the acidity of HZSM-5 could affect the product yield. The maximum aromatic hydrocarbon yield (43% carbon yield) and minimum coke yield (23% carbon yield) occurred at the silica-to-alumina ratio of 30. Aho et al. [44] studied the catalytic pyrolysis of pine wood using Hβ as catalysts in a fluidized bed reactor at 450 °C, and found that the organic oil yield increased from 12.3 wt. % to 17 wt. % when the silica-to-alumina ratio of Hβ increased from 150 to 300. Moreover, the Hβ with a lower silica-to-alumina ratio (more acidic) led to more formation of water and polyaromatic hydrocarbons. Similar results were also observed by Mihalcik et al. [45] when they upgraded oak-derived pyrolysis vapors in a packed bed column using Hβ and calcium exchanged Y-zeolite as catalysts. The pore size of zeolites also play an important role to affect the diffusion and mass transfer of products. The micropores in the zeolites are essential to provide the selectivity to the formation of small aromatics. However, the micropores may also hinder the diffusion of reactants into, and products out of the zeolites, promoting the coke formation. Jae et al. [49] investigated the effect of zeolite pore size on the conversion of glucose to aromatics by catalytic fast pyrolysis. They found that HZSM-5 with moderate internal pore space (6.36 Å) and steric hindrance produced the highest amounts of aromatic hydrocarbons (35.5% carbon yield) and the smallest amounts of coke (30.4% carbon yield).

Depending on the contact method between the catalyst and pyrolysis vapors, the upgrading process can be classified into *in-situ* and *ex-situ*. In the *in-situ* upgrading, which is also known as catalytic fast pyrolysis, the catalyst is mixed with the biomass feedstock [46,50-52]. Biomass pyrolysis and pyrolysis vapor upgrading take place in the same reactor in the *in-situ* upgrading, thus likely reducing the capital and operating costs [53]. Aho et al. [54] investigated the *in-situ* upgrading of pyrolysis vapors from woody biomass in a fluidized bed reactor with zeolite catalysts as bed materials. Their results showed that HZSM-5 gave the highest yield of organic fraction in bio-oil, compared with other types of zeolites. Carlson et al. [50] reported 14% carbon yield of aromatics from catalytic fast pyrolysis of sawdust in a fluidized bed reactor with low biomass weight hourly space velocities and high temperature. Mante and Agblevor [55] studied *in-situ* upgrading of six different biomass resources in a Py-GC/MS system as well as in a fluidized bed reactor. They found that the final hydrocarbon yield was highly affected by the composition of the biomass feedstock. It is worth to note that the results among different researchers varied from each other due to the different reactors and reaction conditions used in experiments. The major disadvantage of *in-situ* upgrading is that the pyrolysis char and coked catalyst cannot be separated. This can be a critical problem if the biomass feedstock has high alkali content such as agricultural residues and algal biomass, since the accumulation of alkali metals from biomass can deactivate or poison the zeolite catalysts right away [56]. In the *ex-situ* upgrading, the catalyst is placed separately from the biomass feedstock in a secondary reactor [52,57]. Compared to the *in-situ* upgrading, the *ex-situ* upgrading provides more control and flexibility to the system. Pyrolysis conditions and catalytic performance could be individually optimized in the *ex-situ* upgrading [57,58]. Multiple serial catalyst beds could apply on the *ex-situ* configuration if necessary [59]. Moreover, pyrolysis char can be separated from the coked catalyst for further applications. Bench-

scale fixed bed reactors or fluidized bed reactors were extensively used for *ex-situ* upgrading process. Diebold and Scahill of the National Renewable Laboratory firstly reported 10 wt. % of gasoline-range hydrocarbons using a pilot vortex reactor followed by a fixed-bed catalytic cracker [59]. French and Czernik [60] screened catalysts for *ex-situ* vapor upgrading in a system consisting of a pyrolysis reactor and a fixed catalyst bed reactor downstream. The highest hydrocarbon yield of 16 wt. % was achieved using nickel-substituted ZSM-5 catalyst. Limited research on direct comparison between *in-situ* and *ex-situ* upgrading has been reported to date. Yildiz et al. [61] compared *in-situ* and *ex-situ* upgrading of pyrolysis vapors from pine wood using HZSM-5 as a catalyst in a continuously operated auger reactor. Similar product yield was observed for the *in-situ* and *ex-situ* upgrading. Compared to the *ex-situ* upgrading, however, the *in-situ* upgrading produced more phenolic and aromatic compounds with less acids and anhydrosugars. Wang et al. [62] recently reported a comparison between *in-situ* and *ex-situ* upgrading for hybrid poplar and dried distillers grains with solubles (DDGS). They concluded that *in-situ* upgrading promoted formation of aromatics, and *ex-situ* upgrading promoted the formation of olefins. Gamliel et al. [63] also performed a comparison between *in-situ* and *ex-situ* catalytic fast pyrolysis (CFP) of miscanthus × giganteus using Py-GC/MS. These results were compared with those from the *in-situ* CFP in a spouted-bed reactor. They found that the *ex-situ* CFP resulted in more permanent gas and aromatics in the bio-oil than *in-situ* CFP, and the results from Py-GC/MS *ex-situ* configuration more closely resembled those of the spouted-bed reactor. In a recent review of *ex-situ* upgrading, Wan and Wang [58] pointed out a serious lack of systematic research for comparison of *in-situ* and *ex-situ* upgrading.

1.4 ABLATIVE PYROLYSIS REACTORS

The reactor is the key component when considering an entire fast pyrolysis system. Many types of reactors including fluidized bed reactor, circulating fluidized bed reactor, free-fall reactor, auger reactor, rotating cone reactor, and ablative reactor have been developed. For most pyrolysis reactor configurations, the biomass feedstock needs to be ground into small particles of around 2 mm, because the process requires high rate of heat transfer through the particles [64]. Kumar estimated that the costs of biomass grinding was about 7-9% of the overall production costs [65]. Forest Concepts also studied the effects of final wood particle size on the total comminution energy cost for the Optimized Crumbler® machine, and found out that the comminution energy cost increases $1.5-4.5 per US ton as wood particle size is reduced from 12 mm to 1-2 mm [66]. In ablative pyrolysis, biomass undergoes melting and/or sublimation reactions as it directly contacts with a hot reactor surface. There is a steep temperature gradient at the biomass surface, leading to the formation of a thin superficial layer of reacting solid [67,68]. The reacting layer moves at constant velocity towards the heart of the cold biomass. Therefore, reaction rates in the ablative reactor are not limited by the heat transfer through the biomass particle, and in principle there is no upper limit to the biomass particle size that can be processed. It is possible to process large pieces of wood instead of only small particles using ablative pyrolyzer to reduce the grinding cost. The work which has made contributions to the field of ablative pyrolysis has been reviewed below.

1.4.1 University of Nancy, France

To the best our knowledge, Lédé et al.'s work has been the only fundamental study on the ablation heat transfer with specific application to wood pyrolysis [68-71]. The experimental setup is shown in Figure. 1.1 [72]. A stainless steel disk with a diameter of 7.5 cm, rotating at a constant and

controlled speed, was heated by four gas burners underneath. A rod of wood was pressed vertically against the hot surface by known weights. In order to prevent the combustion of volatiles, a jet of argon was introduced to the contact surface. The variations of the wood rod ablation rate were studied as a function of contact pressure (0.1-3.5 MPa), disk velocity (0.3-3 m/s), disk temperatures (500-900 °C), and rod diameter (2-10 mm). They found that the ablation rate of wood rod increased linearly with contact pressure at all temperatures. The ablation rate also increased as the relative velocity of the disk increased and then became constant. Unfortunately, Lédé's experiments were not accurate enough to determine the effect of wood rod diameter on the ablation rate. In addition, Lédé's work did not allow the overall product recovery for analytical study and mass balance calculation.

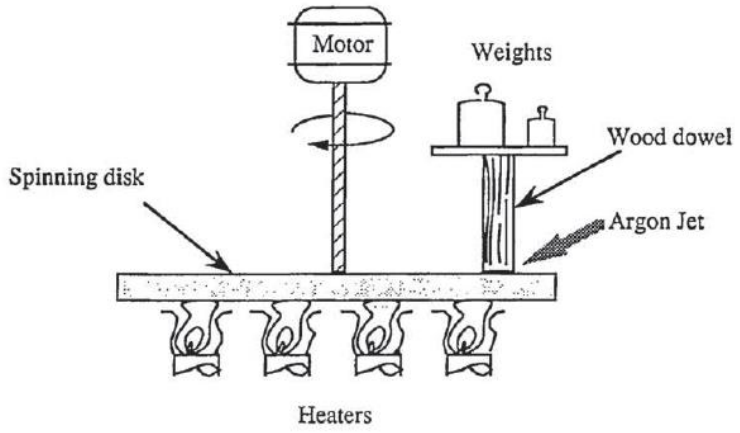

Figure 1.1 Lédé's experimental apparatus [72]

1.4.2 The Colorado School of Mines, USA

Reed and Cowdery designed and constructed a "pyrolysis mill" as shown in Figure 1.2, according to the principles of a conventional grain mill [73,74]. The pyrolysis mill consisted of two "stones" which were both made of copper and heated by Chromalox heaters to the pyrolysis temperature. The upper "stone" was stationary while the lower "stone" was spinning with a speed up to 80 rpm. The contact pressure on the wood particles was controlled by a spring. Wood particles were fed

by a vibratory feeder through upper "stone" and the produced pyrolysis vapors escaped through outlets to a series of four traps. To prevent the condensation of pyrolysis vapors inside reactor, the reactor wall was heated to 300-400 °C. Solid char and ash were left inside the reactor. Liquid bio-oil yield of up to 48.6% based on dry feed has been reported. The composition of bio-oil was not available. The permanent gases from this process were mainly composed of CO, CO_2, and trace amounts of light hydrocarbons.

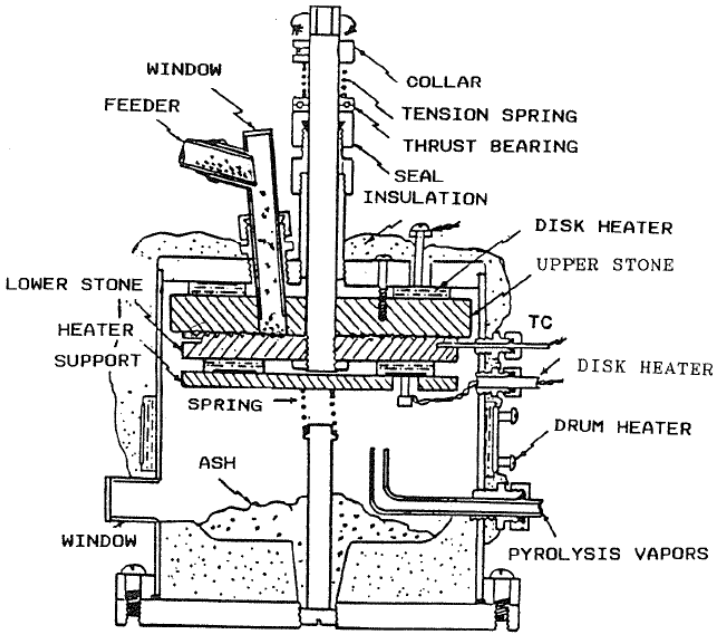

Figure 1.2 Ablative "pyrolysis mill" [74]

The major problem of this system was the slow escape of the pyrolysis vapors from the reactor, lowering the yield of bio-oil. Variable wood chip sizes also led to processing problems due to the disk spacing. Small wood chips could not be ablated and therefore slowly carbonized on the hot plates. Additionally, the copper "stones" were susceptible to deformation under pyrolysis temperatures.

1.4.3 National Renewable Energy Laboratory (NREL), USA

An ablative vortex reactor system was designed and constructed by NREL in 1980s to convert biomass into high value liquids [72,75-77]. The system is shown in Figure 1.3 [76]. The horizontal smooth walled vortex reactor was heated externally by the three-zone cylindrical furnaces. The maximum temperature of the reactor was around 625 °C. Biomass with particle size of 5 mm was fed with a screw feeder. Hot nitrogen or superheated steam was used as carrier gas. Before entering the reactor, a long entrainment tube was used to allow biomass particles to accelerate to a high entering velocity over 400 m/s. The biomass particles then entered the vortex reactor tangentially generating a high centrifugal force, pressing the particles on the hot reactor wall. In order to force biomass flow over the entire reactor heat transfer area, a helical rib was machined on the reactor wall. The gases, vapors, and fine chars left the reactor through the axial exit for further separation and condensation. The partially pyrolyzed biomass and large solid chars were recycled to the reactor by an insulated recycle loop installed at the exit of reactor.

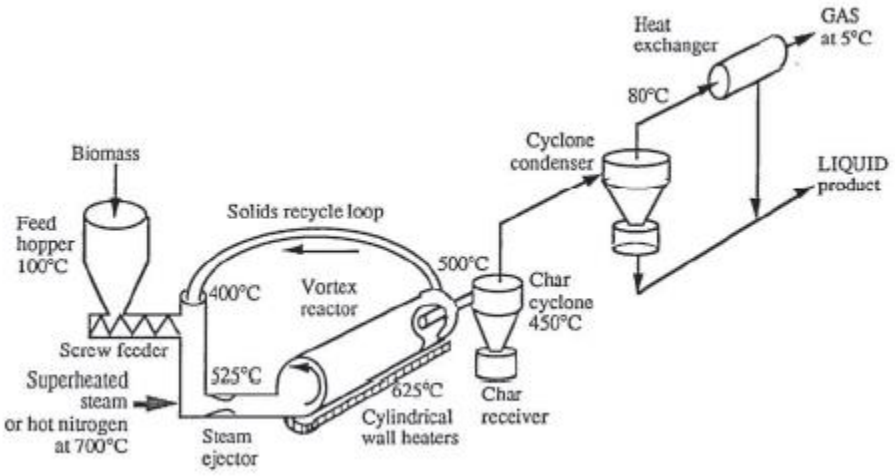

Figure 1.3 NREL ablative vortex pyrolysis reactor system [76]

The original design capacity of this ablative vortex pyrolysis reactor system was 50 kg/h biomass, but the maximum capacity achieved to date was only 36 kg/h biomass. Using this system,

up to 67 wt. % of bio-oil yield based on a dry feed basis has been reported. The bio-oil obtained from this system was highly oxygenated, with a pH of 2-3 and a higher heating value (HHV) of around 22 MJ/kg. The Interchem Industries Inc. founded in 1985 attempted to construct a scaled up reactor based on the NREL vortex reactor concept, but this was not successful [77].

1.4.4 Aston University, UK

Peacocke et al. [72,78,79] designed an ablative reactor with a throughput of 3 kg/h, as shown in Figure 1.4. In this ablative reactor, pine wood particles with particle size of 4.75 – 6.35 mm were fed by a screw feeder. Then, the biomass particles were pressed onto a stationary hot plate (450 – 600 °C) using four rotating asymmetric blades. The speed of the rotating blades was up to 200 rpm. Three-stage ice-cooled condensers were used to recover the liquid products. Up to 67.7% of bio-oil yield on dry feed has been obtained. The major problem of this system was the difficult removal of the char formed on the reactor surface. The char built up below the rotating blades can quickly prevent the incoming particles from being ablated. To solve this problem, a 2 mm diameter blow line was fitted at the surface close to the outlet of the reactor.

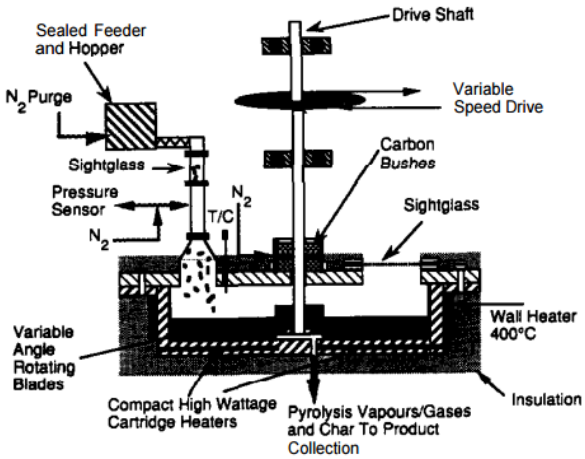

Figure 1.4 Ablative pyrolysis reactor designed by Peacocke et al. [13]

Building on the lessons from the first reactor, Peacocke and Bridgwater later developed another ablative pyrolysis system (Figure 1.5) [80]. This reactor consisted of a cylindrical vessel whose internal surface worked as an ablative heated surface. The feedstock was fed to the reactor against the hot surface (600 °C), and it was scraped along the wall by the rotatable blades. The blades were connected to a central drive shaft, which had an inner drum to reduce the vapor space inside the reactor thereby reducing the resistance time of the products. The drum also provided a suitable surface to which to attach the blades. The problem with this apparatus was the distortion or "flapping" of the blades, which reduced the effectiveness of the reactor. Contact between the blades and the surface can occur, resulting in the blades or the surface being damaged.

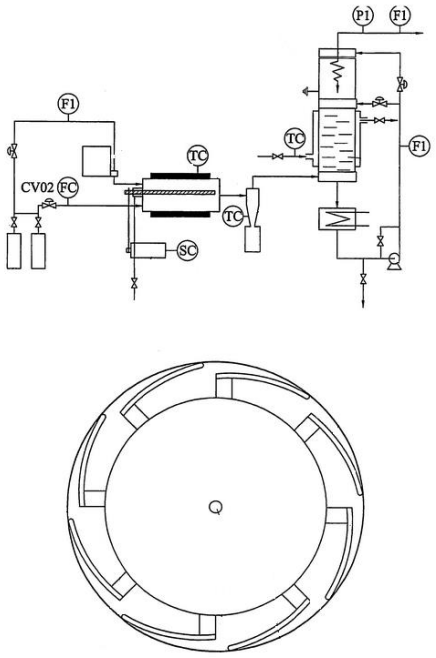

Figure 1.5 Schematic diagram of the ablative thermolysis system and the cross sectional representation of reactor [80]

1.4.5 Others

In the 1990s, BBC Engineering in Canada demonstrated a 10-25 kg/h continuous ablation reactor for waste tyre disposal [77,81]. Detailed information of the reactor is not available. Ablation of tyre particles was achieved by sliding contact on a hot metal surface. Up to 6 mm tyre particles have been tested in the reactor. A liquid yield of 54% has been obtained from pyrolysis of tyres with a particle size of 1.3 mm, at pyrolysis temperature of 470-540 °C and residence time of 0.88 s. No results have been reported on biomass feedstock. This technology was subsequently licensed to the Castle Capital (Canada) who demonstrated a 50 t/day plant in Halifax, Nova Scotia, converting solid waste [77,82]. In 2006, an ablative fast pyrolysis pilot plant with a design capacity of 6 t/d was built by Pytec in Germany [83]. Ablation of wood chips was achieved by compression with a hydraulic cylinder against a hot rotating disk. No other details on this system are available.

1.5 RESEARCH OBJECTIVES

The bark beetle outbreak has severely affected the forests across the western U.S., and the infested trees need to be disposed of to avoid falling and minimize wildfire hazards. Thus, the overall objective of this research is to generate a novel application for beetle-killed trees by converting them into liquid fuel via ablative pyrolysis near the harvesting point, which could significantly reduce the costs of biomass drying, grinding, and transportation. The specific objectives include i) characterize beetle-killed trees at different decay stages, and investigate the effects of their degradation stages on the performance of non-catalytic and catalytic fast pyrolysis using a micro-scale pyrolyzer (Chapter 2); ii) systematically compare the *in-situ* and *ex-situ* upgrading of pyrolysis vapors from beetle-killed trees over a wide range of reaction conditions using a micro-scale pyrolyzer (Chapter 3); iii) design and construct a novel lab-scale ablative pyrolysis unit to

fast pyrolyze beetle-killed trees in the form of entire wood chips and rods into bio-oil (Chapter 4 and 5); and iv) study the effects of different operating parameters in the ablative reactor on the product yield and quality (Chapter 6). Chapter 7 summarizes the work presented in this dissertation and proposes the future work needed to answer the questions raised by this research.

1.6 REFERENCES

[1] U.S. Forest Service, Western Bark Beetle Strategy for Human Safety, Recovery and Resiliency, 2011.

[2] Western Forestry Leadership Coalition (WFLC), Western Bark Beetle Assessment: A Framework for Cooperative Forest Stewardship, 2007.

[3] R.G. Mitchell, H.K. Preisler, Fall rate of lodgepole pine killed by the mountain pine beelte in central Oregon, Western Journal of Applied Forestry, 13 (1998) 23-26.

[4] M. Waterhouse, H. Armleder, Windthrow in partially cut lodgepole pine forests in west-central British Colombia. Extension Note 70, BC Ministry of Forests Research Branch, Victoria, 2004.

[5] J.A. Hicke, M.C. Johnson, J.L. Hayes, H.K. Preisler, Effects of bark beetle-caused tree mortality on wildfire, Forest Ecol. Manag. 271 (2012) 81-90.

[6] J.J. Kim, E.A. Allen, L.M. Humble, C. Breuil, Ohiostomatoid and basidiomycetous fungi associated with green, red, and grey lodgepole pines after mountain pine beetle (*Dendroctonus ponderosae*) infestation, Canadian Journal of Forest Research, 35 (2005) 274-284.

[7] S.M. Ewanick, Bioconversion of mountain pine beetle-killed lodgepole pine to ethanol, Master Thesis, University of British Columbia, Canada, 2006.

[8] T. Byrne, C. Stonestreet, B. Peter, Chapter 9: Characteristics and utilization of post-mountain pine beetle wood in solid wood products, in: L. Safranyik, B. Wilson (Eds), Mountain Pine Beetle: A Synthesis of Biology, Management, and Imapcts on Lodgepole Pine, Canadian Forest Service, 2007, pp 233-253.

[9] P. Watson, Chapter 10: Impact of the mountain pine beetle on pulp and papermaking, in: L. Safranyik, B. Wilson (Eds), Mountain Pine Beetle: A Synthesis of Biology, Management, and Imapcts on Lodgepole Pine, Canadian Forest Service, 2007, pp 233-253.

[10] R.W. Reid, Moisture changes in lodgepole pine before and after attack by the mountain pine beetle, The Forest Chronicle, 34 (1961) 368-375.

[11] E. Sjöström, Wood Chemistry: Fundamentals and Applications, Academic Press Inc., San Diego, California, 1993.

[12] K.L. Woo, P. Watson, S.D. Manfield, The effects of mountain pine beetle and associated blue staining fungi on wood morphology and chemistry, Paprican University Report 831, Paprican and Department of Wood Science, University of BC, Vancouver, BC, 2003.

[13] K.L. Woo, P. Watson, S.D. Manfield, The effects of mountain pine beetle and associated blue staining fungi on wood morphology and chemistry: Implications for wood and fiber quality, Wood and Fiber Science, 37 (2005) 112-126.

[14] P. Bicho, C. Woo, B. Dalpke, Quantifying the effects of extractives from mountain pine beetle-attacked lodgepole pine pulp and papermaking. Natural Resources Canada, Canadian Forest Service, Pacific Forestry Centre, Victoria, BC, Canada, 2008

[15] P.J. Lieu, R.G. Kelsey, F. Shafizadeh, Some chemical characteristics of green and dead lodgepole pine and western white pine, USDA forest Service research note INT-256, 1979.

[16] R.J.M. Westerhof, D.W.F. Brilman, M. Garcia-Perez, Z. Wang, S.R.G. Oudenhoven, S.R.A. Kersten, Stepwise fast pyrolysis of pine wood, Energy Fuel 26 (2012) 7263-7273.

[17] C.E. Greenhalf, D.J. Nowakowski, A.B. Harms, J.O. Titiloye, A.V. Bridgwater, A comparative study of straw, perennial grasses and hardwoods in terms of fast pyrolysis products, Fuel 108 (2013) 216-230.

[18] F.A. Agblevor, S. Besler, A.E. Wiselogel, Production of oxygenated fuels from biomass: impact of feedstock storage. Fuel Science & Technology International, 14 (1996) 589-612.

[19] C. Di Blasi, G. Signorelli, C. Di Russ, G, Rea, Product distribution from pyrolysis of wood and agricultural residues. Industrial & Engineering Chemistry Research, 38 (1999) 2216-2224.

[20] K. Wang, R.C. Brown, Catalytic pyrolysis of microalgae for production of aromatics and ammonia, Green Chem. 15 (2013) 675-681

[21] H.J. Park, H.S. Heo, Y.K. Park, J.H. Yim, J.K. Jeon, J. Park, C. Ryu, S.S. Kim. Clean bio-oil production from fast pyrolysis of sewage sludge: Effects of reaction conditions and metal oxide catalysts, Bioresources Technology, 101 (2010) S83-S85.

[22] H. Yang, R. Yan, H. Chen, D.H. Lee, C. Zheng, Characteristics of hemicellulose, cellulose and lignin pyrolysis, Fuel, 86 (2007)1781-1788.

[23] A.V. Bridgwater, D. Meier, D. Radlein, An overview of fast pyrolysis of biomass, Organic Geochemisty, 30 (1999) 1479-1493.

[24] A.V. Bridgwater, Principles and practice of biomass fast pyrolysis processes for liquids, Journal of Analytical and Applied Pyrolysis, 51 (1999) 3-22.

[25] D. Mohan, C.U. Pittman, P.H. Steele, Pyrolysis of wood/biomass for bio-oil: a critical review. Energy & Fuels, 20 (2006) 848-889.

[26] P.R. Patwardhan, J. A. Satrio, R.C. Brown, B.H. Shanks, Product distribution from fast pyrolysis of glucose-based carbohydrates, Journal of Analytical and Applied Pyrolysis, 86 (2009) 323-330.

[27] P.R. Patwardhan, R.C. Brown, B.H. Shanks, Product distribution from the fast pyrolysis of hemicellulose, ChemSusChem, 4 (2011) 636-643.

[28] P.R. Patwardhan, R.C. Brown, B.H. Shanks, Understanding the fast pyrolysis of lignin, ChemSusChem, 4 (2011) 1629-1636.

[29] P.R. Patwardhan, J. A. Satrio, R.C. Brown, B.H. Shanks, Influence of inorganic salts on the primary pyrolysis products of cellulose, Bioresources Technology, 101 (2010) 4646-4655.

[30] C.J, Ellens, Design, optimization and evaluation of a free fall biomass fast pyrolysis reactor and its products, Master Thesis, Iowa State University, 2009.

[31] Z. Luo, S, Wang, Y, Liao, J. Zhou, Y. Gu, K. Cen, Research on biomass fast pyrolysis for liquid fuel, Biomass and Bioenergy, 26 (2004) 455-462.

[32] M. Garcia-Perez, X.S. Wang, J. Shen, M.J. Rhodes, F. Tian, W.J. Lee, H. Wu, C.Z. Li, Fast pyrolysis of oil mallee woody biomass: Effect of temperature on the yield and quantity of pyrolysis products, Industrial & Engineering Chemistry Research, 47 (2008) 1864-1854.

[33] S. Thangalazhy-Gopakumar, S. Adhikari, Ravindran H, R.B. Gupta, O. Fasina, M. Tu, S.D. Fernando, Physiochemical properties of bio-oil produced at various temperatures from pine wood using an auger reactor, Bioresources Technology, 101 (2010) 8389-8395.

[34] Q. Zhang, J. Chang, T. Wang, Y. Xu, Review of biomass pyrolysis oil properties and upgrading research, Energy Conversion and Management, 48 (2007) 87-92.

[35] A. Oasmaa, S. Czernic, Fuel oil quality of biomass pyrolysis oils-state of the art for the end-users, Energy & Fuels, 13 (1999) 914-921.

[36] R. He, X.P. Ye, B.C. English, J.A. Satrio, Influence of pyrolysis condition on switchgrass bio-oil yield and physicochemical properties, Bioresource Technology, 100 (2009) 5305-5311.

[37] Q. Lu, W. Li, X. Zhu, Overview of fuel properties of biomass fast pyrolysis oils, Energy Conversion and Management, 50 (2009) 1376-1383.

[38] H. Aubin, C. Roy, Study on the corrosiveness of wood pyrolysis oils, Fuel Science Technology International, 8 (1990) 77-86.

[39] S. Czernik, A.V. Bridgwater, Overview of Applications of Biomass Fast Pyrolysis Oil, Energy & Fuels, 18 (2004) 590-598.

[40] H.J. Park, J.I. Dong, J.K Jeon, K.S. Yoo, J.H. Yim, J.M. Sohn, Y.K. Park, Conversion of the pyrolysis vapor of radiata pine over zeolites, Journal of Industrial and Engineering Chemistry, 13 (2007) 182-189.

[41] S. Vitolo, M. Seggiani, P. Frediani, G. Ambrosini, L. Politi, Catalytic upgrading of pyrolytic oils to fuel over different zeolites, Fuel, 78 (1999) 1147-1159.

[42] M. Asadieraghi, W.M.A.W. Daud, H.F. Abbas, Heterogeneous catalysts for advanced bio-fuel production through catalytic biomass pyrolysis vapor upgrading: a review, RSC Advances, 5 (2015) 22234-22255.

[43] C. Liu, H. Wang, A.M. Karim, J. Sun, Y. Wang, Catalytic fast pyrolysis of lignocellulosic biomass, Chemistry Society Reviews, 43 (2014) 7594-7623.

[44] A. Aho, N. Kumar, K. Eränen, T. Salmi, M. Hupa, D.Y. Murzin, Catalytic pyrolysis of biomass in a fluidized bed reactor: Influence of the acidity of H-beta zeolite, Process Safety and Environmental Protection, 85 (2007) 473-480.

[45] D.J. Mihalcik, A.A. Boateng, C.A. Mullen, N.M. Goldberg, Packed-bed catalytic cracking of oak-derived pyrolytic vapors, Industrial & Engineering Chemistry Research, 50 (2011) 13304-13312.

[46] T.R. Carlson, G.A. Tompsett, W.C. Conner, G.W. Huber, Aromatic production from catalytic fast pyrolysis of biomass-derived feedstocks, Topics in Catalysis, 52 (2009) 241-252.

[47] D.J. Mihalcik, C.A. Mullen, A.A. Boateng, Screening acidic zeolites for catalytic fast pyrolysis of biomass and its components, Journal of Analytical and Applied Pyrolysis, 92 (2011) 224-232.

[48] A.J. Foster, J. Jae, Y.T. Cheng, G.W. Huber, R.F. Lobo, Optimizing the aromatic yield and distribution from catalytic fast pyrolysis of biomass over ZSM-5, Applied Catalysis A: General, 423 (2012) 154-161.

[49] J. Jae, G.A. Tompsett, A.J. Foster, K.D. Hammond, S.M. Auerbach, R.F. Lobo, G.W. Huber, Investigation into the shape selectivity of zeolite catalysts for biomass conversion, Journal of Catalysis, 279 (2011) 257-268.

[50] T.R. Carlson, Y.-T. Cheng, J. Jae, G.W. Huber, Production of green aromatics and olefins by catalytic fast pyrolysis of wood sawdust, Energy & Environmental Science, 4 (2011) 145-161.

[51] T.R. Carlson, J. Jae, Y.-C. Lin, G.A. Tompsett, G.W. Huber, Catalytic fast pyrolysis of glucose with HZSM-5: the combined homogeneous and heterogeneous reactions, Journal of Catalysis, 270 (2010) 110-124.

[52] C. Liu, H. Wang, A.M. Karim, J. Sun, Y. Wang, Catalytic fast pyrolysis of lignocellulosic biomass, Chemical Society Reviews, 43 (2014) 7594-7623.

[53] M. Biddy, A. Dutta, S. Jones, A. Meyer, In-Situ Catalytic Fast Pyrolysis Technology Pathway, in, National Renewable Energy Laboratory, 2013.

[54] A. Aho, N. Kumar, K. Eränen, T. Salmi, M. Hupa, D.Y. Murzin, Catalytic pyrolysis of woody biomass in a fluidized bed reactor: Influence of the zeolite structure, Fuel, 87 (2008) 2493-2501.

[55] O.D. Mante, F.A. Agblevor, Catalytic pyrolysis for the production of refinery-ready biocrude oils from six different biomass sources, Green Chemistry, 16 (2014) 3364-3377.

[56] G. Yildiz, F. Ronsse, R. Venderbosch, R. van Duren, S.R. Kersten, W. Prins, Effect of biomass ash in catalytic fast pyrolysis of pine wood, Applied Catalysis B: Environmental, 168 (2015) 203-211.

[57] M. Biddy, A. Dutta, S. Jones, A. Meyer, Ex-Situ Catalytic Fast Pyrolysis Technology Pathway, in, National Renewable Energy Laboratory, 2013.

[58] S. Wan, Y. Wang, A review on ex situ catalytic fast pyrolysis of biomass, Frontiers of Chemical Science and Engineering, 8 (2014) 280-294.

[59] J. Diebold, J. Scahill, Biomass to gasoline (BTG): upgrading pyrolysis vapors to aromatic gasoline with zeolite catalysis at atmospheric pressure, Preprints of Papers, American Chemical Society, Division of Fuel Chemistry, 1987.

[60] R. French, S. Czernik, Catalytic pyrolysis of biomass for biofuels production, Fuel Processing Technology, 91 (2010) 25-32.

[61] G. Yildiz, M. Pronk, M. Djokic, K.M. van Geem, F. Ronsse, R. Van Duren, W. Prins, Validation of a new set-up for continuous catalytic fast pyrolysis of biomass coupled with vapour phase upgrading, Journal of Analytical and Applied Pyrolysis, 103 (2013) 343-351.

[62] K. Wang, P.A. Johnston, R.C. Brown, Comparison of *in-situ* and *ex-situ* catalytic pyrolysis in a micro-reactor system, Bioresour Technol, 2014; 173: 124-131.

[63] D.P. Gamliel, S. Du, G.M. Bollas, J.A. Valla, Investigation of in situ and ex situ catalytic pyrolysis of miscanthus× giganteus using a PyGC–MS microsystem and comparison with a bench-scale spouted-bed reactor, Bioresour Technol, 2015; 191: 187-196.

[64] A.V. Bridgwater, Renewable fuels and chemicals by thermal processing of biomass, Chemical Engineering Journal, 91 (2003) 87-102.

[65] A. Kumar, A conceptual comparison of bioenergy options for using mountain pine beetle infested wood in Western Canada, Bioresource Technology, 100 (2009) 387-399.

[66] Forest Concepts, Forest Concepts Completes US Department of Energy SBIR Phase I Project to Demonstrate Technical Feasibility of Milling Green and High Moisture Biomass to Biofuel Feedstocks, 2014.

[67] J. Lédé, Comparison of contact and radiant ablative pyrolysis of biomass, Journal of Analytical and Applied Pyrolysis, 70 (2003) 601-618.

[68] J. Lédé, J. Panagopoulos, J. Villermaux, Experimental measurement of ablation rate of wood pieces, undergoing fast pyrolysis by contact with heated wall, Preprints of Papers – American Chemical Society, Division of Fuel Chemistry, 38 (1983) 383-389.

[69] J. Lédé, J. Panagopoulos, H.Z. Li, J. Villermaux, Fast pyrolysis of wood: direct measurement and study of ablation rate, Fuel, 64 (1985) 1514-1520.

[70] H. Martin, J. Lédé, H.Z. Li, J. Villermaux, C. Moyne, A. Degiovanni, Ablative melting of a solid cylinder perpenticularly pressed against a heated wall, International Journal of Heat and Mass Transfer, 29 (1986) 1407-1415.

[71] J. Lédé, J. Panagopoulos, H.Z. Li, J. Villermaux, H. Martin, Fusion-like behavior of wood pyrolysis, Journal of Analytical and Applied Pyrolysis, 10 (1987) 291-308.

[72] G.V.C. Peacocke, Ablative pyrolysis of biomass, doctoral dissertation, Aston University, Birmingham, UK, 1994.

[73] T.B. Reed, C.D. Cowdery, Heat flux requirements for fast pyrolysis and a new method for generating biomass vapor, American Chemical Society Spring Symposium, 32 (1987) 68-81.

[74] T.B. Reed, Contact pyrolysis in a “pyrolysis mill”, Research in Thermochemical Biomass Conversion, 1988.

[75] J. Diebold, J. Scahill, Ablative entrained-flow fast pyrolysis of biomass, proceedings of the 16th Biomass Thermochemical Conversion Contractor’s Meeting, Washington, Portland, Oregon, 1984.

[76] J. Diebold, A. Power, Engineering aspects of the vortex pyrolysis reactor to produce primary pyrolysis oil vapors for use in resins and adhesives, Research in Thermochemical Biomass Conversion, 1988.

[77] A.V. Bridgwater, G.V.C. Peacocke, Fast pyrolysis processes for biomass, Renewable and Sustainable Energy Reviews, 4 (2000) 1-73.

[78] G.V.C. Peacocke, A.V. Bridgwater, Ablative plate pyrolysis of biomass for liquids, Biomass and Bioenergy, 7 (1994) 147-154.

[79] G.V.C Peacocke, E.S. Madrali, C.Z. Li, A.J. Güell, F. Wu, R. Kandiyoti, A.V. Bridgwater, Effect of reactor configuration on the yields and structures of pine-wood derived pyrolysis liquids: a comparison between ablative and wire-mesh pyrolysis, Biomass and Bioenergy, 7 (1995) 155-167.

[80] A.V. Bridgwater, G.V.C. Peacocke, N.M.R. Robinson, Ablative thermolysis reactor, Patent No. US7,625,532, 2009.

[81] J.W. Black, D.B. Brown, Preliminary mass testing of the continuous ablation reactor, Biomass Thermal Processing, proceedings of the 1st Canada/European Community R &D Contractor’s Meeting, 1990.

[82] R.H. Venderbosch, W. Prins, Fast pyrolysis technology development, Biofuels, Bioproducts and Biorefining, 4 (2010) 178-208.

[83] D. Meier, S. Schöll, H. Klauber, J, Markgraf, Practical results from Pytech's biomass-to-oil (BTO) process with ablative pyrolyser and diesel CHP plant, Success & Visions for Bioenergy, 2007, ISBN 978-1-872691-28-2.

CHAPTER 2. ANALYTICAL FAST PYROLYSIS OF BEETLE-KILLED TREES[1]

2.1 ABSTRACT

In this article, we propose beetle-killed lodgepole pine (BKLP) as a feedstock for fast pyrolysis due to its low moisture and high energy content. To the best of our knowledge, no previous studies on fast pyrolysis of beetle-killed trees have been reported. Samples of healthy lodgepole pine and three decay-stage BKLPs were used as feedstock to investigate the effects of the decay stage on the performance of both non-catalytic and catalytic fast pyrolysis using a Py-GC/MS. Compared to the healthy tree, BKLPs were found to have slightly more extractives and less lignin. The decay stage, however, did not affect the product yield and selectivity for both non-catalytic and catalytic fast pyrolysis. A variety of oxygenated compounds were produced in non-catalytic fast pyrolysis, but most of those were converted into aromatic hydrocarbons in the presence of HZSM-5. For non-catalytic fast pyrolysis, the yield of char decreased from 22 wt. % to 11 wt. % as the pyrolysis temperature increased from 450 °C to 650 °C. The average HHV of volatile compounds was found to be around 26 MJ/kg. For the catalytic fast pyrolysis, the yield of hydrocarbons was as high as 40 wt. %, and the yield of char was as low as 5 wt. %. The average HHV of volatiles was found to be about 41 MJ/kg, which is close to the HHV of commercial gasoline and diesel (~46 MJ/kg). A high yield of toluene (11 wt. %) and xylenes (9 wt. %) was also observed in the catalytic fast pyrolysis process. Our work suggests that beetle-killed trees are a good feedstock for fast pyrolysis, because the bio-oil derived from the trees that have been dead for four years showed the same quality as that from the healthy trees.

[1]Published: G. Luo, F.L.P. Resende, Fast pyrolysis of beetle-killed trees, Journal of Analytical and Applied Pyrolysis, 110 (2014): 100-107.

2.2 INTRODUCTION

Recently, climate change combined with unhealthy forest conditions have led to a large bark beetle outbreak in the western United States. Across the landscape from the West Coast through the Rocky Mountains, more than 41.7 million acres of conifer forests have been infested by bark beetles since 1996 and this number is expected to increase in the near future (5-10 years) [1]. Although bark beetles are natural components of western forest ecosystems; recent bark beetle epidemic with high levels of tree mortality has negatively impacted public benefits from forests [2]. Bark beetle-caused tree mortality may also change forest fuel distributions and therefore wildfire characteristics [3]. As bark beetle-killed trees decay and fall to the ground, surface fuel loads start to accumulate. Heavy surface fuel loads not only act as ladders to carry a surface fire into tree crowns but also increase the heat intensity and duration of the fire on the forest floor [2]. Thus, the potential for high-severity wildfire increases without changing the probability of fire occurrence. What is worse, wildfires increase the susceptibility of trees to the bark beetle attack [2].

In order to minimize the wildfire hazard, beetle-killed trees should be properly disposed of. Traditionally, the forest industry uses pile or broadcast burning to dispose of forest residues, which unfortunately causes air pollution and wastes energy and nutrients [4]. Moreover, some undesirable properties of beetle-killed trees limit applications for solid wood and wood panel manufacturing. For example, mountain pine beetles carry a diversity of fungi on the surface of their bodies when attacking. The introduction and propagation of these fungi, mainly staining fungi, cause a bluish discoloration in the timber; consequently reducing the commercial value of infested trees for wood product manufacturing [5]. Additionally, staining fungi lower the wood moisture content, particularly for sapwood. Reid [6] found that the sapwood moisture content of

beetle-killed trees decreased from 85-165% of oven dry weight to around 16% after one-year of attack. Once the moisture content falls below the fiber saturation point (30%, dry basis), checking and splitting are observed in the wood, making it improper for wood product manufacturing [7, 8]. Low moisture content and high energy content, however, are excellent feedstock characteristics for bioenergy and biofuel production, because the costs of biomass drying could be reduced or even eliminated.

We propose fast pyrolysis, the rapid thermal decomposition of organic matter in the absence of oxygen, as a potential way to convert beetle-killed trees into bio-oil that could be further upgraded into commodity chemicals and fuels. Fast pyrolysis has been extensively studied for different feedstocks such as woody biomass (softwood and hardwood), agricultural residues (e.g. rice husk and wheat straw) and algae [9-12]. The products of fast pyrolysis include primarily a liquid that is commonly called bio-oil, permanent gases (i.e. CO, H_2, CO_2, and light hydrocarbons), and some solid char. Around 70 wt. % (dry basis) yield of bio-oil has been reported for fast pyrolysis of woody biomass [13]. Bio-oil is a mixture of hundreds of oxygenated compounds. Its high oxygen content results in some undesirable properties, such as high viscosity, high acidity, instability, and relatively low energy density; therefore, further upgrading of the bio-oil through a heterogeneous catalytic process is required before it can be used for the production of commodity chemicals and transportation fuels. Upgrading of bio-oil can be performed either *in-situ* or *ex-situ*. The *in-situ* upgrading process is called catalytic fast pyrolysis (CFP) and has drawn significant attention recently. During the CFP process, upgrading takes place immediately after the formation of pyrolysis vapors in a single reactor. Due to its short residence time, less char is produced compared to the *ex-situ* process, in which pyrolysis vapors are upgraded in a secondary reactor [14, 15]. A variety of zeolites have been tested using CFP, including HY, SN-27, MSM-15, and

HZSM-5 [16, 17]. HZSM-5 is widely accepted to be the most effective and selective catalyst to produce gasoline-range hydrocarbons, which is mainly attributed to its acidity and network structure [18].

Lodgepole pine is one of the most prevalent tree species in the Pacific Northwest of the United States. It is also the main target of the mountain pine beetle (MPB, *Dendroctonus ponderosae*), out of the other varieties of pine species that coexist in this region [19]. To the best of our knowledge, there are no previous studies on fast pyrolysis of beetle-killed trees. The main goal of this study was to investigate the effects of different decay stages of BKLP on the performance (i.e. product yield and selectivity) of both non-catalytic and catalytic fast pyrolysis. The effect of non-catalytic fast pyrolysis temperature has also been studied.

2.3 MATERIALS AND METHODS

2.3.1 Materials

Lodgepole pine (*Pinus contorta*) samples were purchased from Forest Concepts, LLC, for use in this study. The samples were wood Crumbles® (2 mm × 2 mm) from: i) green uninfected trees (LP); ii) partially green but terminally infected trees (BKLP1); iii) standing dead trees with red needles and intact bark (BKLP2); and iv) standing dead trees without needles, and 2-4 years after death (BKLP3) (Figure 2.1). All trees were collected from the same forest field in Steamboat Springs, Colorado, and were in the age range of 70-80 years old. Thus, we assumed that all the differences found between the four types of feedstock used in this study could be attributed to their unique stages of decay. The particle size of these wood Crumbles® was reduced into 40 mesh (420 μm), using a Thomas Wiley mill, for the non-catalytic pyrolysis, in order to generate uniform decayed lodgepole pine samples which fit the small CDS pyroprobe tube. For the catalytic

pyrolysis, the wood particle size was further reduced to 140 mesh (105 μm), which sis the same particle size as the catalyst, generating a uniformly sized mixture of wood samples and catalyst. The catalyst was CBV2314 ZSM-5 (Zeolyst International, SiO_2/Al_2O_3 = 23, ≤ 140 mesh) in the form of the ammonium salt. Prior to use, the catalyst was converted to the acid form, HZSM-5, by calcination at 600 °C for 5 h. Oxygenated and hydrocarbon compounds used as standards were purchased from Sigma Aldrich and Fisher Scientific and used as received.

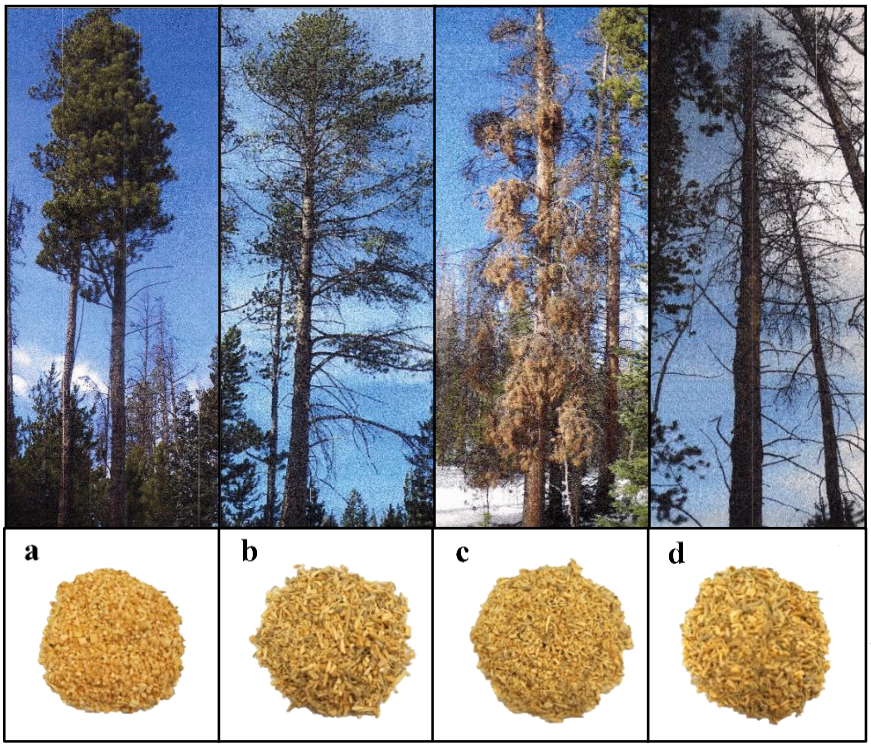

Figure 2.1 Four types of feedstocks. a) Green uninfected trees (LP); b) partially green but terminally infected trees (BKLP1); c) standing dead trees with red needles and intact bark (BKLP2); and d) standing dead trees without needles, and 2-4 years after death (BKLP3).

2.3.2 Feedstock characterization

Chemical constituents (i.e. extractives, carbohydrates, and lignin), moisture content (dry basis) and ash content of the four types of feedstocks were measured, according to "Standard Biomass

Analytical Procedures" developed by the National Renewable Energy Laboratory [20]. To measure the extractives, ethanol was used as a solvent. High-performance liquid chromatography (HPLC, Dionex ICS-3000) was used for monomer sugar analysis. CHNO elemental analysis of the feedstock was performed using an elemental analyzer (Series II 2400, PerkinElmer).

2.3.3 Fast pyrolysis

Fast pyrolysis experiments were carried out using a commercial micro-pyrolyzer (Pyroprobe model 5200, CDS Analytical Inc.). The pyroprobe contained a computer-controlled heating element (a platinum coil), which held an open-ended quartz tube (25 mm × 1.9 mm I.D.). Powdered samples were loaded in the middle of the tube with loose quartz wool packed at both ends. According to the CDS manufacturer's manual, the actual temperature inside the quartz tube is estimated to be about 100 °C lower than the temperature of the heating element. The pyrolysis temperature reported in this study is the set-up heating element temperature.

Feedstock amounts used in the fast pyrolysis experiments were weighed with an autobalance (AD 6, PerkinElmer) with an accuracy of 0.1 μg. Samples of LP and three decay-stage BKLPs (0.5 mg, 420 μm) were pyrolyzed at a temperature of 550 °C and a heating rate of 1000 °C/s. Fast pyrolysis of representative feedstock, BKLP3 (the highest stage of degradation), was also conducted at temperatures of 450 °C and 650 °C to evaluate the effect of temperature. For each experiment, the probe temperature was held for 45 s to minimize the temperature gradient inside the quartz tube. For the CFP process, only LP and BKLP3 were used as feedstocks. Prior to pyrolysis, LP and BKLP3 (105 μm) were evenly mixed with HZSM-5 (105 μm) at a catalyst-to-biomass ratio of 20. In order to avoid saturating the analytical detector (see section 2.3.4), 0.1 mg of the LP and BKLP3 samples were used in CFP. CFP was operated at 550 °C with a holding time of 45 s and a heating rate of 1000 °C/s. The pyroprobe interface temperature was set to 300 °C.

Triplicates were employed at each condition; error bars shown in later figures express the standard deviations. The solid residues from non-catalytic fast pyrolysis and CFP are defined as char and coke, respectively. The yields of char or coke were calculated by weighing the mass of samples before and after pyrolysis, taking the moisture content of the quartz wool and HZSM-5 catalyst into account.

2.3.4 GC/MS analysis

Pyrolysis vapors were carried with high-purity helium via a transfer line (300 °C, 1 m in length) to a gas chromatograph (GC, 2010 Plus, Shimadzu) that was equipped with a mass spectrometer (MS, QP2010 Ultra, Shimadzu). The chromatographic separation of pyrolysis products was achieved on a SHRXI-5MS column (30 m × 0.25 mm I.D. × 0.25 μm film thickness, Shimadzu). An injection temperature of 300 °C and a split ratio of 125:1 were used. The GC oven was programmed to hold at 35 °C for 2 min, followed by heating to 200 °C at 5 °C/s, holding at this temperature for 4 min. The GC oven was then ramped at 5 °C/s to a final temperature of 300 °C that was kept for 5 min. The mass spectra were recorded in the electron ionization mode over a mass per charge (*m/z*) range of 45-550. Peak identification was performed by comparing the produced mass spectra with the NIST 2010 mass spectral library and matching the retention times of the identified compounds with those of known standards. After the peaks were identified, external calibration standards were prepared using GC/MS for quantification. Forty-one oxygenated products were quantified from the total ion chromatogram, using only twenty-nine standards because isomers or chemicals with similar structure were used to quantify some compounds. For CFP, seventy-three compounds were quantified using thirty-seven standards. The elemental composition of the Py-GC/MS products from each process was estimated according to

the compound weight percentage and chemical formula. The higher heating value (HHV) could then be calculated according to the following equation:

$$\text{HHV (MJ/kg)} = \text{C\%} \times 0.3578 + \text{H\%} \times 1.1356 + \text{N\%} \times 0.0594 - \text{O\%} \times 0.0854 - 0.974 \quad (2.1)$$

The HHV values reported for the Py-GC/MS products are only representative of the volatiles from fast pyrolysis that can be detected by GC/MS; whereas non-volatile compounds are not included in this estimate.

2.4 RESULTS AND DISCUSSION

2.4.1 Feedstock characterization

The elemental composition of LP and BKLP samples are given in Table 2.1, and no statistical difference was observed between the four types of feedstocks. All the samples had high C and O contents of ca. 49.6% and 42.6%, and low H and N contents of ca. 6.3% and 0.5%, respectively. Therefore, the approximate chemical formula for the feedstock is $C_{4.1}H_{6.3}O_{2.7}N_{0.03}$, corresponding to an HHV of 20.3 MJ/kg.

Table 2.1 Elemental composition of LP and BKLPs

Feedstock	Elemental percentage (%)			
	C	O	H	N
LP	49.50 ± 0.11	42.53 ± 0.81	6.12 ± 0.04	0.53 ± 0.05
BKLP1	49.71 ± 0.10	42.02 ± 1.18	6.27 ± 0.04	0.50 ± 0.02
BKLP2	49.60 ± 0.25	43.17 ± 0.38	6.23 ± 0.09	0.49 ± 0.01
BKLP3	49.62 ± 0.29	43.29 ± 0.46	6.37 ± 0.02	0.44 ± 0.01

Results for the chemical composition of the samples are shown in Table 2.2. The four samples were found to have similar moisture (5.0%), ash (0.3%), glucose (38.0%), mannose (10.0%), and xylose (6.5%) contents, considering the standard deviations. However, BKLPs, in particular BKLP1 (shortly after attack) exhibited slightly higher extractives content than LP. Lodgepole pines have two responses after attack of MPBs; namely, an initial response of a redistribution of existing oleoresins to the wound site followed by a secondary resinosis, that is, the synthesis of resinous compounds in the parenchyma cells [21]. Thus, the higher extractives content seen with BKLPs may be due to the secondary resinosis. Compared to LP, BKLPs were found to have a relatively lower content of lignin (Klason lignin and acid soluble lignin) and higher contents of galactose and arabinose. However, for beetle-infested trees, the losses of both lignin and carbohydrates have been reported in the literature [22]. The presence of accompanying decay fungi, such as white-rot fungi, may cause the decrease of lignin [23]. The lower carbohydrate content of the beetle-infested trees may be attributed to the consumption of lower molecular, soluble carbohydrates by the microorganism in the infested trees [24]. The Klason lignin analysis only shows the relative weight percentage for each analyte. If the weight percentage of one analyte decreases, the weight percentage of one or more analytes will increase, since they add up to nearly 100 wt.%. Therefore, in our study the statistically significant loss of lignin observed in BKLPs, compared to LP, leads to merely an apparent increase of galactose and arabinose, so our results are indeed consistent with literature results.

Table 2.2 Chemical constituents of LP and BKLPs

	LP	BKLP1	BKLP2	BKLP3
Moisture content [a]	4.87 ± 0.28	5.05 ± 0.12	4.82 ± 0.15	4.85 ± 0.19
Ash [a]	0.29 ± 0.03	0.32 ± 0.01	0.40 ± 0.16	0.29 ± 0.02
Extractive [a]	4.83 ± 0.26	5.98 ± 0.13	5.11 ± 0.21	5.48 ± 0.18
Klason lignin [b]	30.15 ± 0.56	28.07 ± 0.65	28.12 ± 0.74	28.53 ± 0.23

Acid-soluble lignin [b]	0.37 ± 0.01	0.42 ± 0.04	0.28 ± 0.00	0.31 ± 0.03
Carbohydrates [b]				
Glucose	36.39 ± 1.80	37.74 ± 1.59	43.61 ± 4.99	38.96 ± 2.86
Mannose	8.97 ± 0.53	9.74 ± 0.90	11.41 ± 1.42	9.59 ± 0.64
Xylose	6.30 ± 0.32	6.30 ± 0.34	6.91 ± 0.78	6.80 ± 0.48
Galactose	3.22 ± 0.16	3.95 ± 0.16	3.80 ± 0.38	3.84 ± 0.26
Arabinose	1.58 ± 0.17	1.98 ± 0.15	1.97 ± 0.40	1.99 ± 0.22

a. % of O.D. dry wood
b. % of O. D. extractive-free wood

2.4.2 Non-catalytic fast pyrolysis

When lignocellulosic biomass undergoes fast pyrolysis, it produces permanent gases, bio-oil, and solid char. In this study, only the volatile constituents of bio-oil at 300 °C (this is the temperature of the transfer line) and solid char were quantitatively analyzed, due to the limitations of the experimental setup and GC/MS technique. Permanent gases, typically contributing about 10 wt. % to fast pyrolysis products, and non-volatiles at 300 °C cannot be measured. In the discussion that follows, the yield of a compound or char is defined as:

$$Yield\ (wt.\%) = \frac{Mass\ of\ a\ compound\ or\ char}{Mass\ of\ raw\ biomass\ (LP\ or\ BKLPs)} \times 100 \quad (2.2)$$

2.4.2.1 Effect of BKLP decay stages on non-catalytic fast pyrolysis

Fast pyrolysis of LP and BKLP feedstocks at 550 °C, in the absence of a catalyst, produced a wide range of compounds, most of which were oxygenated compounds including acids, furfurals, phenols and anhydrosugars (Figure 2.2). Peaks observed before the retention time of 40 min were found to be nearly identical for the four samples. A group of peaks present at 40-45 min, however, were only observed for BKLPs, and increased in intensity with degradation. Unfortunately, the

peak indexes in this range were too small to be accurately identified or even quantified by GC/MS. The area of these peaks was around 1-2% of total peak area.

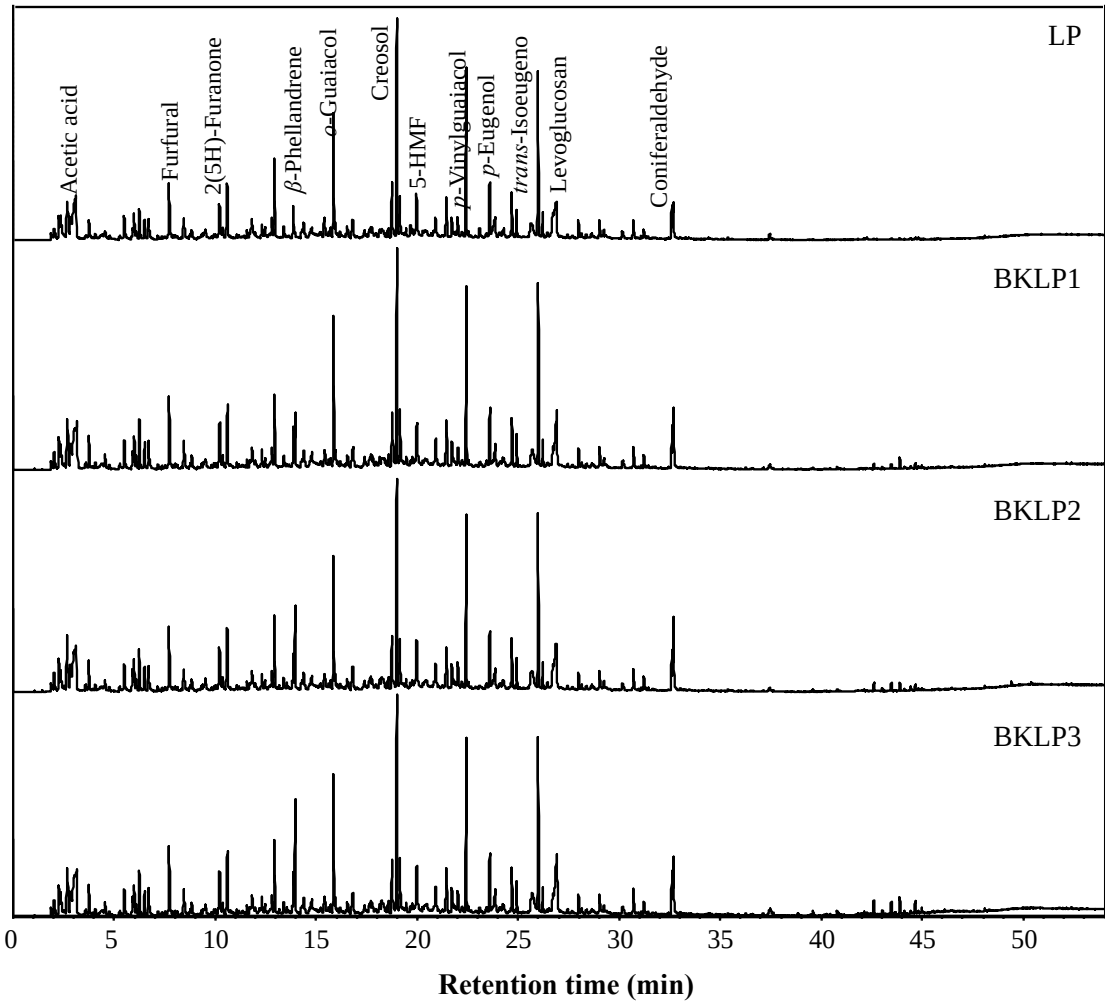

Figure 2.2 Total ion chromatograms of fast pyrolysis products from LP and BKLPs at 550 °C

Figure 2.3 shows the yield of char and total volatiles as a function of decay stage. No statistical difference was seen for char yield among BKLP1, BKLP2, and BKLP3. However, BKLP3 had slightly lower char yield (14.3 wt. %) than LP (16.6 wt. %), which may be due to its relatively lower lignin content. Lignin is the most thermally resistant component in biomass, gradually decomposing over a wide temperature range of 300-800 °C [25, 26]. At the temperature of 550 °C in this study, some lignin may have not completely decomposed, resulting in the formation of char.

In addition, the primary pyrolysis products of lignin are likely to oligomerize to form char [27]. For the yield of total volatiles, no significant difference was observed between the four types of feedstocks, and it is around 12-13 wt. % of raw feedstock.

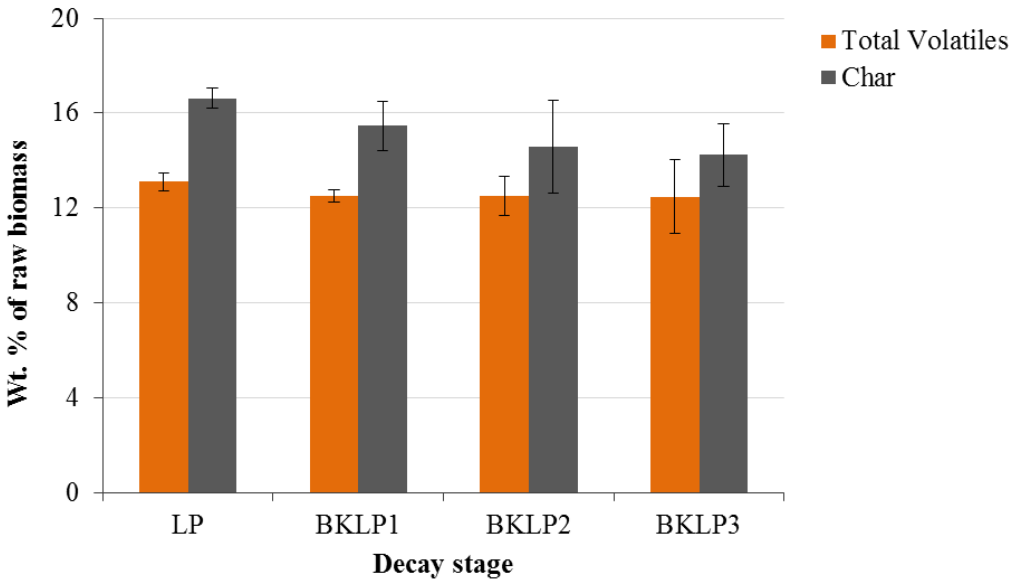

Figure 2.3 Yield of fast pyrolysis products from LP and BKLPs at 550 °C

The volatile compounds were further classified into alcohols (i.e. ethanol), acids, ketones, furans, anhydrosugars, phenols, guaiacols, aromatics, and monoterpenes (i.e. β-phellandrene). The yield of each type of compound is shown in Figure 2.4. Guaiacols were found to be the major type of compounds with a yield of 3.5-4.0 wt. % of raw feedstock since lodgepole pine is mainly composed of guaiacyl-lignin, followed by furans (~3.0 wt. %) and anhydrosugars (~2.8 wt. %). The most abundant compounds among those categories were identified to be levoglucosan (1.3-1.5 wt. %), followed by 5-hydroxymethylfurfural (~1.1 wt. %) and furfural (~1.0 wt. %). No significant effect of the decay stage on the yield of different types of compounds was seen. The only exception was the yield of monoterpenes (i.e. β-phellandrene), which was found to be higher for BKLPs than for LP; whereas no statistical difference was observed between BKLPs. Other

studies have identified β-phellandrene as the predominant component of extractives in lodgepole pine [21]. As mentioned above, the extractives increase during resinosis after bark beetle attack. Although a statistical difference was observed in this study between LP and BKLPs, the yield of β-phellandrene was less than 0.1 wt. %. The elemental composition of the volatile compounds was also calculated and is given in Table 2.3. Compounds from LP and BKLPs were estimated to have similar elemental composition with C, O, and H contents of 59.6%, 34.1% and 6.3%, respectively. The corresponding HHV was calculated to be around 25.6 MJ/kg, which is higher than that of the original BKLP feedstock (20.3 MJ/kg). The HHV is also slightly higher than that of bio-oil reported (18-23 MJ/kg) in the literature, since only volatile components were considered for the HHV calculation here [11, 28].

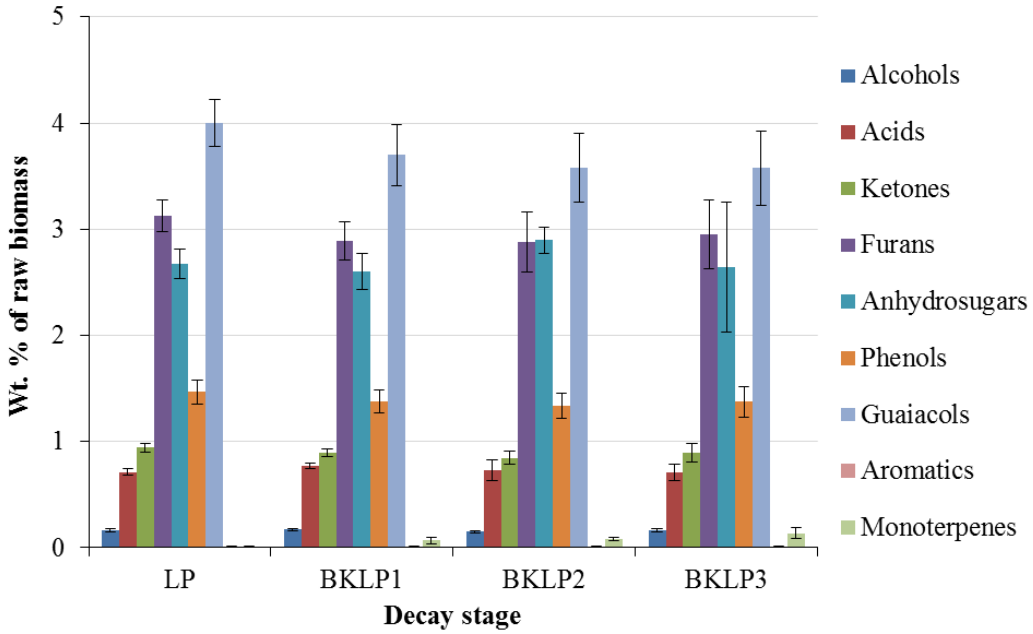

Figure 2.4 Yield of volatile components for LP and BKLPs at 550 °C

As time since beetle attack lengthens, the commercial value of lodgepole pine for wood manufacturing decreases as a result of an increasing risk of secondary attacks by rot-fungi or/and

insect-seeking birds [8]. Since BKLP3 represents the highest level of degradation and could potentially lead to the results that differ from what has been observed for other feedstocks previously studied, it was selected as the feedstock for the remaining experiments.

2.4.2.2 Effect of temperature on non-catalytic fast pyrolysis

The effect of temperature was studied using BKLP3 as feedstock. The quantitative data including the yield of pyrolysis products and different types of volatile compounds are shown in Figure 2.5 and Figure 2.6, respectively. As the pyrolysis temperature increased from 450 °C to 650 °C, the yield of char decreased from 21.8 wt. % to 10.5 wt. % (Figure 2.5). The decrease of char yield with increasing temperature could result from the higher rate of wood decomposition, in particular for the lignin fraction, at higher temperatures [27, 29]. The trend of decreasing char yield with increasing temperature obtained in this study is in agreement with the results reported in the literature [28-30], indicating that the degradation caused by beetle attack did not change the effect of temperature on char yield. We did not attempt to compare the actual char amount with those from other studies, because other studies used different feedstock types, reactor configurations, and operational conditions. For reasons similar to those of char yield, given above, the yields of alcohols and phenols were found to increase as pyrolysis temperature increased. The yield of aromatic compounds, mainly toluene, also became notable at 550 °C (Figure 2.6).

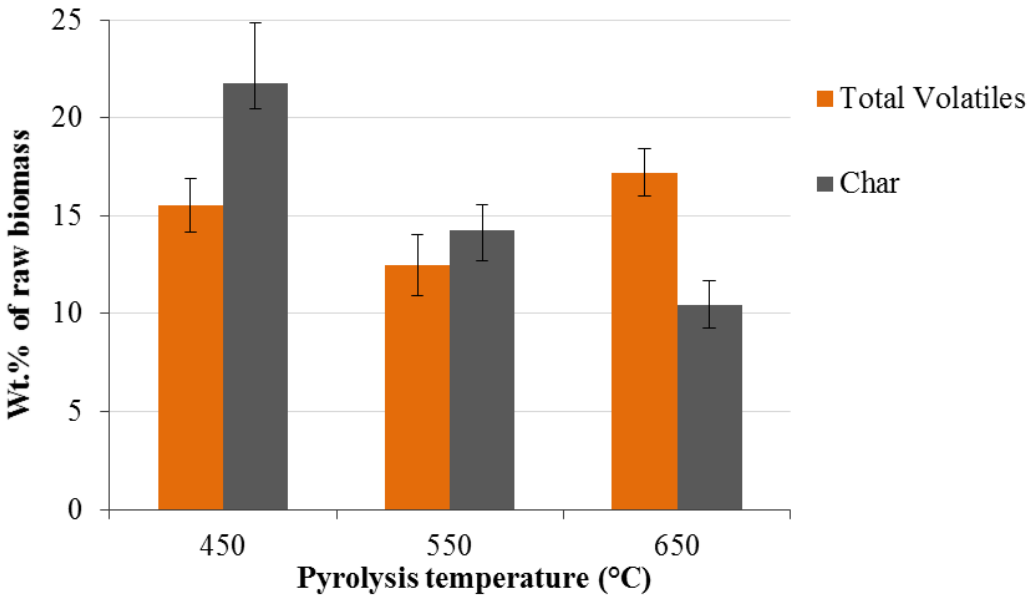

Figure 2.5 Yield of fast pyrolysis products of BKLP3 at 450, 550, and 650 °C

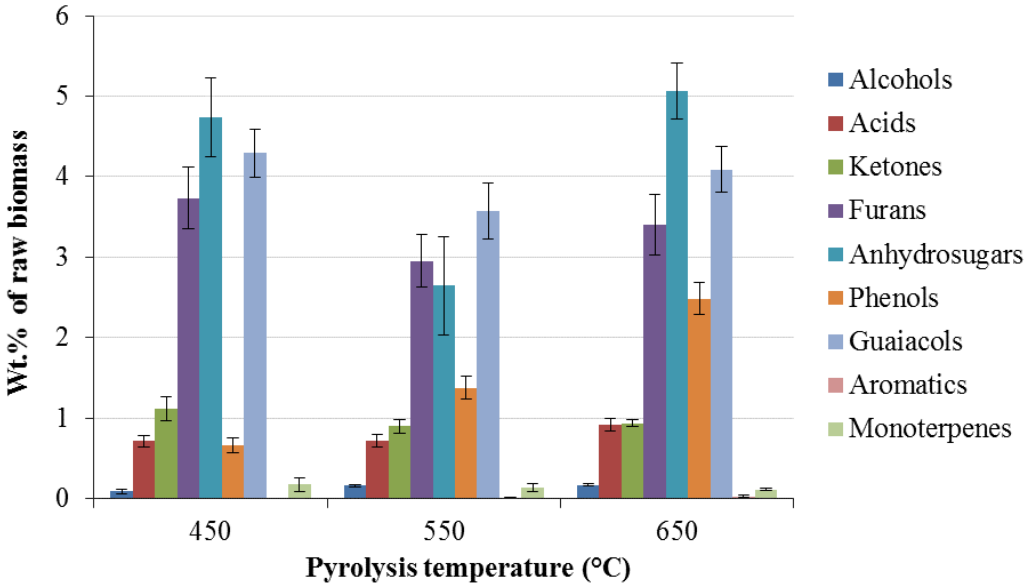

Figure 2.6 Yield of volatile components for BKLP3 at 450, 550, and 650 °C

The yield of total volatiles went through a minimum yield of 12.5 wt. % at 550 °C (Figure 2.5), which is mainly due to a minimum in the yield of anhydrosugars (Figure 2.6). As temperature increased from 450 °C to 650 °C, the yield of anhydrosugars first decreased from 4.7 wt. % to 2.6

wt. %, and then increased to 5.0 wt. % (Figure 2.6). The decrease of anhydrosugars yield from 450 °C to 550 °C may result from decomposition of some anhydrosugars into small molecules; while the increase of anhydrosugars yield from 550 °C to 650 °C could be due to the decomposition of larger oligomers that are not detectable by GC/MS at higher temperature. The effect of temperature on the yield of anhydrosugars is a controversial topic. Demirbas [31] found that the yield of levoglucosan decreased as pyrolysis temperature increased from 350-600 °C. Thangalazhy-Gopakumar et al. [32] reported that a maximum yield of levoglucosan was achieved at 450 °C for the fast pyrolysis of pine wood in an auger reactor. However, Thangalazhy Gopakumar et al. [33] also reported that for fast pyrolysis of pine wood using Py-GC/MS, the yield of levoglucosan and other anhydrosugars was not significantly affected as temperature increased from 450 °C to 750 °C. The discrepancies in the results of anhydrosugars could be explained as a combination of the following factors: (i) anhydrosugars, like levoglucosan, have a boiling point higher than 300 °C (the temperature of the transfer line), resulting in a tailed peak in total ion chromatograms that lowers the accuracy for its integration and quantification; (ii) some anhydrosugars are not commercially available and therefore their quantifications are based on estimates using similar standards like levoglucosan; and (iii) feedstock type, operation conditions, and reactor configurations are different in each study.

The effect of pyrolysis temperature on the yield of other types of compounds, including acids, ketones, furans, guaiacols, and monoterpenes, was not found to be significant (Figure 2.6). At each pyrolysis temperature, levoglucosan, 5-hydroxymethyfurfural and furfural were identified as the major products. As temperature increased from 450 °C to 650 °C, the yield of levoglucosan decreased from 2.8 wt. % to 1.3 wt. %, and then increased to 3.5 wt. %; the yield of 5-hydroxymethyfurfural decreased from 1.4 wt. % to a constant value of around 1.0 wt. %, and the

yield of furfural remained constant at 1.0 wt. %. In addition, a temperature range of 450 °C to 650 °C was found to have no significant effect on the elemental composition of volatile compounds. The average C, O, and H contents were calculated to be 59.2%, 34.5%, and 6.3%, corresponding to an HHV of 25.4 MJ/kg (Table 2.3).

Table 2.3 Elemental composition of non-catalytic and catalytic total identified compounds

Pyrolysis types	Conditions (Feedstock, T(°C))	Elemental percentage (%)		
		C	O	H
Non-catalytic	BKLP3, 450	58.25 ± 0.89	35.49 ± 0.96	6.27 ± 0.07
	LP, 550	59.23 ± 0.59	34.60 ± 0.66	6.17 ± 0.07
	BKLP1,550	59.33 ± 0.22	34.44 ± 0.26	6.23 ± 0.04
	BKLP2, 550	59.69 ± 1.25	34.01 ± 1.37	6.30 ± 0.12
	BKLP3, 550	60.35 ± 1.16	33.31 ± 1.30	6.34 ± 0.15
	BKLP3, 650	58.87 ± 1.48	34.83 ± 1.62	6.30 ± 0.14
CFP	LP, 550	89.27 ± 0.06	2.05 ± 0.06	8.68 ± 0.01
	BKLP3, 550	89.28 ± 0.15	2.04 ± 0.17	8.68 ± 0.02

2.4.3 Catalytic fast pyrolysis

LP and BKLP3 were used to investigate the effect of the BKLP decay stage on the performance of CFP at the catalyst-to-biomass ratio of 20 and the pyrolysis temperature of 550 °C. Instead of the oxygenated compounds produced from non-catalytic fast pyrolysis, most compounds obtained during CFP were hydrocarbons, such as benzene, toluene, xylenes, and naphthalenes. According to Figure 2.7, the BKLP decay stages had no significant influence on the yield of coke (4.5-4.6 wt. %), oxygenates (3.7-3.8 wt. %), and hydrocarbons (39.2-40.0 wt. %) in CFP. The category “others” in Figure 2.7 refers to the unidentified compounds such as non-volatiles and the undetected permanent gaseous products.

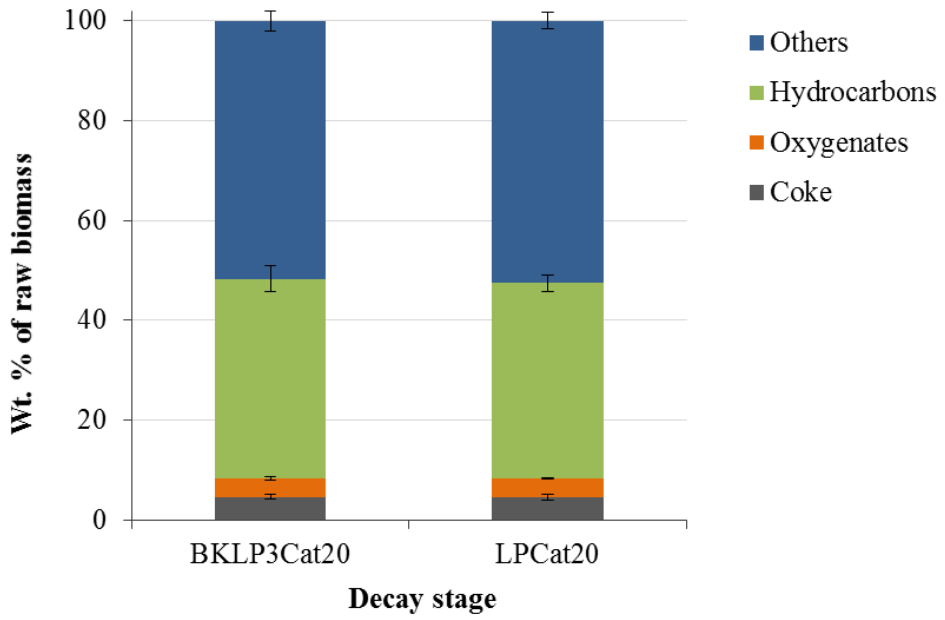

Figure 2.7 CFP products yield of LP and BKLP3 at the catalyst-to-biomass ratio of 20, and 550 °C

The selectivity to various hydrocarbon products is shown in Figure 2.8. No significant difference of hydrocarbon selectivity was visible between LP and BKLP3. Hydrocarbons with a carbon number of 7 or 8 (i. e. toluene, ethylbenzene, xylenes and styrene) are shown to be the most abundant products, and each of them had a selectivity of ca. 27%. The actual yield of toluene and xylenes was 10.7 wt. % and 8.9 wt. % of raw BKLP biomass, respectively. Toluene and xylenes produced in CFP are very important petrochemicals. Both of them can be added to motor gasoline to enhance the octane number. Furthermore, *para* and *ortho* xylenes are also important precursors for the production of plasticizers and polymers [34]. The lower selectivity to heavier hydrocarbons could be explained by their slower diffusions in HZSM-5 due to steric constraints [35, 36]. Results from Figure 2.7 and Figure 2.8 indicate that the decay stage did not affect the yield and composition of products for CFP, similar to what was observed for non-catalytic fast pyrolysis. Study of Wang et al. [26] has shown that product selectivity from catalytic pyrolysis of

lignocellulosic biomass highly depends on its composition. Thus, the equivalent compositions of the feedstocks as shown in Table 2.1 and Table 2.2 may partly explain the similar product selectivity here.

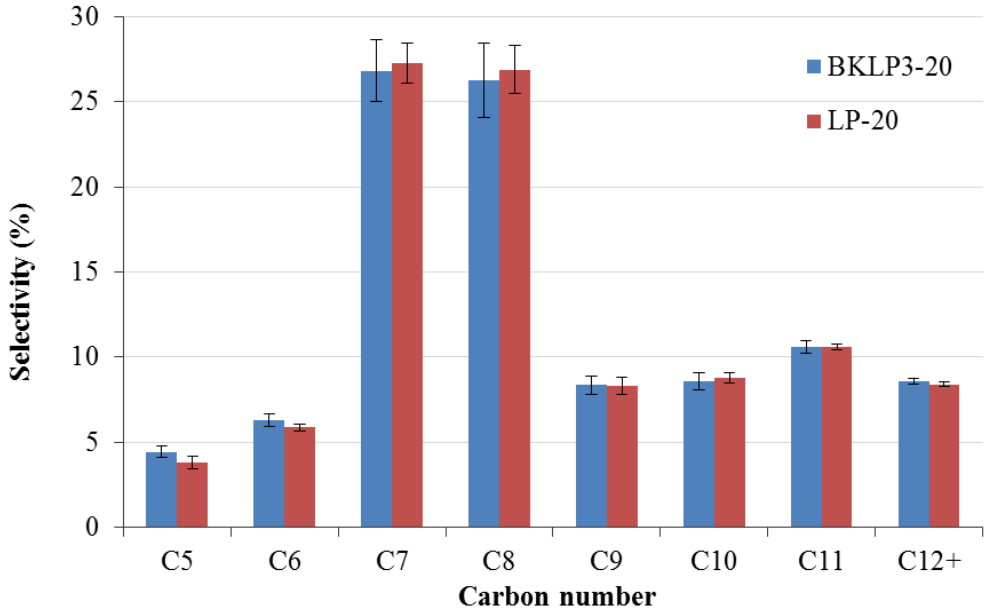

Figure 2.8 Selectivity of hydrocarbons from CFP of LP and BKLP3 at the catalyst-to-biomass ratio of 20, and 550 °C

2.4.4 Non-catalytic pyrolysis vs. catalytic pyrolysis

Both non-catalytic and catalytic fast pyrolysis processes were carried out on LP and BKLPs in this study. Generally, with increasing time-since-death, beetle-infested trees become less appropriate for solid wood and fiber wood products (e.g. pulp, oriented strand board, and particle board) manufacturing as a result of secondary decay [37]. Based on our results, nevertheless, the decay stages of lodgepole pine did not affect the quality of the products obtained from both non-catalytic and catalytic fast pyrolysis processes. This result suggests that even trees that have been dead for four years can be used for fuel and chemical production via fast pyrolysis. The major products for non-catalytic fast pyrolysis were found to be oxygenated compounds, but most of them were

converted into aromatic hydrocarbons during CFP, because the deoxygenation reactions occurred in the presence of an HZSM-5 catalyst. Table 2.3 shows the elemental composition of total identified products obtained from both processes. For non-catalytic fast pyrolysis, products derived from BKLP3 at 550 °C had the C, O, and H contents of 60.4%, 33.3%, and 6.3%, respectively, corresponding to an HHV of 26.0 MJ/kg. In the presence of HZSM-5, the C and H contents increased to 89.3% and 8.0%, respectively, while the O content decreased to 2.0%. Thus, products from CFP were found to have a much higher HHV of 40.9 MJ/kg, which is close to the HHV of commercial gasoline and diesel fuels (~45.5 MJ/kg). Additionally, less coke yield was observed for CFP (4.5-4.6 wt. %, Figure 7) compared to non-catalytic fast pyrolysis (14.3-16.6 wt. %, Figure 3). In CFP, there are two types of coke, namely, thermal coke (char) and catalytic coke. The term "coke" used in this study refers to the total carbonaceous residues formed in CFP, without distinguishing its thermal and catalytic origin. Williams and Nugranad [38] made a comparison of non-catalytic and catalytic fast pyrolysis of rice husks in a fluidized bed reactor. They found that the presence of HZSM-5 increased yield of total carbonaceous residues with higher yield of catalytic coke and lower yield of thermal coke. Zhang et al. [39] showed similar results when using corncob as feedstock in a fluidized-bed reactor. Ma et al. [40] investigated non-catalytic and catalytic fast pyrolysis of lignin using a pyroprobe. However, they found that CFP with HZSM-5/lignin ratio of 20 produced more char than that of non-catalytic fast pyrolysis, while CFP with higher HZSM-5/lignin ratios (i.e. 50 and 80) produced less char, compared to that in the absence of catalyst. It is evident, therefore, that the relative amount of total carbonaceous residues between non-catalytic and catalytic fast pyrolysis is a strong function of the catalyst-to-biomass ratio and the reactor configuration.

2.4.5 Availability of beetle-killed trees for fast pyrolysis

Our work has shown the potential to produce gasoline and commodity chemicals such as toluene and xylenes from beetle-killed trees. Around 42 million acres of conifer forests have been infested by bark beetles in the western United States since 1996 [1]. To do a conservative estimation, we assume that the infestation density is 40 trees per acre, the average tree height and diameter are 15 m and 30 cm, wood density is 0.4×10^3 kg/m^3, and the tree utilization percentage is 50 wt. %; therefore, the available mass of beetle-killed trees in the western United States for fast pyrolysis is around 356 million tons. According to the results above, around 142 million tons of hydrocarbons, 38 million tons of toluene, and 32 million tons of xylenes could be produced from current beetle-killed tree stocks in the western United States. If these hydrocarbons were used to produce drop-in fuels, 52 billion gallon fuels would be produced ($\rho_{gasoline}$ = 719.7 kg/m^3), which is about 39% of the annual gasoline consumption in the U. S. (~133 billion gallons). In addition, the estimated toluene production would be three times more than the current annual production of toluene from fossil fuels worldwide (~10 million tons) [18]. However, several factors are not taken into account in the estimate. For instance, the scale-up and reactor types may affect the product yield. The number of trees that will be infested in the future is also not included. Thus, this is only a rough conservative estimate aiming to provide an order of magnitude of the potential for the production of fuels and chemicals from existing beetle-killed trees via fast pyrolysis.

2.5 CONCLUSIONS

This study explored fast pyrolysis and CFP as a means to convert LP and BKLPs in three decay stages into biofuels and chemicals. Compared to LP, BKLPs have relatively higher extractives and lower lignin content due to the degradation of decay fungi. However, no practical differences of

non-catalytic and catalytic fast pyrolysis products yields and selectivity were observed between different decay-stage lodgepole pine samples. For non-catalytic fast pyrolysis, products had an HHV value of 25.4 MJ/kg. For CFP, products were found to have an HHV value of 40.9 MJ/kg, as well as a high selectivity to certain important petrochemicals like toluene and xylenes. Currently, beetle-killed trees that have been dead for a long time are underutilized in the solid wood and fiber wood product manufacturing. Our work indicates that both non-catalytic and catalytic fast pyrolysis are attractive ways to convert beetle-killed trees into high-value chemicals and fuels.

2.6 REFERENCES

[1] U.S. Forest Service, Western Bark Beetle Strategy for Human Safety, Recovery and Resiliency, 2011.

[2] Western Forestry Leadership Coalition (WFLC), Western Bark Beetle Assessment: A Framework for Cooperative Forest Stewardship, 2007.

[3] J.A. Hicke, M.C. Johnson, J.L. Hayes, H.K. Preisler, Effects of bark beetle-caused tree mortality on wildfire, Forest Ecol. Manag. 271 (2012) 81-90.

[4] R.D. Perlack, L.L. Wright, A.F. Turhollow, R.L. Graham, B.J. Stockes, D.C. Erbach, Biomass as feedstock for a bioenergy and bioproducts industry: The technical feasibility of a billion-ton annual supply, Oak Ridge Nation Laboratory, Oak Ridge, Tennessee, 2005.

[5] J.J. Kim, E.A. Allen, L.M. Humble, C. Breuil, Ophiostomatoid and basidiomycetous fungi associated with green, red, and grey lodgepole pines after mountain pine beetle (Dendroctonus ponderosae) infestation, Can. J. For. Res. 35 (2005) 274-284.

[6] R.W. Reid, Moisture changes in lodgepole pine before and after attack by the mountain pine beetle, For. Chron. 34 (1961) 368-375.

[7] K.L. Woo, P. Watson, S.D. Manfield, The effects of mountain pine beetle and associated blue staining fungi on wood morphology and chemistry, Paprican University Report 831, Paprican and Department of Wood Science, University of BC, Vancouver, BC, 2003.

[8] K.L. Lewis, I. Hartley, Rate of deterioration, degrade and fall of trees killed by mountain pine beetle: A synthesis of the literature and experiential knowledge, Mountain Pine Beetle Initiative Working Paper 2005-14, Natural Resources Canada, Canadian Forest Service, Victoria, BC, 2005.

[9] W.T. Tsai, M.K. Lee, Y.M. Chang, Fast pyrolysis of rice husk: Product yields and compositions, Bioresour. Technol. 98 (2007) 22-28.

[10] R.J.M. Westerhof, D.W.F. Brilman, M. Garcia-Perez, Z. Wang, S.R.G. Oudenhoven, S.R.A. Kersten, Stepwise fast pyrolysis of pine wood, Energy Fuel 26 (2012) 7263-7273.

[11] C.E. Greenhalf, D.J. Nowakowski, A.B. Harms, J.O. Titiloye, A.V. Bridgwater, A comparative study of straw, perennial grasses and hardwoods in terms of fast pyrolysis products, Fuel 108 (2013) 216-230.

[12] K. Wang, R.C. Brown, Catalytic pyrolysis of microalgae for production of aromatics and ammonia, Green Chem. 15 (2013) 675-681.

[13] K.H. Kim, T. Kim, S. Lee, D. Choi, H. Yeo, I. Choi, J.W. Choi, Comparison of physicochemical features of biooils and biochars produced from various woody biomasses by fast pyrolysis, Renew. Energ. 50 (2013) 188-195.

[14] A.P. Horne, P.T. Williams, The effect of zeolite HZSM-5 catalyst deactivation during the upgrading of biomass-derived pyrolysis vapors, J. Anal. Appl. Pyrolysis 34 (1995) 65-85.

[15] T.R. Carlson, T.P. Vispute, G.W. Huber, Green gasoline by catalytic fast pyrolysis of solid biomass derived compounds, ChemSusChem 1 (2008) 397-400.

[16] A.M. Azeez, D. Meier, J. Odermatt, T. Willner, Effects of zeolites on volatile products of beech wood using analytical pyrolysis, J. Anal. Appl. Pyrolysis 91 (2011) 296-302.

[17] H.W. Lee, T.H. Kim, S.H. Park, J. Jeon, D.J. Suh, Y. Park, Catalytic fast pyrolysis of lignin over mesoporous Y zeolite using Py-GC/MS, J. Nanosci. Nanotechnol. 13 (2013) 2640-2646.

[18] M. Zhang, F.L.P. Resende, A. Moutsoglou, Catalytic fast pyrolysis of aspen lignin via Py-GC/MS, Fuel 116 (2014) 358-369.

[19] B.H. Aukema, A.L. Carroll, J. Zhu, K.F. Raffa, T.A. Sickley, S.W. Taylor, Landscape level analysis of mountain pine beetle in British Columbia, Canada: Spatiotemporal development and spatial synchrony within the present outbreak, Ecography 29 (2006) 427-441.

[20] J. Sluiter, A. Sluiter, Summative Mass Closure – Laboratory Analytical Procedure Review and Integration. National Renewable Energy Laboratory, Golden, Colorado, 2011.

[21] P. Bicho, C. Woo, B. Dalpke, Quantifying the effects of extractives from mountain pine beetle-attacked lodgepole pine pulp and papermaking. Natural Resources Canada, Canadian Forest Service, Pacific Forestry Centre, Victoria, BC, Canada, 2008.

[22] K.L. Woo, P. Watson, S.D. Manfield, The effects of mountain pine beetle attack on lodgepole pine wood morphology and chemistry: Implications for wood and fiber quality, Wood Fiber Sci. 37 (2005) 112-126.

[23] G.M. Scott, D.W. Bormett, N.R. Sutherland, S. Abubakr, E. Lowell, Pulpability of beetle-killed spruce, United States Department of Agriculture Forest Products Laboratory, Madison, WI, 1996.

[24] R.A. Zabel, J.J. Morrell, Wood Microbiology: Decay and Its Prevention, Academic Press, Inc., New York, 1992.

[25] H. Yang, R. Yan, H. Chen, D.H. Lee, C. Zheng, Characteristics of hemicellulose, cellulose and lignin pyrolysis, Fuel 86 (2007)1781-1788.

[26] K. Wang, K.H. Kim, R.C. Brown, Catalytic pyrolysis of individual components of lignocellulosic biomass, Green Chem. 16 (2014) 727-735.

[27] P.R. Patwardhan, R.C. Brown, B.H. Shanks. Understanding the fast pyrolysis of lignin, ChemSuschem 4 (2011) 1629-1636.

[28] M. Garcia-Perez, X.S. Wang, J. Shen, M.J. Rhodes, F. Tian, W. Lee, H. Wu, C. Li, Fast pyrolysis of oil mallee woody biomass: Effect of temperature on the yield and quality of pyrolysis products, Ind. Eng. Chem. Res. 47 (2008) 1846-1854.

[29] S. Zhou, M. Garcia-Perez, B. Pecha, S.R.A. Kersten, A.G. McDonald, R.J.M. Westerhof, Effect of the fast pyrolysis temperature on the primary and secondary products of lignin, Energy Fuel 27 (2013) 5867-5877.

S. Şensöz, M. Can, Pyrolysis of pine (Pinus Brutia Ten.) chips: 1. Effect of pyrolysis temperature and heating rate on the product yields, Energ. Source 24 (2002) 347-355.

[30] R.J.M. Westerhof, D.W.F. Brillman, W.P.M. van Swaajj, S.R.A. Kersten, Effect of temperature in fluidized bed fast pyrolysis of biomass: Oil quality assessment in test units, Ind. Eng. Chem. Res. 49 (2010) 1160-1168.

[31] A. Demirbas, The influence of temperature on the yields of compounds existing in bio-oils obtained from biomass samples via pyrolysis, Fuel Process. Technol. 88 (2007) 591-597.

[32] S. Thangalazhy-Gopakumar, S. Adhikari, Ravindran H, R.B. Gupta, O. Fasina, M. Tu, S.D. Fernando, Physiochemical properties of bio-oil produced at various temperatures from pine wood using an auger reactor, Bioresour. Technol. 101 (2010) 8389-8395.

[33] S. Thangalazhy-Gopakumar, S. Adhikari, R.B. Gupta, S.D. Fernando, Influence of pyrolysis operating conditions on bio-oil components: A microscale study in a pyroprobe, Energy Fuel 25 (2011) 1191-1199.

[34] S. D. Barnicki, Chapter 10: Synthetic organic chemicals, in: J.A. Kent (Ed), Handbook of Industrial Chemistry and Biotechnology: Volume 1 and 2, Springer Science+Business Media, New York, 2012, pp. 318-320.

[35] M. Bjørgen, S. Svelle, F. Joensen, J. Nerlov, S. Kolboe, F. Bonino, L. Palumbo, S. Bordiga, U. Olsbye, Conversion of methanol to hydrocarbons over zeolite H-ZSM-5: On the origin of the olefinic species, J. Catal. 249 (2007) 195-207.

[36] G. Luo, A.G. McDonald, Conversion of methanol and glycerol into gasoline via ZSM-5 catalysis, Energy Fuel 28 (2014) 600-606.

[37] K.J. Lewis, L.D. Hartley, Rate of deterioration, degrade, and fall of trees killed by mountain pine beetle, JEM 7 (2006) 11-19.

[38] P.T. Williams, N. Nugranad, Comparison of products from the pyrolysis and catalytic pyrolysis of rice husks, Energy 25 (2000) 493-513.

[39] H. Zhang, R. Xiao, H. Huang, G. Xiao, Comparison of non-catalytic and catalytic fast pyrolysis of corncob in a fluidize bed reactor, Bioresour Technol 100 (2009) 1428-1434.

[40] Z. Ma, E. Troussard, J.A. van Bokhoven, Controlling the selectivity to chemicals from lignin via catalytic fast pyrolysis, Appl. Catal., A 423-424 (2012) 130-136.

CHAPTER 3. *IN-SITU* AND *EX-SITU* UPGRADING OF PYROLYSIS VAPORS FROM BEETLE-KILLED TREES[2]

3.1 ABSTRACT

In this article, we systematically studied the effects of several parameters on the product yield and selectivity for the *in-situ* and *ex-situ* upgrading of pyrolysis vapors from beetle-killed trees using a micro-pyrolyzer equipped with an online GC/MS-FID. HZSM-5 was used as catalyst for both processes. The *in-situ* upgrading was highly affected by the catalyst-to-biomass ratio. At the ratio of 10, the highest aromatic yield of 25% was obtained with the carbonaceous residues yield of 41%. For the *ex-situ* upgrading, the most important variable to affect the product yield is the secondary reactor temperature. The highest aromatic yield of 22% and lowest coke yield of 14% was achieved at the secondary reactor temperature of 600 °C. Alkylation and dealkylation of alkyl aromatics over HZSM-5 played an important role in determining product selectivity in both processes. Dealkylation reactions were favored at higher temperature and the alkylation reactions were promoted at lower temperature, which is consistent with the exothermic nature of alkylation. A direct comparison between the *in-situ* and *ex-situ* upgrading processes was made under identical conditions. The comparison shows largely similar yields of aromatic volatiles and solid residues between the two upgrading processes, with differences primarily on species selectivity. As a result of the alkylation/dealkylation reactions, the *in-situ* upgrading had higher selectivity to xylenes and aromatics with nine carbons, and the ex-situ upgrading exhibited higher selectivity to benzene and toluene.

[2] Published: G. Luo, F.L.P. Resende, In-situ and ex-situ upgrading of pyrolysis vapors from beetle-killed trees, Fuel, 166 (2016) 367-375.

3.2 INTRODUCTION

Bark beetles have infested more than 41.7 million acres of conifer forests in the Western United States since 1996. It is expected that the outbreak of bark beetles will continue to increase in the near future [1]. This bark beetle epidemic with high levels of tree mortality leads to high risk of wildfire hazard and falling trees, threatening the regional economics and public safety [2]. To minimize the negative impacts, beetle-killed trees need to be properly disposed of. When the bark beetle successfully attacks a tree, it also introduces a diversity of fungi into it. The fungal attack causes bluish discoloration, low moisture content, and checking (small cracks) in the wood, which significantly reduce the value of the infested wood in the solid wood market [3-5]. As the time-since-death increases, beetle-killed trees become even less appropriate for solid wood manufacturing due to the secondary decay [5]. Thus, our group has been carrying out fast pyrolysis to convert beetle-killed trees into a useful product: bio-oil [6].

The low moisture content of beetle-killed trees makes them an excellent feedstock for fast pyrolysis, since the costs of feedstock drying could be reduced or even eliminated. In our previous work [6], the effect of the degradation stage of beetle-killed trees on the performance of both non-catalytic and catalytic fast pyrolysis were investigated. We found that pyrolysis of beetle-killed trees that have been dead for up to four years led to similar product yield and quality compared to that of healthy trees, indicating that beetle-killed trees are a promising feedstock for fast pyrolysis. This is true for both catalytic and non-catalytic pyrolysis. Volatile products derived from non-catalytic fast pyrolysis were composed of various oxygenated compounds, resulting in a relatively low higher heating value (HHV) of 26 MJ/kg. In the presence of HZSM-5, most oxygenates were converted into aromatic hydrocarbons. Thus, the HHV of the volatile products from catalytic pyrolysis was upgraded to 41 MJ/kg, which is close to that of gasoline.

According to the contact method between the catalyst and pyrolysis vapors, the catalytic upgrading process can be classified into *in-situ* and *ex-situ*. In the *in-situ* upgrading, which is also known as catalytic fast pyrolysis, the catalyst is mixed with the biomass feedstock [7-13]. Biomass pyrolysis and pyrolysis vapor upgrading take place in the same reactor for the in-situ upgrading, thus likely reducing the capital and operating costs [14]. In the *ex-situ* upgrading, the catalyst is placed separately from the biomass feedstock in a secondary reactor [13, 15]. Compared to the *in-situ* upgrading, the *ex-situ* upgrading provides more control and flexibility to the system. Pyrolysis conditions and catalytic performance could be individually optimized in the *ex-situ* upgrading [15, 16]. Moreover, multiple serial catalyst beds could apply on the *ex-situ* configuration if necessary [16]. To date, limited research on direct comparison between *in-situ* and *ex-situ* upgrading has been reported. Yildiz et al. [17] compared *in-situ* and *ex-situ* upgrading of pyrolysis vapors from pine wood using HZSM-5 as a catalyst in a continuously operated auger reactor. Similar product yield was observed for the *in-situ* and *ex-situ* upgrading. Compared to the *ex-situ* upgrade, however, the *in-situ* upgrading produced more phenolic and aromatic compounds with less acids and anhydrosugars. Wang et al. [18] recently reported a comparison between *in-situ* and *ex-situ* upgrading for hybrid polar and dried distillers grains with solubles (DDGS). They concluded that *in-situ* upgrading promoted formation of aromatics, and *ex-situ* upgrading promoted the formation of olefins. Gamliel et al. [19] also performed a comparison between *in-situ* and *ex-situ* catalytic fast pyrolysis (CFP) of miscanthus x giganteus using Py-GC/MS. These results were compared with those from the *in-situ* CFP in a spouted-bed reactor as well. They found that the *ex-situ* CFP resulted in more permanent gas and aromatics in the bio-oil than *in-situ* CFP, and the results from Py-GC/MS *ex-situ* configuration more closely resembled those of the spouted-bed reactor. In a recent review of *ex-situ* upgrading, Wan and Wang [16] pointed out a serious lack of systematic

research for comparison of *in-situ* and *ex-situ* upgrading. The present paper addresses this need by reporting a systematic study over a wide range of reaction parameters (e.g. pyrolysis temperature, secondary reactor temperature, and biomass-to-catalyst ratio) for both *in-situ* and *ex-situ* upgrading, and by comparing results from *in-situ* and *ex-situ* upgrading under identical conditions. The results also allow us to discuss the effect of alkylation/dealkylation reactions on aromatics selectivity, and their corresponding effect on the *in-situ* and *ex-situ* upgrading processes.

Our motivation for comparing the *in-situ* and *ex-situ* upgrading stems from the potential use of mobile units for the pyrolysis of beetle-killed trees. The cost of producing bio-oil from forest residues such as beetle-killed trees is associated with harvesting and transportation of solid biomass. Handling solid forms of biomass is expensive, because of the long distance to conversion facilities, numerous required operations, and the low bulk density of biomass [20, 21]. Depending on the moisture content of woody biomass, the energy density of bio-oil is 6 to 7 times higher than that of green wood chips [21-24]. Wright [25] made a techno-economic analyses of biofuel technologies and reported that the transportation costs per mile of bio-oil were only 20% of that for transporting raw biomass. Using mobile pyrolysis units to convert woody biomass on-site will eliminate the need of transporting the low-value woody biomass over long distances. To upgrade pyrolysis vapors with a mobile unit, *ex-situ* upgrading may be more appropriate for some reactor configurations, like auger and ablative reactors. It is therefore important to understand the differences between *in-situ* and *ex-situ* upgrading. In this study, a systematic comparison of the *in-situ* and *ex-situ* upgrading of pyrolysis vapors from beetle-killed lodgepole pine over a wide range of reaction conditions was performed using a micro-pyrolyzer.

3.3 MATERIALS AND METHODS

3.3.1 Materials

Beetle-killed lodgepole pine (*Pinus contorta*) Crumbles® (2 mm × 2 mm) that were from standing dead trees without needles, and 2-4 years after death, were purchased from Forest Concepts, LLC. To be used as feedstock, these wood Crumbles® were ground into a particle size of less than 200 mesh (74 μm) using a ball mill. The elemental and chemical composition of the beetle-killed lodgepole pine is listed in Table 3.1 [6]. The catalyst used in this study was CBV2314 ZSM-5 (Zeolyst International, SiO_2/Al_2O_3 = 23) in the form of ammonium salt. Prior to use, ZSM-5 was calcined at 600 °C for 5 h, converting into the acid form, HZSM-5. Aromatic standards were purchased from Sigma Aldrich and Fisher Scientific and used as received.

Table 3.1 Elemental and chemical composition of beetle-killed lodgepole pine feedstock

Elemental composition (wt. %)	
C	49.62
O[a]	43.29
H	6.37
N	0.44
Chemical composition (wt. %)	
Moisture[b]	4.85
Ash[b]	0.26
Extractive[b]	5.48
Klason lignin[c]	28.53
Acid-soluble lignin[c]	0.31
Carbohydrates[c]	
Glucose	38.96
Mannose	9.59
Xylose	6.80
Galactose	3.84

Arabinose	1.99

a. O% was measured with O-mode using an elemental analyzer (Series II 2400, PerkinElmer)
b. wt.% of oven dry wood
c. wt.% of oven dry extractive-free wood

3.3.2 Methods

A commercial micro-pyrolyzer (Pyroprobe model 5200, CDS Analytical Inc.) was used for fast pyrolysis and pyrolysis vapor upgrading experiments. The pyroprobe contains two reactors in series. The first reactor (denoted "pyrolysis reactor") is an open-ended quartz tube (25 mm × 1.9 mm I.D.) heated by a platinum coil. The second one is a stainless steel reactor (155 mm × 4 mm I.D., denoted "secondary reactor") surrounded by a tubular heater in coil form. The temperature of these two reactors can be independently controlled. The actual temperatures of the first and secondary reactors are lower than the temperatures of the heating elements. The temperature reported in this study is the set-up heating element temperature. The interface between the two reactors and the transfer line between the pyrolyzer and gas chromatograph were maintained at the CDS recommended maximum temperature of 300 °C, minimizing the condensation of the product vapors. Helium was used as carrier gas in this system. The vaporized products were first swept into a trap at 50 °C, in which volatiles condensed while non-condensable gases vented out. The trap was then heated up to 300 °C, vaporizing the volatiles and then sending them to the GC for detailed compositional analysis. This is referred to as "trap mode" and is one of the differences between the experiments reported here and those from our previous work [6], when the volatiles were sent directly to the GC (py-mode). The trap mode may lead to some losses of product vapors. However, preliminary experiments comparing py-mode and trap mode indicate that losses in the trap mode are in trace amounts. The trap mode was originally designed to allow for runs at high

pressure or with a reactant gas, but it is also a component of the system for any runs including the secondary reactor. In order to make direct comparisons between *in-situ* and *ex-situ* upgrading possible, all experiments reported here were performed under trap mode. Due to the limitations of the experimental setup and GC technique, the permanent gases and non-volatiles at 300 °C cannot be measured and are not reported in this study. According to the literature, non-condensable gases typically correspond to a carbon yield of 20-30% [18, 19].

As illustrated in Figure 3.1, for the *in-situ* pyrolysis vapor upgrading, 0.5 mg of beetle-killed lodgepole pine sample was mixed with HZSM-5 and loaded in the pyrolysis reactor while the secondary reactor was empty. For the *ex-situ* upgrading, 0.5 mg of beetle-killed lodgepole pine sample was pyrolyzed in the pyrolysis reactor. The pyrolysis vapors were then sent to the secondary reactor containing HZSM-5. Different pyrolysis temperatures (500, 600, and 700 °C), secondary reactor temperatures (300, 400, 500, 600, and 700 °C), and catalyst-to-biomass ratios (5, 10, 20, and 40) were tested for both *in-situ* and *ex-situ* upgrading.

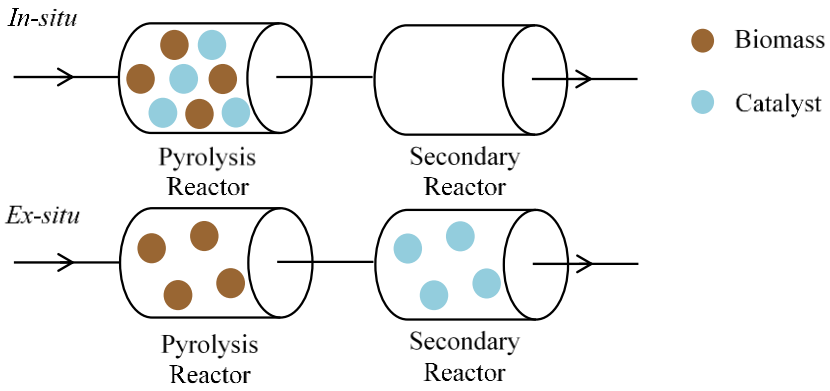

Figure 3.1 Reactor setup for the *in-situ* and *ex-situ* upgrading

Volatile products were analyzed by a gas chromatograph (GC, 2010 Plus, Shimadzu) equipped with a mass spectrometer (MS, QP2010, Ultra, Shimadzu) and a flame ionization

detector (FID, Shimadzu). To separate the volatile compounds, a capillary column, SHRXI-5MS (30 m × 0.25 mm I.D. × 0.25 μm film thickness, Shimadzu) was used. The GC inlet was kept at 300 °C and the inlet split ratio was 250: 1. The GC oven temperature program was started with an isothermal step of 4 min at 40 °C followed by a ramp of 10 °C/min up to a final temperature of 300 °C that was then held constant for 5 min. The mass spectra were recorded using the electron ionization mode over a mass per charge (m/z) range of 45-550. Identification of compounds was achieved by mass spectra comparison with NIST 2010 library and quantification of those compounds was obtained with an FID using external calibration standards. Fifteen standards were used to quantify twenty-nine compounds, since some compounds were quantified by isomers or compounds with similar structures. For all upgrading experiments reported in this work, the volatiles identified and quantified mainly consist of aromatic hydrocarbons. Peaks representing oxygenates were too small for quantification and were neglected. The HHV of all the aromatic hydrocarbons that can be detected by GC/MS-FID was calculated based on the following equation [26]:

$$HHV(MJ/kg) = 0.3491\ C\% + 1.1783\ H\% + 0.1005\ S\% - 0.1034\ O\% - 0.0151\ N\% - 0.0211\ Ash\% \quad (3.1)$$

The HHVs calculated here are only representative of the detectable aromatic volatiles; whereas water and other non-detectable compounds are not included in this estimate.

In this study, char was defined as carbonaceous residues derived from fast pyrolysis of biomass, and coke was defined as carbonaceous residues deposited on HZSM-5. The carbon content in the carbonaceous residues including both char and coke was quantified using an elemental analyzer (Series II 2400, PerkinElmer). For the in-situ upgrading, char and coke could not be separated, since biomass and HZSM-5 were mixed together. For the ex-situ upgrading, char

was generated in the pyrolysis reactor and the coke deposited on HZSM-5 in the secondary reactor. They were quantified separately.

All measurements mentioned above were performed in triplicates to verify the reproducibility of the data. We report averages and error bars that represent standard deviations. The yield of aromatic volatiles (29 quantified aromatic hydrocarbons) and carbonaceous residues was expressed as carbon yield, defined as the mass ratio of carbon in the specific product to the carbon in the original biomass, namely, beetle-killed lodgepole pine. The aromatic selectivity was calculated as the ratio of mass of the aromatics with certain carbon number to the total mass of all the quantified aromatics.

3.4 RESULTS AND DISCUSSION

3.4.1 Effect of pyrolysis temperature

3.4.1.1 In-situ upgrading

Figure 3.2 shows the carbon yield of the products as a function of pyrolysis temperature (pyrolysis reactor) for the *in-situ* upgrading. In this experiment, 0.5 mg of beetle-killed lodgepole pine sample was used. We varied the pyrolysis temperature from 500 °C to 700 °C and kept the secondary reactor temperature at 300 °C. The catalyst-to-biomass ratio was 10. The carbon yield of aromatic volatiles slightly increased from 21% to 25% as the pyrolysis temperature increased from 500 °C to 600 °C and remained unchanged at the pyrolysis temperature of 700 °C. The carbon yield of carbonaceous residues (which include pyrolysis char and coke deposited on HZSM-5 catalyst) decreased from 47% to 36% as the pyrolysis temperature increased from 500 °C to 700 °C. A similar tendency was also observed by Wang and his coworker on the catalytic fast pyrolysis of microalgae with a micro-pyrolyzer [27]. They observed that the carbon yield of aromatics

increased from 18% to 23%, and the carbon yield of solid residues decreased from 44% to 34% as the pyrolysis temperature increased from 500 °C to 700 °C. The increase in the temperature of non-catalytic fast pyrolysis promotes the thermal decomposition of biomass, in particular the lignin fraction, resulting in higher yields of low molecular weight species, with low yield of pyrolysis char [28-31]. The small molecules are easier to diffuse into the pores of HZSM-5 to produce desirable hydrocarbons and less coke [32]. Thus, the decrease in the yield of carbonaceous residues with the increasing pyrolysis temperature in Figure 3.2 may be related to the decrease in both pyrolysis char and catalytic coke. The formation of small oxygenated molecules produced at higher pyrolysis temperature favors the formation of aromatic volatiles. On the other hand, high temperature also favors the formation of permanent gases, consuming carbon that otherwise could end up as aromatics [29, 33]. We hypothesize that this is the reason why the carbon yield of aromatic volatiles does not increase substantially with increasing pyrolysis temperature.

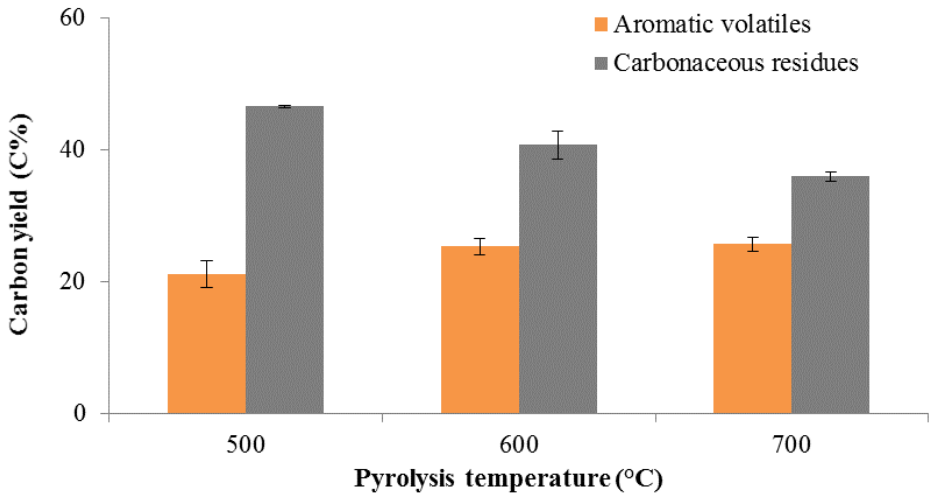

Figure 3.2 Product yields as a function of pyrolysis temperature for the *in-situ* upgrading (biomass loading: 0.5 mg, catalyst-to-biomass ratio: 10, secondary reactor temperature: 300 °C)

The aromatic selectivity as a function of the pyrolysis temperature is shown in Figure 3.3. At all the pyrolysis temperatures, toluene (C7) and xylenes (C8) are the major components in the aromatic volatiles with a selectivity of 24-30%. As the pyrolysis temperature increased, the selectivity to benzene (C6) and toluene (C7) slightly increased and the selectivity to xylenes and aromatics with a carbon number of nine (C9) slightly decreased. The results suggest the increase in the dealkylation rates of heavier aromatics at higher temperature, consuming xylenes, trimethylbenzenes, and methylethylbenzenes, and producing additional benzene and toluene. Carlson et al. [11] studied the catalytic fast pyrolysis of glucose and found a similar tendency. As pyrolysis temperature increased from 400 °C to 800 °C, the selectivity to benzene increased while the selectivity to xylenes and other heavier aromatics slightly decreased [11].

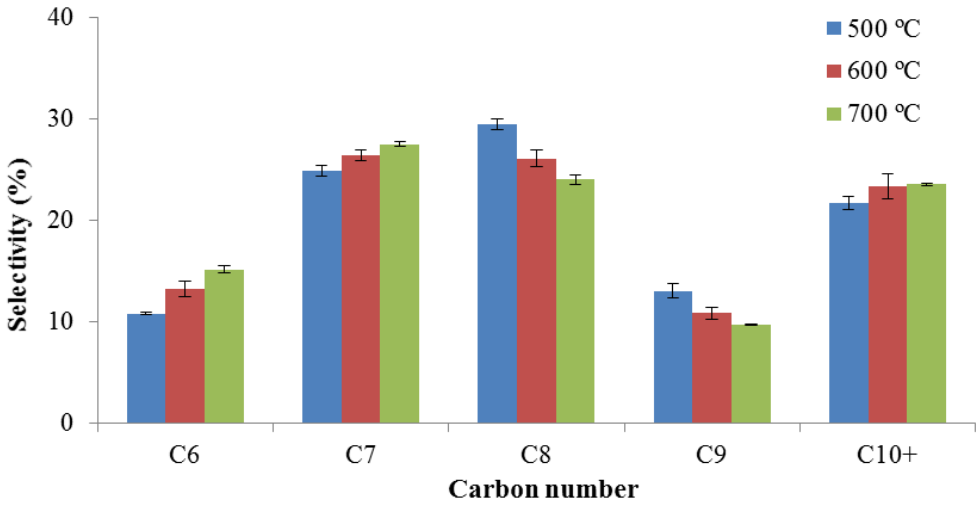

Figure 3.3 Aromatic selectivity as a function of pyrolysis temperature for the *in-situ* upgrading (biomass loading: 0.5 mg, catalyst-to-biomass ratio: 10, secondary reactor temperature: 300 °C; C6: benzene, C7: toluene, C8: ethylbenzene, and xylenes; C9: trimethylbenzenes, indane, and indene, etc., C10+: methylindenes, naphthalenes, and higher aromatics with a carbon number up to 15)

3.4.1.2 Ex-situ upgrading

Figure 3.4 shows the carbon yield of the products as a function of pyrolysis temperature (pyrolysis reactor) for the *ex-situ* upgrading. In this experiment, 0.5 mg of biomass was placed in the first reactor and 10 mg of HZSM-5 catalyst were located separately from biomass in the secondary reactor, resulting in a catalyst-to-biomass ratio of 20. The pyrolysis temperature was varied from 500 °C to 700 °C and the secondary reactor temperature was kept at 600 °C. As the pyrolysis temperature increased from 500 °C to 700 °C, the carbon yield of pyrolysis char decreased from 27% to 17%. Similar to the *in-situ* upgrading, this trend may be a result of the higher rate of biomass decomposition at higher pyrolysis temperature [28, 29]. Taking the standard deviation into consideration, the pyrolysis temperature did not significantly affect the carbon yield of aromatic volatiles. At all pyrolysis temperatures, the yield was around 21%. As explained for the in-situ upgrading, the aromatic yield was a result of two counteracting processes. The increase in the pyrolysis temperature promotes simultaneous increases in the yield of light oxygenates (e.g. small acids, alcohols, and aldehydes) and non-condensable gases [28, 29]. Light oxygenates with small molecular size are easy to diffuse into the pores of HZSM-5, enhancing the formation of aromatics [32, 34]. On the other hand, volatiles can further decompose at higher temperatures, producing non-condensable gases. In addition, the carbon yield of coke remained almost unchanged as the pyrolysis temperature increased. It is possible that the increase in light oxygenates that resulted from higher pyrolysis temperature were not enough to significantly reduce the coke formation on HZSM-5. In Figure 3.5, it can be observed that the pyrolysis temperature did not significantly affect the aromatic selectivity, since the secondary reactor temperature was kept constant. All temperatures showed high selectivity to benzene and toluene of around 28% and 32%, respectively.

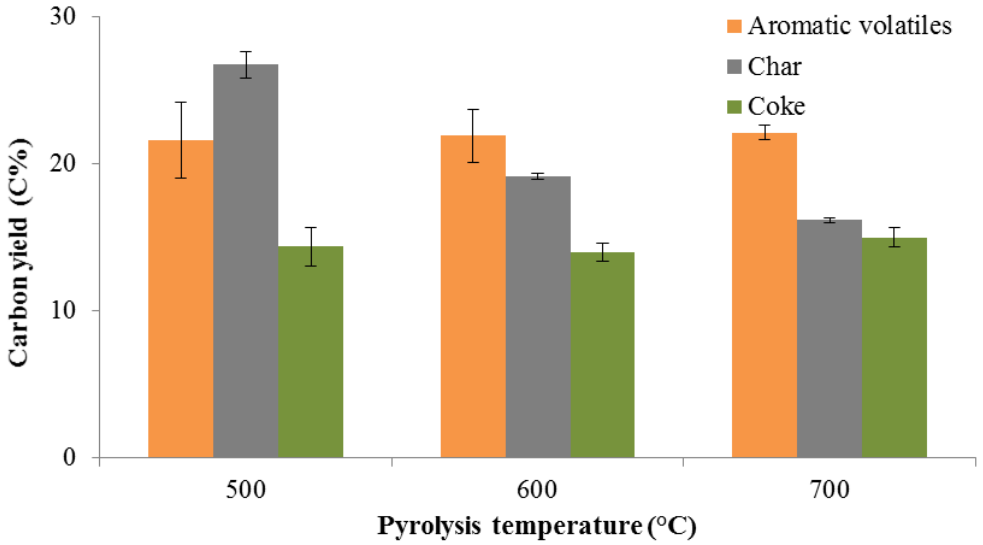

Figure 3.4 Product yields as a function of pyrolysis temperature for the *ex-situ* upgrading (biomass loading: 0.5 mg, catalyst-to-biomass ratio: 20, secondary reactor temperature: 600 °C)

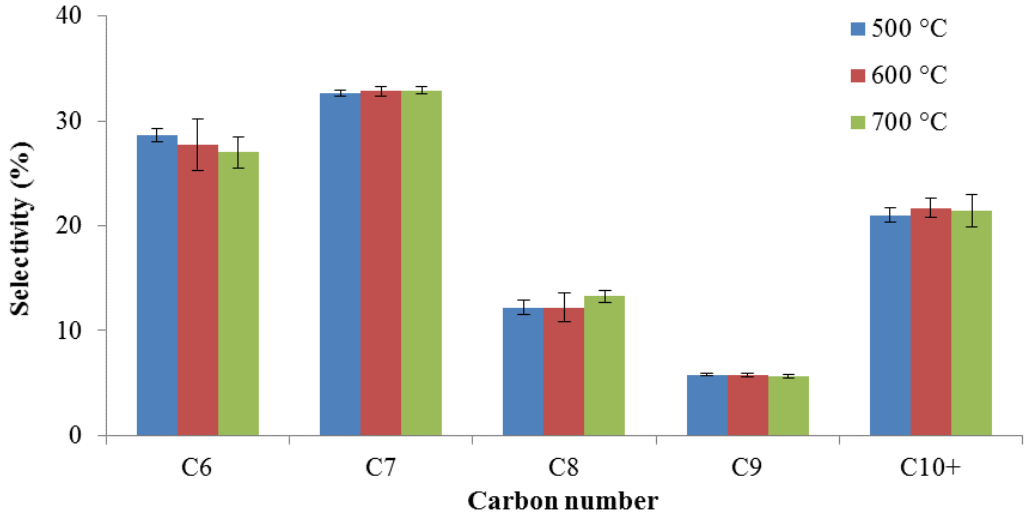

Figure 3.5 Aromatic selectivity as a function of pyrolysis temperature for the *ex-situ* upgrading (biomass loading: 0.5 mg, catalyst-to-biomass ratio: 20, secondary reactor temperature: 600 °C; C6: benzene, C7: toluene, C8: ethylbenzene, and xylenes; C9: trimethylbenzenes, indane, and indene, etc., C10+: methylindenes, naphthalenes, and higher aromatics with a carbon number up to 15)

3.4.2 Effect of secondary reactor temperature

3.4.2.1 In-situ upgrading

To investigate the effect of secondary reactor temperature on the performance of *in-situ* upgrading, we varied the secondary reactor temperature from 300 °C to 700 °C. 0.5 mg of beetle-killed lodgepole pine sample was used. The pyrolysis temperature was 600 °C and the catalyst-to-biomass ratio was 10. Though the secondary reactor was empty for the *in-situ* upgrading, we had anticipated that a high temperature in this reactor might cause cracking of aromatic volatiles. We observed, however, that the product yields did not change as the secondary reactor temperature increased from 300 °C to 700 °C (Table 3.2). At all temperatures, the carbon yield of aromatics was around 25% and the yield of carbonaceous residues was around 41%. The selectivity to aromatic volatiles also remained unchanged with a high selectivity to toluene (~26%) and xylenes (~26%) in this wide range of secondary reactor temperature. We hypothesize that the heat transfer rates from the wall of the empty tube (155 mm long) to the aromatic vapors were not high enough to cause the vapors to crack (the temperature of this reactor was measured at the outside of the wall).

Table 3.2 Product yields and aromatic selectivity as a function of the secondary reactor temperature for the *in-situ* upgrading (biomass loading: 0.5 mg, catalyst-to-biomass ratio: 10, pyrolysis temperature: 600 °C)

2^{nd} reactor temperature/ C°	300	400	500	600	700
Product yield/ C%					
Volatiles	25.30±1.29	25.92±2.82	25.45±1.26	24.97±0.21	24.60±1.99
Carbonaceous residues	40.71±2.05	42.27±3.05	42.82±1.19	40.60±0.73	41.81±1.26
Aromatic selectivity/ %					
Benzene	13.28±0.75	12.45±1.10	12.12±1.07	13.79±1.08	14.76±1.59
Toluene	26.42±0.55	25.58±0.42	25.80±0.78	27.03±0.78	27.72±0.50

Ethylbenzene and xylenes	26.11±0.83	26.87±1.71	27.53±1.84	27.25±1.10	26.62±3.36
C9 aromatics [a]	10.85±0.58	11.52±0.42	11.66±0.99	10.01±0.93	9.23±0.31
C10+ aromatics [b]	23.37±1.19	23.60±1.08	22.92±1.24	21.92±1.48	21.71±1.63

a. C9 aromatics include trimethylbenzenes, indane, and indene
b. C10+ aromatics include methylindenes, naphthalenes, and higher polyaromatics with a carbon number up to 15

3.4.2.2 Ex-situ upgrading

The effect of secondary reactor temperature on the performance of *ex-situ* upgrading was also studied, varying the secondary reactor temperature from 300 °C to 700 °C. The pyrolysis temperature was 600 °C. 0.5 mg of biomass feedstock and 10 mg catalyst were used, resulting in a catalyst-to-biomass ratio of 20. Unlike the *in-situ* upgrading, the product yields for the *ex-situ* upgrading were significantly affected by the secondary reactor temperature. According to Figure 3.6, the carbon yield of pyrolysis char was around 19% and remained unchanged with the increase in the secondary reactor temperature, which is expected since the char yield is mainly affected by the pyrolysis temperature here. As the secondary reactor temperature increased from 300 °C to 600 °C, the carbon yield of aromatic volatiles dramatically increased from 3% to 22%, while the carbon yield of coke decreased from 45% to 14%. When the secondary reactor temperature was further increased to 700 °C, the carbon yield of aromatics decreased to 14% and the coke yield did not change. Similar temperature behavior has been reported for the conversion of bio-oil model compounds over HZSM-5. Cheng and Huber [35] studied the temperature effect on furan conversion over HZSM-5. They found that high temperature of 600 °C favored the formation of aromatics and lowered the coke formation. When the temperature further increased to 650 °C, the yield of aromatics started decreasing and the yield of olefins was enhanced. The yield of CO and CO_2 increased constantly from 6.7 % to 19.0% as the temperature increased from 450 °C to 650

°C. The conversion of anisole into aromatics via HZSM-5 was also found to be favorable at high temperature of 550 °C [36, 37]. The pyrolysis vapors from beetle-killed lodgepole pine in the absence of catalyst are mainly composed of alcohols, furans, ketones, phenols, guaiacols, and anhydrosugars. The selectivity to furans, phenols, and guaiacols was as high as 60-70% [6]. Many different reactions, such as dehydration, decarboxylation, decarbonylation, alkylation, and cracking occurred for the conversion of these compounds inside HZSM-5. Decarbonylation of furan and benzofuran that is a product of furan Diels-Alder condensation is an essential step to convert furans into olefins and aromatics [35]. This decarbonylation reaction is thermodynamically favorable at high temperatures, such as 600 °C [35]. Aromatics are generated from phenols via decarboxylation, which also occurs at high temperature [37]. This is the reason why the carbon yield of aromatic volatiles increased dramatically as the secondary reactor temperature increased from 300 °C to 600 °C. However, at even higher temperature, such as 700 °C, the decomposition of oxygenated volatiles that are the carbon sources for the formation of aromatic volatiles may be promoted to produce more permanent gases.

The secondary reactor temperature also had a significant impact on the aromatic selectivity, as shown in Figure 3.7. At 300 °C, the selectivity to benzene is 31% and to toluene is 34%. The yield of aromatic volatiles at 300 °C was only around 3%; therefore, the aromatic selectivity at 300 °C is less relevant than those at higher temperatures. As the temperature increased from 400 °C to 700 °C, the selectivity to benzene increased from 15% to 42% while the selectivity to C8 and C9 decreased. The selectivity to toluene increased first to a maximum value at 600 °C and then decreased at 700 °C. Dealkylation of alkyl aromatics is favorable at high temperature, consuming heavier aromatics like trimethylbenzenes, ethylmethylbenzenes, and xylenes and producing additional less substituted aromatics like benzene and toluene [38, 39]. The selectivity

to toluene decreased at 700 °C because the dealkylation of toluene might occur at that temperature, producing benzene. The selectivity to naphthalenes and even higher aromatics was kept almost unchanged within the wide temperature range.

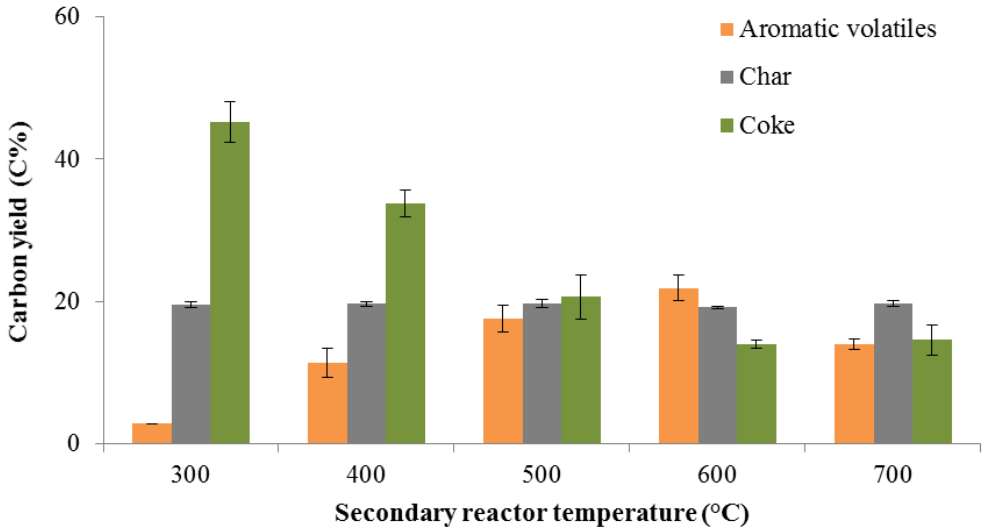

Figure 3.6 Product yields as a function of secondary temperature for the *ex-situ* upgrading (biomass loading: 0.5 mg, catalyst-to-biomass ratio: 20, pyrolysis temperature: 600 °C)

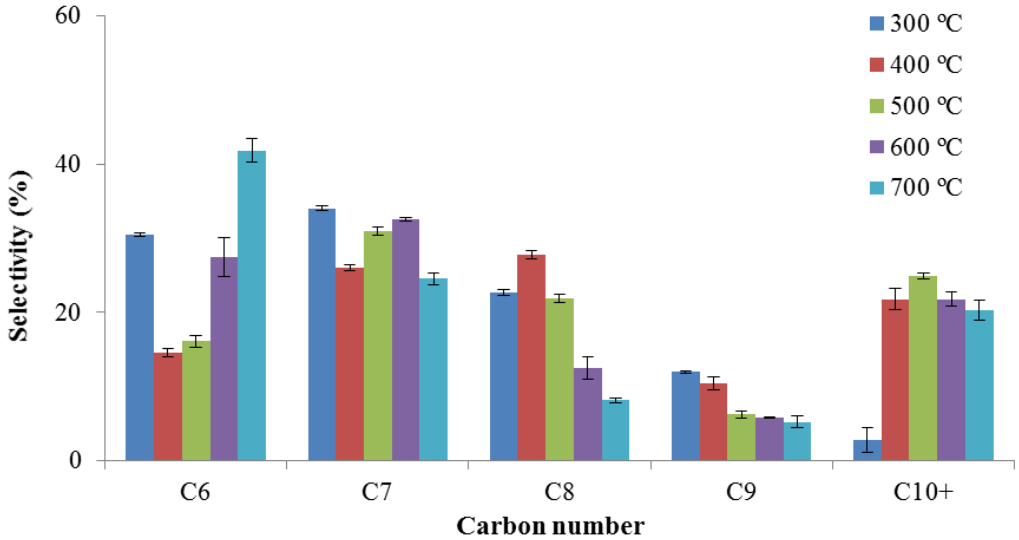

Figure 3.7 Aromatic selectivity as a function of secondary temperature for the *ex-situ* upgrading (biomass loading: 0.5 mg, catalyst-to-biomass ratio: 20, pyrolysis temperature:

600 °C; C6: benzene, C7: toluene, C8: ethylbenzene, and xylenes; C9: trimethylbenzenes, indane, and indene, etc., C10+: methylindenes, naphthalenes, and higher aromatics with a carbon number up to 15)

3.4.3 Effect of the catalyst-to-biomass ratio

3.4.3.1 In-situ upgrading

The catalyst-to-biomass ratios used were 5, 10, 20, and 40. The effects were tested using 0.5 mg beetle-killed lodgepole pine sample and varying the mass of catalyst. The pyrolysis and secondary reactor temperature were 600 °C and 300 °C, respectively. Figure 3.8 shows the product yield as a function of catalyst-to-biomass ratio for the *in-situ* upgrading. As the catalyst-to-biomass ratio increased from 5 to 10, the carbon yield of aromatic volatiles increased from 17% to 25%. However, when the catalyst-to-biomass ratio further increased to 20, the carbon yield of volatiles decreased to 18% and remained unchanged at the ratio of 40. The carbon yield of carbonaceous residues also decreased initially and then increased with increasing catalyst-to-biomass ratio. The minimum carbonaceous residues yield of 41% was obtained at the catalyst-to-biomass ratio of 10. When the catalyst-to-biomass ratio increased from 5 to 10, the exposed active sites of HZSM-5 increased, leading to a higher yield of aromatic volatiles and lower yield of coke. Since the same amount of biomass (0.5 mg) was used for all the tests, the total amount of material in the small pyrolysis quartz tube was much larger for the catalyst-to-biomass ratios of 20 and 40. Thus, the lower yield of aromatics and higher yield of carbonaceous residues at the ratios of 20 and 40 may have resulted from higher resistances to heat and mass transfer. Slow diffusion rates of volatiles and lower temperatures promoted the secondary reactions that produce more solid residues. A similar effect of the catalyst-to-biomass ratio on the product yield has also been reported in the literature. Zhang et al. [40] investigated the effect of the catalyst-to-biomass ratio on the catalytic

pyrolysis of lignin. They found that the aromatic yield increased from 6 wt. % to 21 wt.% as the catalyst-to-lignin ratio increased from 1 to 3. Further increase of the HZSM-5 catalyst loading in turn decreased the aromatic production.

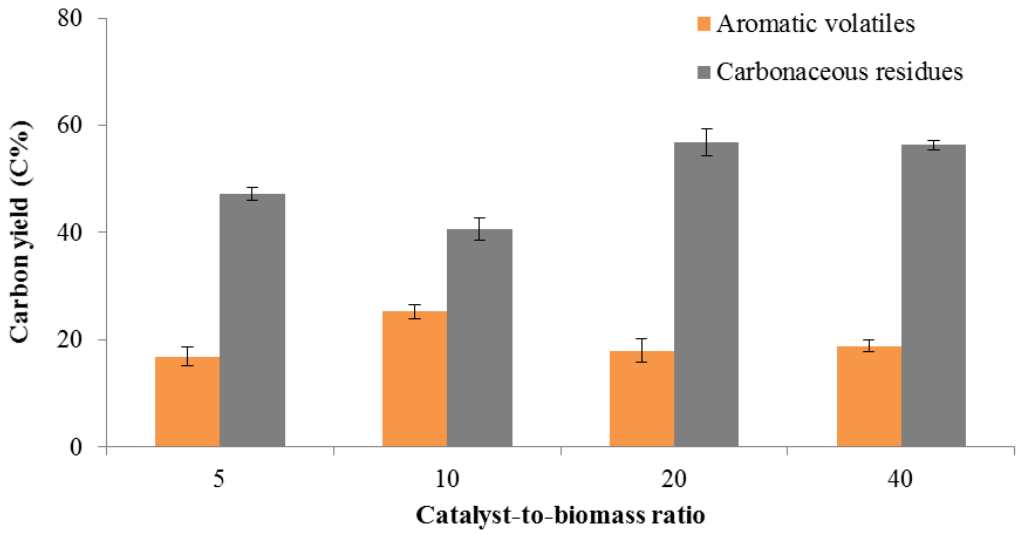

Figure 3.8 Product yields as a function of the catalyst-to-biomass ratio for the *in-situ* upgrading (biomass loading: 0.5 mg, pyrolysis temperature: 600 °C, secondary reactor temperature: 300 °C)

Figure 3.9 shows the aromatic selectivity as a function of the catalyst-to-biomass ratio. As catalyst-to-biomass ratio increased, the selectivity to benzene, toluene, and xylenes slightly increased and the selectivity to higher aromatics like those with carbon number of nine and larger decreased. Indene (C9) and methylindenes (C10) were observed to be consumed. We hypothesize that longer residence times resulted from the higher catalyst-to-biomass ratio, and that promoted the secondary reactions/polymerization of indene and methylindenes to form coke on the catalyst surface. In addition, because of the increase in heat and mass transfer limitations, it is possible that the volatiles were exposed to lower temperatures inside the catalyst pores of the zeolite, which

would promote alkylation reactions. This is consistent with the observation that the increase in C7 and C8 was larger than the increase in C6, as shown in Figure 3.9. Thus, the overall selectivity of aromatic volatiles did not change dramatically with increasing catalyst-to-biomass ratios. Our results are also consistent with the study on catalytic fast pyrolysis of glucose conducted by Carlson et al. [11].

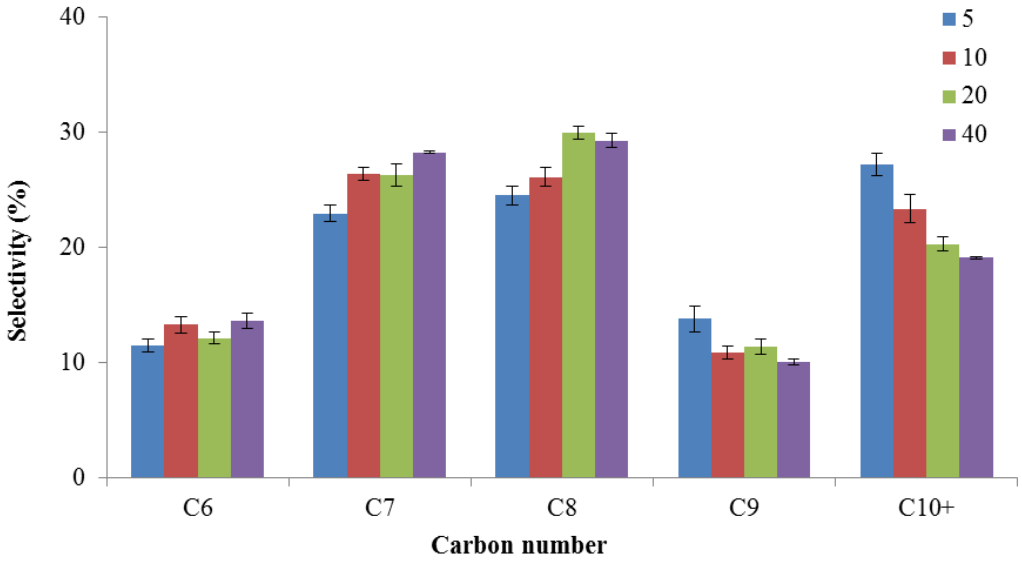

Figure 3.9 Aromatic selectivity as a function of the catalyst-to-biomass ratio for the *in-situ* upgrading (biomass loading: 0.5 mg, pyrolysis temperature: 600 °C, secondary reactor temperature: 300 °C; C6: benzene, C7: toluene, C8: ethylbenzene, and xylenes; C9: trimethylbenzenes, indane, and indene, etc., C10+: methylindenes, naphthalenes, and higher aromatics with a carbon number up to 15)

3.4.3.2 Ex-situ upgrading

The catalyst-to-biomass ratios of 5, 10, 20, and 40 were also used to investigate its effect on the performance of *ex-situ* upgrade. 0.5 mg of beetle-killed lodgepole pine was used as feedstock. The pyrolysis and secondary reactor temperature were both 600 °C. Table 3 shows the product yields and aromatic selectivity as a function of the catalyst-to-biomass ratios. For the *ex-situ* upgrading,

no significant differences in product yield and aromatic selectivity were observed with increasing catalyst-to-biomass ratio (Table 3.3). The carbon yield of aromatic volatiles, char, and coke were around 20%, 19%, and 15%, respectively, for all catalyst loadings. Moreover, catalyst-to-biomass ratios did not have significant effect on the aromatic selectivity. For all catalyst loadings, the aromatics had highest selectivity to toluene (~32%) followed by benzene (~27%) and xylenes (~12%). It appears that, even at catalyst-to-biomass ratio of 5, most of the pyrolysis volatiles are being converted to aromatic hydrocarbons. This way, any further increase in catalyst loading does not change yield and composition of products and are therefore unnecessary. Note that the same observation cannot be made for the *in-situ* upgrading, since an increase in the catalyst-to-biomass ratio from 5 to 10 led to an increase in yield. This suggests that the *ex-situ* upgrading is more effective in ensuring the volatiles react inside the catalyst pores, and indicates the mixing difficulties for the *in-situ* upgrading.

Table 3.3 Product yields and aromatic selectivity as a function of the catalyst-to-biomass ratios for the *ex-situ* upgrading (biomass loading: 0.5 mg, pyrolysis temperature: 600 °C, secondary reactor temperature: 600 °C)

Catalyst-to-biomass ratio	5	10	20	40
Product yield/ C%				
Volatiles	21.07±1.01	21.26±0.96	21.90±1.82	22.26±2.77
Char	19.56±0.72	19.60±0.72	19.15±0.17	19.63±0.65
Coke	15.24±2.54	14.37±1.82	14.41±1.10	15.19±1.17
Carbonaceous residues	34.80±3.08	33.98±1.10	33.56±0.97	34.82±0.54
Aromatic selectivity/ %				
Benzene	27.49±0.45	27.29±0.44	27.68±2.53	27.38±0.43
Toluene	33.27±1.23	31.62±0.68	32.74±0.36	33.36±0.74
Ethylbenzene and xylenes	13.21±0.74	12.82±0.47	12.19±1.34	12.19±0.37
C9 aromatics[a]	5.75±0.47	5.87±0.21	5.80±0.10	5.47±0.49

C10+ aromatics[b]	22.28±0.70	22.69±0.27	21.81±0.97	21.60±0.25

a. C9 aromatics include trimethylbenzenes, indane, and indene
b. C10+ aromatics include methylindenes, naphthalenes, and higher polyaromatics with a carbon number up to 15

3.4.4 Comparison between *in-situ* and *ex-situ* upgrading

This study has revealed important differences in trends between the *in-situ* and *ex-situ* upgrading processes. The product yields for *in-situ* upgrading were mainly affected by the catalyst-to-biomass ratio, and those for *ex-situ* upgrading were primarily influenced by the secondary reactor temperature. In addition, alkylation and dealkylation reactions play an important role in adjusting the aromatics selectivity for both *in-situ* and *ex-situ* upgrading. In the presence of HZSM-5, dealkylation reactions of alky aromatics were promoted at higher temperature. When mass and heat transfer limitations increased, lower temperatures led to alkylation reactions on HZSM-5. It has been reported that alkyl aromatics can react on HZSM-5 by transfer of alkyl groups (transalkylation/disproportionation) [41]. However, the trends observed in our work for consumption/production of alkyl aromatics were not consistent with the stoichiometry of transalkylation reactions (including disproportionation) involving C6-C9 aromatics. This suggests that, in the alkylation/dealkylation reactions mentioned previously, the source of the alkyl group was not an aromatic species. It is possible aliphatic species, such as ethylene, react with the aromatics to provide the alkyl groups. Wang et al. [18] reported that the selectivity to ethylene increased with increasing temperature in the *ex-situ* upgrading, which is consistent with our hypothesis above. The proposed pathway for alkylation/dealkylation is shown in Figure 3.10.

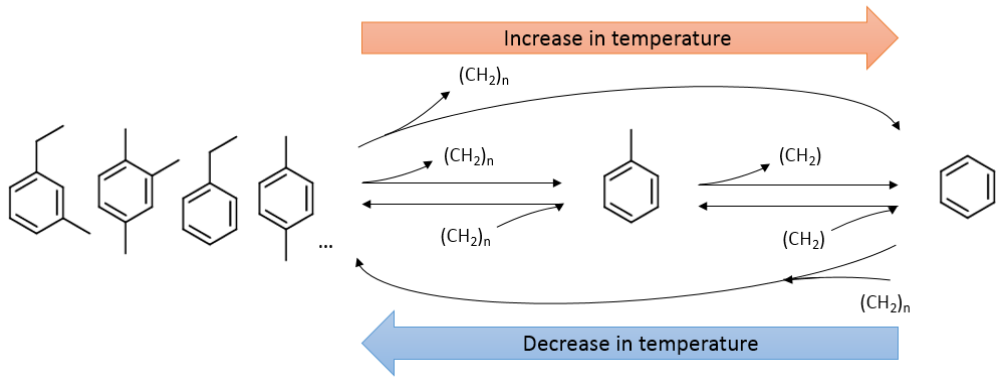

Figure 3.10 Alkylation and dealkylation reaction pathway in the presence of HZSM-5 for both *in-situ* and *ex-situ* upgrading

To make a direct comparison between *in-situ* and *ex-situ* upgrading of pyrolysis vapors from beetle-killed trees, the same reaction conditions were selected. The amounts of beetle-killed lodgepole pine sample and HZSM-5 catalyst used in the tests were 0.5 mg and 5 mg, respectively, resulting in a catalyst-to-biomass ratio of 10. The highest yield for *in-situ* upgrading was achieved at the catalyst-to-biomass ratio of 10, and the catalyst-to-biomass ratio did not significantly affect yield for *ex-situ* upgrading. This is the reason why the catalyst-to-biomass ratio of 10 was selected here. For the same reason, the pyrolysis and secondary reactor temperatures were both set up at 600 °C. The only difference between these two processes was the location of catalyst. For the *in-situ* upgrading, the HZSM-5 catalyst was mixed with biomass in the pyrolyzer and the secondary reactor was empty; whereas for the *ex-situ* upgrading the catalyst was placed separately from the biomass in the secondary reactor.

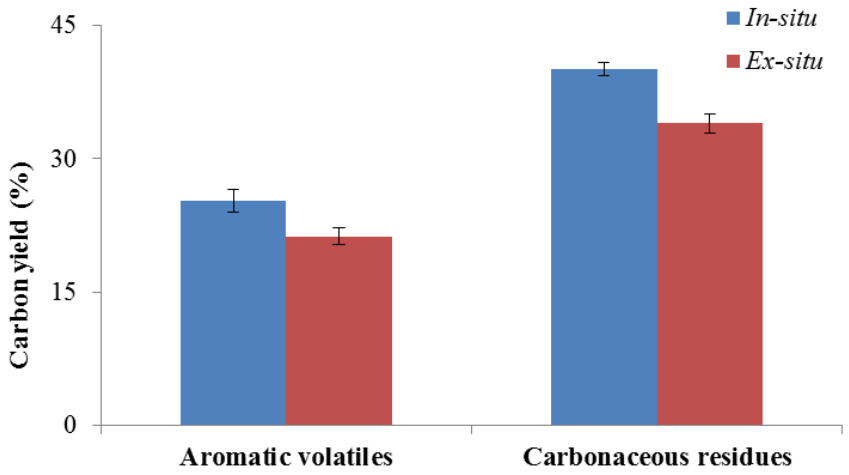

Figure 3.11 Product yields for *in-situ* and *ex-situ* upgrading of pyrolysis vapors from beetle-killed lodgepole pine (*in-situ* and *ex-situ* conditions: biomass loading: 0.5 mg, catalyst-to-biomass ratios: 10, pyrolysis temperature: 600 °C, secondary reactor temperature: 600 °C)

The product yields for the *in-situ* and *ex-situ* upgrading are summarized in Figure 3.11. The carbon yield of aromatic volatiles from the *in-situ* upgrading was around 25%, which is slightly higher than that from the *ex-situ* upgrading (~21%). Yildiz et al. [17] obtained a similar result when comparing the *in-situ* and *ex-situ* upgrading of pyrolysis vapors from pine wood using HZSM-5 as a catalyst in an auger reactor. Wang et al. also found more aromatics were produced in the *in-situ* upgrading using hybrid poplar and DDGS as feedstocks in a micro-pyrolyzer [18]. The *in-situ* upgrading also produced more char and coke, compared to the *ex-situ* case. The yield of carbonaceous residues, including both char and coke from the *in-situ* upgrading was around 40%, and that from *ex-situ* upgrading was around 34%. The results obtained at different catalyst-to-biomass ratios by Gamliel et al. are also consistent with our results [19]. The higher yield of carbonaceous residues for *in-situ* upgrading may be due to the suppressed heat and mass transfer rates caused by the larger amount loading of mixture of biomass and catalyst, which promote the secondary reactions that form more char/coke. For the *ex-situ* upgrading, only 0.5 mg biomass

sample was pyrolyzed in the first reactor and the pyrolysis vapors were contacted with the preheated catalyst bed. Thus, heat transfer limitations were not as evident for the *ex-situ* case. Additionally, the results above suggest that the *ex-situ* upgrading possibly produced more gases than the *in-situ* upgrading, which is consistent with literature. Gamliel et al. [19] reported that *ex-situ* upgrading of pyrolysis vapors from miscanthus x giganteus using Py-GC/MS resulted in a higher yield of permanent gases than the *in-situ* process. Similar results were also obtained by Wang et al., when using hybrid poplar and DDGS as feedstock [18, 42]. The combined carbon yield of aromatic volatiles and carbonaceous residues for *in-situ* and *ex-situ* upgrading were around 65% and 55%, respectively. Assuming that the undetectable gaseous products typically have a carbon yield of 20-30%, the total carbon balance for both processes will be in a range of 75-95%. In terms of the aromatic selectivity (Figure 3.12) the *ex-situ* upgrading had higher selectivity to benzene and toluene, while the *in-situ* upgrading had higher selectivity to xylenes and larger aromatics. Because of the larger mass in the single process, the *in-situ* upgrading is affected by heat and mass transfer limitation to a larger extent than the *ex-situ* upgrading [16]. This, in turn, decreased the temperature of the volatiles, promoting alkylation reactions.

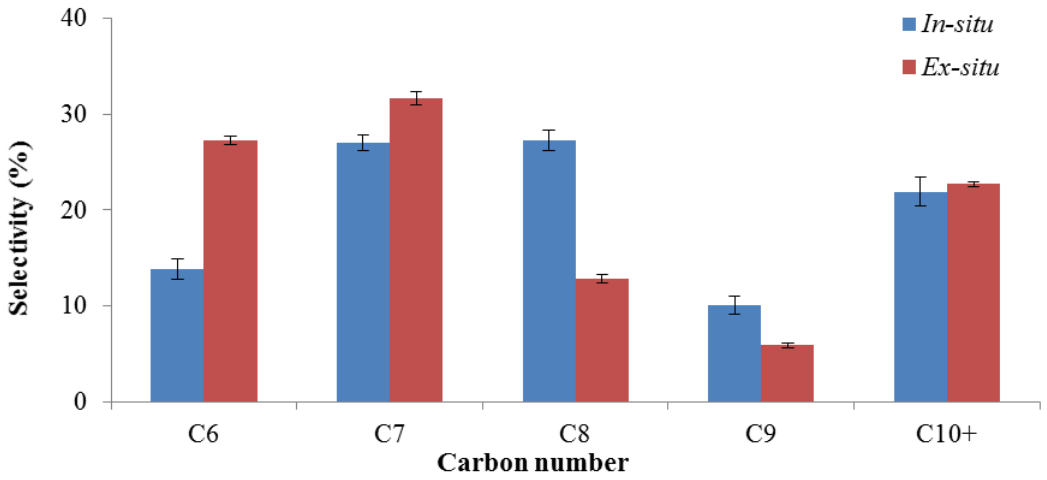

Figure 3.12 Aromatic selectivity for *in-situ* and *ex-situ* upgrading of pyrolysis vapors from beetle-killed lodgepole pine (*in-situ* and *ex-situ* conditions: biomass loading: 0.5 mg, catalyst-to-biomass ratios: 10, pyrolysis temperature: 600 °C, secondary reactor temperature: 600 °C; C6: benzene, C7: toluene, C8: ethylbenzene, and xylenes; C9: trimethylbenzenes, indane, and indene, etc., C10+: methylindenes, naphthalenes, and higher aromatics with a carbon number up to 15)

Our motivation to make a direct comparison between *in-situ* and *ex-situ* upgrading stems from the potential use of a mobile unit for the pyrolysis of beetle-killed trees. According to the results in this study, we were able to upgrade pyrolysis vapors from beetle-killed trees into chemicals and fuels using both *in-situ* and *ex-situ* configurations. Though slightly more aromatic volatiles can be produced from the *in-situ* upgrading, less carbonaceous residues will be produced in the *ex-situ* upgrading. The potential excess of permanent gases produced from the *ex-situ* upgrading can also be collected and burned, providing valuable heat to the system. The HHV of all the detectable aromatic hydrocarbons was also calculated for both *in-situ* and *ex-situ* processes. The aromatic volatiles from both processes had a similar HHV of around 42 MJ/kg. Therefore, the selection of *in-situ* and *ex-situ* configuration will not make a significant difference when using them to upgrade pyrolysis vapors from beetle-killed trees into fuels. When upgrading pyrolysis vapors from beetle-killed trees into chemicals; however, there will be a significant difference between *in-situ* and *ex-situ* configurations. The *in-situ* upgrading had higher selectivity to xylenes and larger aromatics, while the *ex-situ* upgrading had higher selectivity to benzene and toluene. Toluene and xylenes are important petrochemicals. Both of them can be used as an octane booster in motor gasoline [43]. Toluene is also a good solvent for painting and lacquers. Moreover, *para* and *ortho* xylenes are important precursors to produce plasticizers and polymers [43, 44].

In addition to what our results indicate, there are other differences between *in-situ* and *ex-situ* upgrading. In the *in-situ* upgrading, pyrolysis char and inorganic minerals existing in the biomass feedstock cannot be separated from catalytic coke. Although the accumulation of char and coke can be reduced by continuous catalyst regeneration like the regeneration process in the conventional fluid catalytic cracking (FCC) technology, the accumulation of alkali metals on the catalyst can still deactivate or poison the zeolite catalyst eventually [45], which will reduce the catalyst lifetime. In contrast, pyrolysis char along with the alkali metals are separated from catalytic coke in the *ex-situ* upgrading. As a consequence, the activity and lifetime of the zeolite catalyst will be improved, since it is not affected by alkali metals. In addition, compared to the *in-situ* upgrading, the *ex-situ* upgrading is more flexible to different configurations of the pyrolyzer, such as auger and ablative reactors. Thus, the selection of *in-situ* or *ex-situ* configuration for the mobile pyrolysis of beetle-killed trees will also depend on the ash content of the trees and the configuration of the mobile pyrolysis unit.

3.5 CONCLUSIONS

The effects of pyrolysis temperature, secondary temperature, and catalyst-to-biomass ratio on the product yield and selectivity for *in-situ* and *ex-situ* upgrading of pyrolysis vapors from beetle-killed trees have been investigated using a micro-pyrolyzer. HZSM-5 was used as catalyst. The only variable that significantly affected the *in-situ* upgrading was the catalyst-to-biomass ratio. At a catalyst-to-biomass ratio of 10, the highest aromatic carbon yield of 25% was achieved. Higher catalyst-to-biomass ratios increase mass and heat transfer resistances and limit aromatic production. Thus, less aromatic volatiles and more carbonaceous residues were produced at ratios higher than 10. For the *ex-situ* upgrading, most of the pyrolysis volatiles were converted to aromatic hydrocarbons at the catalyst-to-biomass ratio of 5, indicating the *ex-situ* upgrading is

more effective in ensuring the volatiles react inside the catalyst pores. The product yields from *ex-situ* upgrading were highly affected by the temperature of the secondary reactor. At the secondary reactor temperature of 600 °C, the highest aromatic carbon yield of 22% was obtained. The rates of alkylation and dealkylation reactions of alkyl aromatics play an important role on the product selectivity for both *in-situ* and *ex-situ* upgrading, which has been extensively discussed in this article. To the best of our knowledge, this aspect has not been reported by others previously in the literature. Because of its exothermicity, alkylation reactions were promoted at lower temperature, and dealkylation reactions were favored at higher temperature. Based on the results, it was also speculated that the alkyl groups involved in the alkylation/dealkylation reactions originate from species other than aromatics, such as ethylene. A direct comparison between the *in-situ* and *ex-situ* upgrading has been performed under identical reaction conditions. Some differences existed between the *in-situ* and *ex-situ* upgrading processes with respect to aromatic hydrocarbon selectivity. However, the product yields from both processes were largely similar. The *in-situ* upgrading had higher selectivity to xylenes and aromatics with carbon number of 9 while the *ex-situ* upgrading exhibited higher selectivity to benzene and toluene, indicating that the selection of *in-situ* or *ex-situ* configuration could determine the product distribution when producing chemicals. The HHV of all the detectable aromatic volatiles from both processes were similar (~42 MJ/kg); thus, the selection of *in-situ* or *ex-situ* upgrading will not significantly affect fuel production.

3.6 REFERENCES

[1] U.S.F. Service, Western Bark Beetle Strategy for Human Safety, Recovery and Resiliency, 2011.

[2] W.F.L. Coalition, WESTERN BARK BEETLE ASSESSMENT: A Framework for Cooperative Forest Stewardship, in, 2007.

[3] J.-J. Kim, E.A. Allen, L.M. Humble, C. Breuil, Ophiostomatoid and basidiomycetous fungi associated with green, red, and grey lodgepole pines after mountain pine beetle (Dendroctonus ponderosae) infestation, Can J For Res, 2005; 35: 274-284.

[4] R. Reid, Moisture changes in lodgepole pine before and after attack by the mountain pine beetle, The Forestry Chronicle, 1961; 37: 368-375.

[5] K.J. Lewis, I.D. Hartley, Rate of deterioration, degrade, and fall of trees killed by mountain pine beetle, J Ecosys Manage, 2006; 7.

[6] G. Luo, F.L. Resende, Fast pyrolysis of beetle-killed trees, J Anal Appl Pyrol, 2014; 110: 100-107.

[7] T.R. Carlson, Y.-T. Cheng, J. Jae, G.W. Huber, Production of green aromatics and olefins by catalytic fast pyrolysis of wood sawdust, Energy Environ Sci, 2011; 4: 145-161.

[8] P.T. Williams, N. Nugranad, Comparison of products from the pyrolysis and catalytic pyrolysis of rice husks, Energy, 2000; 25: 493-513.

[9] H. Zhang, J. Zheng, R. Xiao, Y. Jia, D. Shen, B. Jin, G. Xiao, Study on Pyrolysis of Pine Sawdust with Solid Base and Acid Mixed Catalysts by Thermogravimetry–Fourier Transform Infrared Spectroscopy and Pyrolysis–Gas Chromatography/Mass Spectrometry, Energ Fuel, 2014; 28: 4294-4299.

[10] H. Zhang, R. Xiao, D. Wang, Z. Zhong, M. Song, Q. Pan, G. He, Catalytic fast pyrolysis of biomass in a fluidized bed with fresh and spent fluidized catalytic cracking (FCC) catalysts, Energ Fuel, 2009; 23: 6199-6206.

[11] T.R. Carlson, J. Jae, Y.-C. Lin, G.A. Tompsett, G.W. Huber, Catalytic fast pyrolysis of glucose with HZSM-5: the combined homogeneous and heterogeneous reactions, Journal of Catalysis, 2010; 270: 110-124.

[12] O.D. Mante, F. Agblevor, R. McClung, A study on catalytic pyrolysis of biomass with Y-zeolite based FCC catalyst using response surface methodology, Fuel, 2013; 108: 451-464.

[13] C. Liu, H. Wang, A.M. Karim, J. Sun, Y. Wang, Catalytic fast pyrolysis of lignocellulosic biomass, Chem Soc Rev, 2014.

[14] M. Biddy, A. Dutta, S. Jones, A. Meyer, In-Situ Catalytic Fast Pyrolysis Technology Pathway, in, National Renewable Energy Laboratory, 2013.

[15] M. Biddy, A. Dutta, S. Jones, A. Meyer, Ex-Situ Catalytic Fast Pyrolysis Technology Pathway, in, National Renewable Energy Laboratory, 2013.

[16] S. Wan, Y. Wang, A review on ex situ catalytic fast pyrolysis of biomass, Front Chem Sci Eng, 2014; 8: 280-294.

[17] G. Yildiz, M. Pronk, M. Djokic, K.M. van Geem, F. Ronsse, R. Van Duren, W. Prins, Validation of a new set-up for continuous catalytic fast pyrolysis of biomass coupled with vapour phase upgrading, J Anal Appl Pyrol, 2013; 103: 343-351.

[18] K. Wang, P.A. Johnston, R.C. Brown, Comparison of *in-situ* and *ex-situ* catalytic pyrolysis in a micro-reactor system, Bioresour Technol, 2014; 173: 124-131.

[19] D.P. Gamliel, S. Du, G.M. Bollas, J.A. Valla, Investigation of in situ and ex situ catalytic pyrolysis of miscanthus× giganteus using a PyGC–MS microsystem and comparison with a bench-scale spouted-bed reactor, Bioresour Technol, 2015; 191: 187-196.

[20] A. Kumar, A conceptual comparison of bioenergy options for using mountain pine beetle infested wood in Western Canada, Bioresour Technol, 2009; 100: 387-399.

[21] R.C. Brown, T.R. Brown, Biorenewable resources: engineering new products from agriculture, John Wiley & Sons, 2013.

[22] P.C. Badger, P. Fransham, Use of mobile fast pyrolysis plants to densify biomass and reduce biomass handling costs—A preliminary assessment, Biomass Bioenerg, 2006; 30: 321-325.

[23] J. Meng, J. Park, D. Tilotta, S. Park, The effect of torrefaction on the chemistry of fast-pyrolysis bio-oil, Bioresour Technol, 2012; 111: 439-446.

[24] X. Ren, J. Meng, A.M. Moore, J. Chang, J. Gou, S. Park, Thermogravimetric investigation on the degradation properties and combustion performance of bio-oils, Bioresour Technol, 2014; 152: 267-274.

[25] M.M. Wright, Techno-economic evaluations of biofuel technologies, in: MecEn, Iowa State University, 2008.

[26] S. Channiwala, P. Parikh, A unified correlation for estimating HHV of solid, liquid and gaseous fuels, Fuel, 2002; 81: 1051-1063.

[27] K. Wang, R.C. Brown, Catalytic pyrolysis of microalgae for production of aromatics and ammonia, Green Chem, 2013.

[28] P.R. Patwardhan, R.C. Brown, B.H. Shanks, Product distribution from the fast pyrolysis of hemicellulose, ChemSusChem, 2011; 4: 636-643.

[29] P.R. Patwardhan, R.C. Brown, B.H. Shanks, Understanding the fast pyrolysis of lignin, ChemSusChem, 2011; 4: 1629-1636.

[30] M. Zhang, F.L. Resende, A. Moutsoglou, D.E. Raynie, Pyrolysis of lignin extracted from prairie cordgrass, aspen, and Kraft lignin by Py-GC/MS and TGA/FTIR, J Anal Appl Pyrol, 2012; 98: 65-71.

[31] S. Zhou, B. Pecha, M. van Kuppevelt, A.G. McDonald, M. Garcia-Perez, Slow and fast pyrolysis of Douglas-fir lignin: Importance of liquid-intermediate formation on the distribution of products, Biomass Bioenerg, 2014; 66: 398-409.

[32] K. Wang, K.H. Kim, R.C. Brown, Catalytic pyrolysis of individual components of lignocellulosic biomass, Green Chem, 2014; 16: 727-735.

[33] S. Du, Y. Sun, D.P. Gamliel, J.A. Valla, G.M. Bollas, Catalytic pyrolysis of miscanthus× giganteus in a spouted bed reactor, Bioresour Technol, 2014; 169: 188-197.

[34] K. Wang, J. Zhang, B.H. Shanks, R.C. Brown, Catalytic conversion of carbohydrate-derived oxygenates over HZSM-5 in a tandem micro-reactor system, Green Chem, 2015.

[35] Y.-T. Cheng, G.W. Huber, Chemistry of furan conversion into aromatics and olefins over HZSM-5: a model biomass conversion reaction, ACS Catal, 2011; 1: 611-628.

[36] P.A. Horne, P.T. Williams, Reaction of oxygenated biomass pyrolysis model compounds over a ZSM-5 catalyst, Renew Energ, 1996; 7: 131-144.

[37] X. Zhu, R.G. Mallinson, D.E. Resasco, Role of transalkylation reactions in the conversion of anisole over HZSM-5, Appl Catal, A, 2010; 379: 172-181.

[38] Y. Ono, H. Kitagawa, Y. Sendoda, Transformation of lower alkanes into aromatic hydrocarbons over ZSM-5 zeolites, Catal Rev, 1992; 34: 179-226.

[39] S. Al-Khattaf, Catalytic transformation of toluene over a high-acidity Y-zeolite based catalyst, Energ Fuel, 2006; 20: 946-954.

[40] M. Zhang, F.L. Resende, A. Moutsoglou, Catalytic fast pyrolysis of aspen lignin via Py-GC/MS, Fuel, 2014; 116: 358-369.

[41] S. Waziri, A. Aitani, S. Al-Khattaf, Transformation of toluene and 1, 2, 4-trimethylbenzene over ZSM-5 and mordenite catalysts: a comprehensive kinetic model with reversibility, Ind Eng Chem Res, 2010; 49: 6376-6387.

[42] K. Wang, R.C. Brown, Catalytic pyrolysis of corn dried distillers grains with solubles to produce hydrocarbons, ACS Sustainable Chem Eng, 2014; 2: 2142-2148.

[43] T.R. Carlson, G.A. Tompsett, W.C. Conner, G.W. Huber, Aromatic production from catalytic fast pyrolysis of biomass-derived feedstocks, Top Catal, 2009; 52: 241-252.

[44] S.D. Barnicki, Synthetic Organic Chemicals, in: Handbook of Industrial Chemistry and Biotechnology, Springer, 2012, pp. 307-389.

[45] C.A. Mullen, A.A. Boateng, Accumulation of Inorganic Impurities on HZSM-5 Zeolites during Catalytic Fast Pyrolysis of Switchgrass, Ind Eng Chem Res, 2013; 52: 17156-17161.

CHAPTER 4. DESIGN AND CONSTRUCTION OF A NOVEL ABLATIVE PYROLYSIS REACTOR

4.1 INTRODUCTION

The reactor is the key component when considering an entire fast pyrolysis system. Many types of reactors, including fluidized bed reactor, circulating fluidized bed reactor, free-fall reactor, auger reactor, and ablative reactor have been developed. For most pyrolysis reactor configurations, the biomass feedstock needs to be ground into small particles of 1-2 mm, because the process requires high rate of heat transfer through the particles [1]. Kumar estimated that the costs of biomass grinding were about 7-9% of the overall production costs [2]. Forest Concepts also studied the effects of the final wood particle size on the total comminution energy cost for the Optimized Crumbler® machine, and found out that the comminution energy cost increases $1.5-4.5 per US ton as the wood particle size is reduced from 12 mm to 1-2 mm [3]. In an ablative pyrolyzer, biomass undergoes melting and/or sublimation reactions as it directly contacts with a hot reactor surface. There is a steep temperature gradient at the biomass surface, leading to the formation of a thin superficial layer of reacting solid [4]. The reacting layer moves at constant velocity towards the heart of the cold biomass. Therefore, the reactive process in the ablative reactor takes place only at the superficial layer rather than the entire biomass particle. For this reason, in principle there is no upper limit to the biomass particle size that can be processed in the ablative pyrolyzer[4, 5]. In order to reduce the grinding costs and the overall costs of the fast pyrolysis process, we designed and constructed a lab-scale ablative pyrolysis reactor to convert large wood chips from beetle-killed trees directly into bio-oil.

4.2 REACTOR SYSTEM OVERVIEW

The ablative reactor is composed of a chamber, which contains a spinning bowl where the wood chips can be placed, and a hot plate at the top which can move down and apply pressure against wood chips. Fast pyrolysis initiates as the hot plate contacts the wood chips, and the inert gas at a high flow rate then rapidly sweeps the generated vapors out of the chamber for condensation. Vacuum is applied at the outlet to reduce the residence time of the pyrolysis vapors inside the reactor.

4.2.1 Reactor description

The ablative reactor system is designed to convert wood chips into bio-oil, char, and non-condensable gases via fast pyrolysis in a single step. It is a semi-batch system with a capacity of up to 500 g wood chips per run. Figure 4.1 shows the ablative pyrolysis reactor.

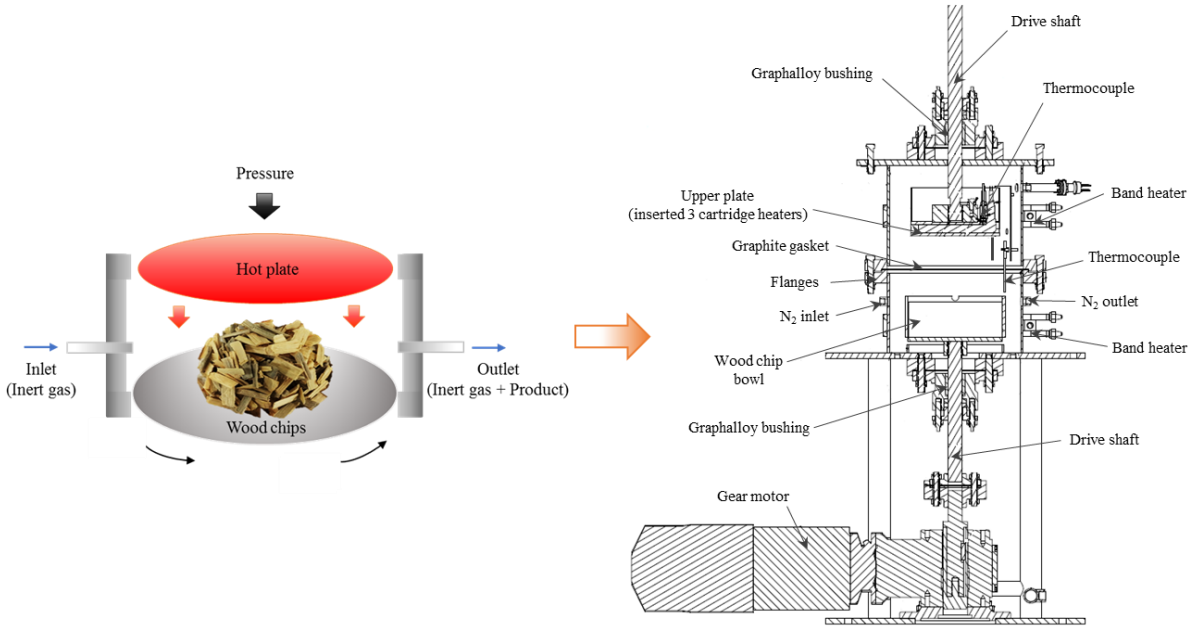

Figure 4.1 Ablative pyrolysis reactor

The reactor chamber is made of A240 304L stainless steel with an internal diameter of 0.30 m and an internal height of 0.42 m. This chamber can be split into an upper chamber and lower chamber, which are connected with flanges. A static seal is created by a graphite gasket placed between the two flanges faces. The wood chip bowl made of A240 304L stainless steel has an internal diameter of 0.21 m and a height of 0.09 m. In order to make the generated pyrolysis vapors escape from the wood chip bowl quickly, 0.05 × 0.01 m rectangular slots were made on the shell of the bowl (Figure 4.2). To prevent wood chips from dropping out of the bowl from the slots, a 1 mm thick perforated T304 liner with 1.6 mm holes on a 3.2 mm 60° triangular pitch was installed inside the shell. The wood chip bowl is driven by a 3 HP SEW-EURODRIVE gear motor, providing a rotation speed up to 160 rpm.

Figure 4.2 Wood chip bowl and its shell with rectangular slots

The lower chamber contains a gas inlet and a gas outlet. To minimize the vapor residence time, the product vapors escaped out of the chamber through a perforated tube bent around the circumference of the bowl (Figure 4.3).

Figure 4.3 N_2 inlet and gas outlet

The upper plate with a diameter of 0.2 m and a thickness of 0.032 m is driven by a piston connected to a hydraulic system, capable of moving vertically and applying a maximum pressure of 1.5 bar against the wood chips (Figure 4.4 and 4.5). The lower and upper drive shafts housing on the reactor chamber contain graphalloy bushings to prevent leakages and ingress of air. Three 1 kW Chromalox CIR cartridge heaters were inserted in the upper plate, and are capable of generating a heat flux up to 10^5 W/m^2 and heating the plate up to 700 °C. Furthermore, two band heaters (Chromalox HBT 120) were used to heat the reactor wall to a minimum temperature of 300 °C, minimizing the condensation of pyrolysis vapors on the reactor wall. Each of the band heaters has a power of 2 kW. The temperatures of the cartridge heaters and band heaters are measured and controlled by inbuilt type K thermocouples that are connected to Chromalox 1/4 DIN temperature controllers. To minimize the heat losses, the entire reactor chamber was insulated using two layers of 1.3 cm thick ceramic sheets and one layer of silica fabric wrap.

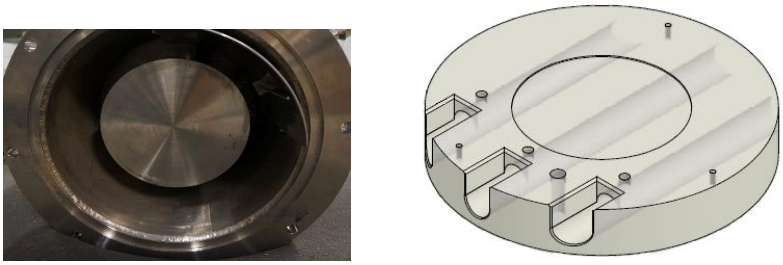

Figure 4.4 Upper plate and slots for cartridge heaters

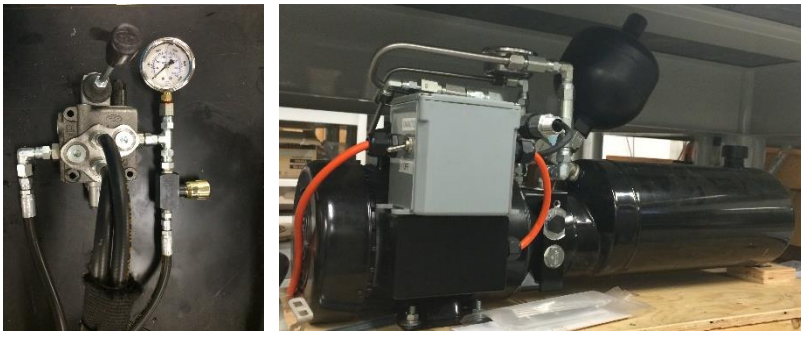

Figure 4.5 Hydraulic system

4.2.2 Reactor operation

Figure 4.6 shows the schematic diagram of the system including reactor, condenser, and gas meter, etc. Prior to the reaction, a specified amount of wood chips is loaded on the wood chip bowl. After sealing the reactor chamber, the upper plate and the reactor wall are pre-heated to the operating temperatures. During the pre-heating time, the upper plate is located at the highest position. The distance between the upper plate and the wood chip bowl bottom is about 0.23 m to minimize the slow pyrolysis of biomass caused by radiation heat transfer during the pre-heating time. At the same time, room temperature N_2 is used as carrier gas being introduced into the system from the gas inlet at the reactor wall. The flow rate of N_2 is controlled by an Aalborg mass flow controller. Once the upper plate and reactor wall reach the operating temperatures, the wood chip bowl driven by the motor starts to rotate and the upper plate driven by the hydraulic system starts moving down towards the wood chips. Ablative contact of the hot upper plate with the wood chips initiates fast pyrolysis. The produced pyrolysis vapors then carried by N_2 quickly escape from the reactor chamber through the gas outlet and enter a multi-stage bio-oil collection system. The first stage is an ice-water cooled impinger, which collects the heavy fractions of the bio-oil. The second stage is a counter-current double-pipe condenser, of which 50/50 vol. % propylene glycol/water is used as cooling fluid in the outer pipe, with an inlet temperature of -10 °C. This stage collects the light (aqueous) fraction of bio-oil. The remaining cooled vapors and non-condensable gases flow through a Swagelok coalescing filter and a packed quartz wool fiber which collect any residual aerosols and water vapors. In addition, building vacuum was connected to the system to drive the pyrolysis vapors out of the reactor chamber. However, the non-condensable gases are sent to the retriever and cannot be collected for further analysis with only building vacuum installed. Thus, a parallel GAST vacuum with a gas outlet was installed for a few runs for gas quantification and

overall mass balance calculation. The specifications of both building vacuum and GAST vacuum pump are summarized in Table 4.1. Solid char is left on the wood chip bowl.

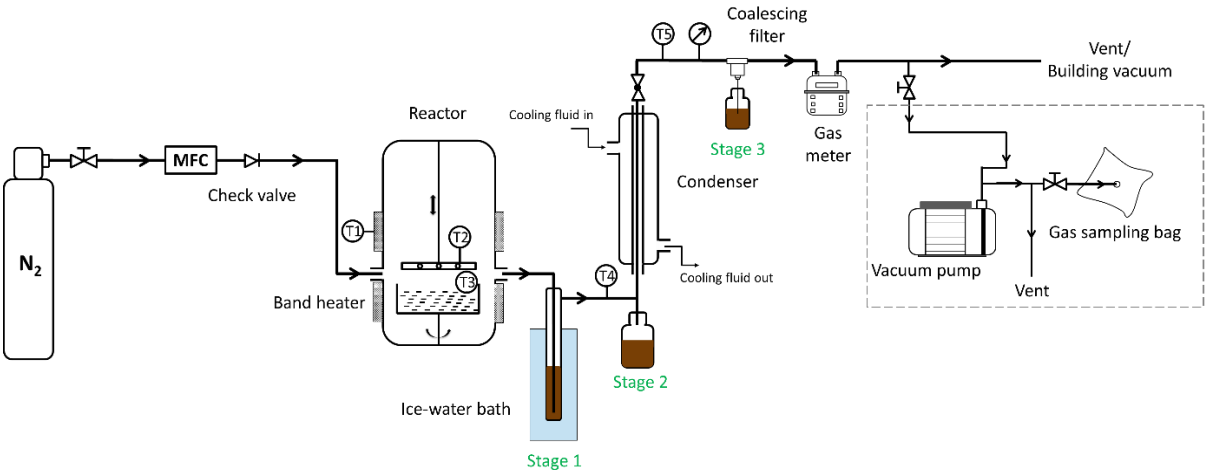

Figure 4.6 Schematic diagram of the system

Table 4.1 Specifications of the building vacuum and GAST vacuum pump

	Building vacuum	Vacuum pump
HP	4.7 HP	0.25 HP
Flow rate	1.7 cfm	1.4 cfm
Vacuum level	22-25” Hg	25” Hg

4.3 REACTOR SYSTEM DESIGN

4.3.1 Determination of operating parameters

The operating parameters required for the specific design of the ablative reactor are temperatures of the upper plate and reactor wall, the flow rate of carrier gas (N_2), the applied pressure on the wood chips, and the rotating speed of the wood chip bowl. These are summarized in Table 4.2.

Table 4.2 Selected values of operating parameters for design

Parameter	Symbol	Value
Upper plate temperature (°C)	T_{plate}	700
Reactor wall temperature (°C)	T_{wall}	≥ 300
N_2 flow rate (SLPM)	$\dot{V}$	100
Applied pressure on biomass (bar)	P	1.5
Rotating speed of wood chip bowl (rpm)	ω	160

Fast pyrolysis is the rapid thermal decomposition of organic material in the absence of oxygen. It usually takes place at moderate temperatures of 400 – 600 °C [6, 7]. In our ablative pyrolysis unit, fast pyrolysis of biomass occurs as the hot upper plate applies pressure on the wood chips. Thus, the selected maximum temperature for the upper plate is 700 °C. Moreover, the reactor wall was designed to have a minimum temperature of 300 °C to minimize the condensation of pyrolysis vapors on the inner wall and improve the liquid bio-oil yield.

N_2 is used as carrier gas and inert medium. The volumetric flow rate of N_2, $\dot{V}$, was determined as a ratio of the reactor chamber volume V to the resulting vapor residence time t (Eq 4.1).

$$\dot{V} = \frac{V}{t} \tag{4.1}$$

Generally, fast pyrolysis has a very short vapor residence time of a few seconds [6, 7]. So t = 2 s was used to calculate the volumetric flow rate of N_2. The reactor dimensions and nitrogen properties are summarized in Table 4.3. Using the volumes of the entire reactor chamber and the lower chamber, the calculated volumetric flow rate of N_2 would be 478 SLPM and 204 SLPM, respectively. These values are too high to be practically feasible with gas cylinders. Because of the relative locations of the N_2 inlet and outlet, we assumed that the carrier gas N_2 would bypass most of the chamber volume; therefore, a maximum flow of 100 SLPM was selected.

Table 4.3 Parameter values for nitrogen flow rate calculation

Parameter	Symbol	Value
Reactor dimension		
Diameter of reactor chamber (m)	d	0.30
Height of reactor chamber (m)	h	0.42
Thickness of reactor chamber wall (m)	w_{wall}	0.0048
Volume of reactor chamber (m^3)	V	0.0308
Volume of lower reactor chamber (m^3)	V'	0.0132
Nitrogen properties		
Density at 300 °C, 1 atm (kg m^{-3})	ρ_{300}	0.5956
Density at 20 °C, 1 atm (kg m^{-3})	ρ_{20}	1.1508

It is essential that the heated surface applies enough pressure on the wood chips. Lédé et al. did a fundamental study using a wood rod on a heated spinning stainless steel disk. The ablation rate of the wood rod was found to be proportional to the pressure applied on it [5, 8]. Diebold et al. [9, 10] did fast pyrolysis of wood chips in an ablative vortex reactor and studied the effect of contact pressure on the ablation rate of wood chips. For the wood particle ablation in a centrifugal movement, the ablation rate decreased as the centrifugal forces on the wood particle decreased [9, 10]. A "pyrolysis mill" was designed by Reed to do the contact ablative pyrolysis of biomass [11]. The pyrolysis mill has a stationary copper upper "stone" and a spinning lower copper "stone", which is similar to the ablative reactor in this work. Based on the experimental results, Reed proposed that the contact pressure on biomass typically needed to be 0.4 bar and 1.5 bar for a small (0.05 g/s) and large scale (20 g/s) pyrolysis mill, respectively [11]. Based on these reported values, the maximum applied pressure of 1.5 bar was selected for designing the ablative reactor.

In Lédé's studies, they found the ablation rate of the wood rod was also related to the extent of relative motion between the contacting wood and the heated disk [5, 12]. The ablation rate of wood first increased as the relative velocity of the spinning heated disk increased, and then became

constant when the velocity was higher than 1.5 m/s. Based on this report, we used a linear velocity u = 1.5 m/s to calculate the design frequency of rotation (ω in rpm) of the wood chip bowl in our ablative pyrolyzer (Eq 4.2).

$$\omega\ (\text{rpm}) = 60\ \text{u}\ /(2\pi\ r_b) \tag{4.2}$$

where r_b is the radius of wood chip bowl in meters. The calculated frequency of rotation was equal to 130 rpm. Thus, the rotating speed of the wood chip bowl was designed to be as high as 160 rpm.

4.3.2 Heaters selection

Two temperatures need to be controlled in our reactor system; namely, the upper plate temperature and the reactor wall temperature. The temperatures of the upper plate and the reactor wall are controlled with cartridge heaters and band heaters, respectively.

4.3.2.1 Cartridge heater

A high heat flux to the wood chips is required in fast pyrolysis of biomass, especially in the case of large biomass particles, in order to improve bio-oil yield [13]. Based on the literature, a heat flux of 10^5 W/m^2 was selected in the design of our ablative pyrolysis unit [11, 14]. The required power of the cartridge heater can be calculated using the selected heat flux:

$$P_{CH} = \emptyset\ A_{plate} \tag{4.3}$$

$$A_{plate} = \pi\ (d_{plate}/2)^2 \tag{4.4}$$

where P_{CH} is the power of cartridge heater, $\emptyset$ is the heat flux, A_{plate} is the heat transfer area which is equal to the surface area of upper plate, and d_{plate} is the diameter of upper plate (Table 4.4). The calculated values of A_{plate} and P_{CH} are 0.03 m^2 and 3,000 W, respectively. Thus, three

Chromalox CIR cartridge heaters, each of which has a power of 1,000 W, were inserted into the upper plate.

Table 4.4 Upper plate dimensions and material properties values

Parameter	Symbol	Value
Upper plate dimensions		
Diameter (m)	d_{plate}	0.20
Thickness (m)	w_{plate}	0.032
Slots volume (m^3)	V_{slots}	1.54×10^{-4}
A240 304L stainless steel properties		
Density (kg m^{-3})	ρ_{304L}	8.0×10^3 [15]
Specific heat (J kg^{-1} K^{-1})	C_{304L}	500 [15]

Without considering the heat losses from the upper plate to the surroundings, the total heat required to heat up the plate from room temperature to the desirable maximum pyrolysis temperature can be estimated:

$$Q_{plate} = C_{304L}\, m_{plate}\left(T_{plate} - T_0\right) \tag{4.5}$$

$$m_{plate} = \rho_{304L} V_{plate} = \rho_{304L}\left(\pi\left(\frac{d_{plate}}{2}\right)^2 w_{plate} - V_{slots}\right) \tag{4.6}$$

where Q_{plate} is the heat required to heat up the plate to the desired pyrolysis temperature, C_{304L} and ρ_{304L} are the specific heat and density of A204 304L stainless steel, of which the upper plate made, m_{plate} is the mass of the upper plate, T_{plate} and T_0 are the final plate temperature (700 °C.) and room temperature (20 °C), V_{plate} is volume of the upper plate, d_{plate} and w_{plate} are the diameter and thickness of the upper plate, and V_{slots} is the volume of the three slots for cartridge heaters. Using the values given in Table 4.4, Q_{plate} is calculated, which is equal to 2,299 kJ. Then, the time required to heat up the upper plate to the pyrolysis temperature can be calculated as the ratio of total required heat to the power of cartridge heaters (Eq. 4.7). We calculated that calculated

that 525 s (~8.8 min) are needed to heat the upper plate from room temperature to 700 °C. In reality, the heat losses from the upper plate to the surroundings significantly increase the heating up time. It was experimentally determined that about 45 min were needed to heat up the heat upper plate from room temperature to 700 °C.

$$t' = \frac{Q_{plate}}{P_{CH}} \tag{4.7}$$

4.3.2.2 Band heater

Two band heaters are used to maintain the reactor wall at 300 °C to minimize condensation of pyrolysis vapors. In order to keep the same heating up time of reactor wall as the upper plate, t' = 525 s is used for calculation to select band heaters. Neglecting the heat transfer between reactor wall and surroundings, the total heat required to heat up the reactor wall was calculated using Eq. 4.8:

$$Q_{wall} = C_{304L}\, m_{wall}(T_{wall} - T_0) \tag{4.8}$$

$$m_{wall} = \rho_{304L}\, V_{wall} = \rho_{304L}\pi d w_{wall} h \tag{4.9}$$

where Q_{wall} is the heat required to heat up the reactor wall, C_{304L} and ρ_{304L} are the specific heat and density of A204 304L stainless steel, of which the reactor wall made (Table 4.4), m_{wall} is the mass of the wall, T_{plate} and T_0 are the final wall temperature (300 °C) and room temperature (20 °C), w_{wall} is the thickness of the reactor wall, and d and h are the diameter and height of the reactor chamber, respectively (Table 4.3). The calculated values of m_{wall} and Q_{wall} are 15 kg and 2059 kJ. According to Eq. 4.10, the minimum power of the band heaters, P_{BH}, can then be estimated to be equal to 3922 W. Thus, two 2" band heaters (Chromalox HBT 120) were selected. Each of them has a power of 2,000 W. Due to the heat losses to the surroundings, the measured

time to heat up the reactor from room temperature to 300 °C was also longer than the calculated value (~8.8 min), which is around 17 min.

$$P_{BH} = \frac{Q_{wall}}{t\prime} \tag{4.10}$$

4.3.3 Motor selection

In the ablative system, a motor drives the rotating wood chip bowl. To select the motor, the load torque M at the motor drive shaft needs to be calculated. The upper plate and the wood chip bowl are brought into contact under an axial force *F*, which is composed of three parts; namely, the force from the hydraulic system F_h, gravity of the upper plate G_{plate}, and gravity of biomass $G_{biomass}$ (Eq. 4.11):

$$F = F_h + G_{plate} + G_{wood} = P_{max}\pi r_b^2 + m_{plate}g + m_{wood}g \tag{4.11}$$

where P_{max} is the maximum pressure that the hydraulic system applies on the plate, r_b is the radius of wood chip bowl, m_{plate} is the mass of the upper plate (see Eq. 4.6), m_{wood} is the maximum mass of wood chips, and g is the standard acceleration due to gravity. The values of these parameters are given in Table 4.5, and the calculated the maximum value of axial force F is 4,784 N.

Table 4.5 Parameter values for axial force *F* calculation

Parameter	Symbol	Value
Maximum pressure from hydraulic system (Pa)	P_{max}	1.5×10^5
Mass of upper plate (kg)	m_{plate}	8.16
Radius of wood chip bowl (m)	r_b	0.11
Maximum mass of biomass (kg)	m_{wood}	0.50
Standard acceleration due to gravity (m s^{-2})	g	9.8

According to Figure 4.7, if p is the normal pressure at any location on the wood chip bowl, the frictional force acting on the elemental area of the wood chip bowl bottom is $\mu\ p\ dA$, where μ is the friction coefficient between the stainless steel and wood, which is around 0.4 [16], and dA ($dA = r\ dr\ d\theta$) is the area of the element. The torque of this elemental friction force about the shaft axis is $\mu\ p\ r\ dA$, where r is the lever arm. Then the total load torque M at the motor drive shaft becomes:

$$M = \int \mu p\ r\ dA \tag{4.12}$$

where we evaluate the integral over the area of the wood chip bowl bottom. Here we can assume that the pressure p is constant and uniformly distributed so that $\pi R^2 p$ is equal to the axial force F, and R is equal to the radius of wood chip bowl, r_b. Substituting the constant value of p in Eq. 4.12 gives us:

$$M = \frac{\mu F}{\pi r_b^2}\int_0^{2\pi}\int_0^{r_b} r^2\ dr\ d\theta = \frac{2}{3}\mu F r_b \tag{4.13}$$

This result can also be interpreted as equivalent to torque due to a friction force μF acting at a distance of 2/3 r_b from the shaft center [17]. So the total load torque applied at the motor shaft is about 127.6 N·m.

The minimum required power of motor P_{motor} can be calculated as follows:

$$P_{motor}(Watt) = M\omega/9.5488 \tag{4.14}$$

where ω is the maximum rotating speed of wood chip bowl, which is 160 rpm. We calculated that the required power of motor was 2138 W, which is equivalent to 2.87 hp. Thus, a 3 hp SEW-EURODRIVE gear motor was selected.

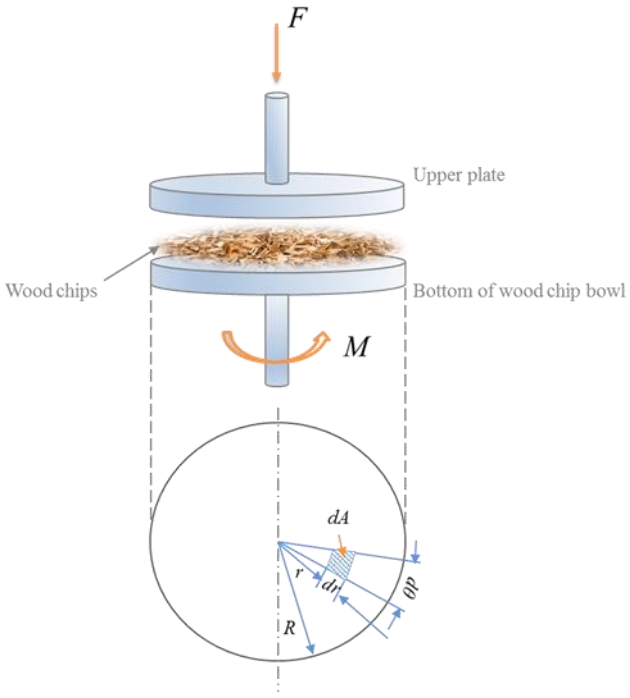

Figure 4.7 Schematic diagram for torque calculation

4.3.4 Condenser design

In the ablative reactor system, a vertical concentric tube condenser with the counter flow arrangement was designed at first to cool down the hot pyrolysis vapors into liquid bio-oil (Figure 4.8). The inner diameter of the inner and outer tubes of the condenser are 0.0221 m (D_i) and 0.0325 m (D_o), respectively. Pyrolysis vapors carried by a large amount of N_2 leave the reactor chamber at 300 °C and then flow into the condenser for quick condensation. The desired outlet temperature for the vapors is 20 °C. A 50/50 vol. % propylene glycol/water (PG 50/50) solution provided by a Fisher Isotemp recirculating chiller with an inlet temperature of -10 °C and a flow rate of 88 ml/s is used as cooling fluid for the condenser. Before the construction, the minimum length of the condenser, L_c, was determined using the logarithmic mean temperature (LMTD) analysis method.

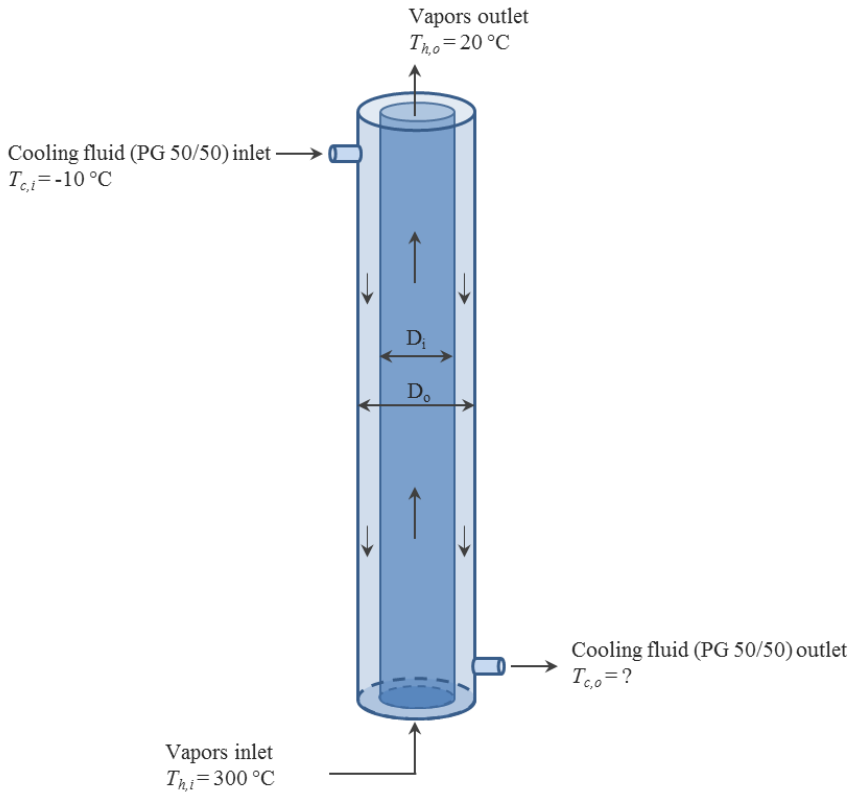

Figure 4.8 Schematic diagram of the concentric tube condenser

The heat transfer rate q from the hot vapors to the cold cooling fluid is given by the following equation:

$$q = UA_s\Delta T_{lm} \tag{4.15}$$

in which

$$A_s = \pi D_i L_c \tag{4.16}$$

Arranging Eq 4.15 and Eq. 4.16, the minimum length of the condenser L_c can be expressed as:

$$L_c = \frac{q}{U\pi D_i \Delta T_{lm}} \tag{4.17}$$

where U is the overall heat transfer coefficient, A_s is the internal heat transfer area between the two fluids, and ΔT_{lm} is a log mean temperature difference.

The heat transfer rate q can be obtained from the overall energy balance for the hot vapors,

$$q = \dot{m}_h \, c_{p.h}(T_{h,i} - T_{h,o}) \tag{4.18}$$

where $\dot{m}_h$ and $c_{p.h}$ are the mass flow rate and heat capacity of the vapors, and $T_{h,i}$ and $T_{h,o}$ are the hot vapors inlet and outlet temperatures, which are known as 300 °C and 20 °C, respectively. N_2 is used to represent the hot vapors in this calculation, since N_2 is used as carrier gas which is the majority of the hot vapors. The maximum volumetric flow rate of N_2 is $\dot{V}$=100 L/min, and thereby $\dot{m}_h$ ($\dot{m}_h = \dot{V}\rho_h$) is 0.1236 kg/min. The properties of N_2 at 300 °C are given in Table 4.6. To use Eq. 4.18, we also assume that the heat loss to the surroundings (well-insulated condenser surface) and the kinetic and potential energy changes are negligible. In addition, vapor properties are constant. Thus, we calculated that the heat transfer rate from the hot vapors to the cooling fluid is 617 W.

Table 4.6 Physical properties of N_2, PG 50/50, and phenol

	N_2 @ 300 °C [18]		PG 50/50 @ -10 °C [19]		Phenol* [18]	
	Symbol	Value	Symbol	Value	Symbol	Value
Density (kg/m^3)	ρ_h	5.87 × 10^{-1}	ρ_c	1.06E+03	ρ_L	1.06 × 10^3
Dynamic viscosity (N·s/m^2)	μ_h	2.83 × 10^{-5}	μ_c	3.45E-02	μ_L	8.00 × 10^3
Heat capacity (J/kg·K)	$c_{p.h}$	1.07 × 10^3	$c_{p,c}$	3.42E+03	$c_{p,L}$	1.43 × 10^3
Thermal conductivity (W/m·K)	--	--	k_c	3.19E-01	k_L	1.90 × 10^{-1}

***** All phenols properties are evaluated at the film temperature $T_{f,L}$= 86 °C, which is the average of the condensate saturation temperature and the inner tube surface temperature.

For a counter flow concentric tube condenser, ΔT_{lm} is given below,

$$\Delta T_{lm} = \frac{\Delta T_1 - \Delta T_2}{\ln(\Delta T_1 / \Delta T_2)} \tag{4.19}$$

where

$$\Delta T_1 = T_{h,i} - T_{c,o} \tag{4.20}$$

$$\Delta T_2 = T_{h,o} - T_{c,i} \tag{4.21}$$

$T_{c,i}$ is the cooling fluid inlet temperature, which is -10 °C. $T_{c,o}$ is the cooling fluid outlet temperature, which can be calculated using following equation:

$$T_{c,o} = \frac{q}{\dot{m}_c c_{p,c}} + T_{c,i} \tag{4.22}$$

$\dot{m}_c$ and $c_{p,c}$ are the mass flow rate and the heat capacity of the cooling fluid PG 50/50. The properties of PG 50/50 are shown in Table 4.6. $\dot{m}_c$ can be obtained from the chiller pumping capacity ($\dot{V}_c$= 88 L/min) and the cooling fluid density ρ_c:

$$\dot{m}_c = \dot{V}_c \, \rho_c \tag{4.23}$$

Thus, $T_{c,o}$ = -8.1 °C is obtained. Plugging in numbers in Eq. 4.19, ΔT_{lm} is equal to 119.4 °C.

To evaluate the overall heat transfer coefficient U, we assume that surface fouling is not significant in our system. Additionally, the inner tube wall made of A240 304L stainless steel has a very small thickness and a high thermal conductivity; therefore, the thermal resistance of the tube is negligible here and $A_i = A_o = A_s$. Then, U can be expressed as:

$$\frac{1}{U} = \frac{1}{h_i} + \frac{1}{h_o} \tag{4.24}$$

where h_i and h_o are the average convection coefficients of the inside vapors and outside cooling fluid, respectively.

For the flow of hot vapors through the inner tube, the Reynolds number is

$$Re_{D,h} = \frac{4\dot{m}_h}{\pi D_i \mu_h} = 4{,}184 \tag{4.25}$$

where μ_h is the dynamic viscosity of N_2 at 300 °C (Table 4.7), since N_2 is used to represent the hot vapors. $Re_{D,h}$ is equal to 4,184 that is higher than 2,300 (critical Reynolds number), indicating the flow is turbulent inside the inner tube. Colburn [20, 21] studied the effect of turbulence on the condensate film, and his results shown in Figure 4.9 are generally used to design vertical tube condensers.

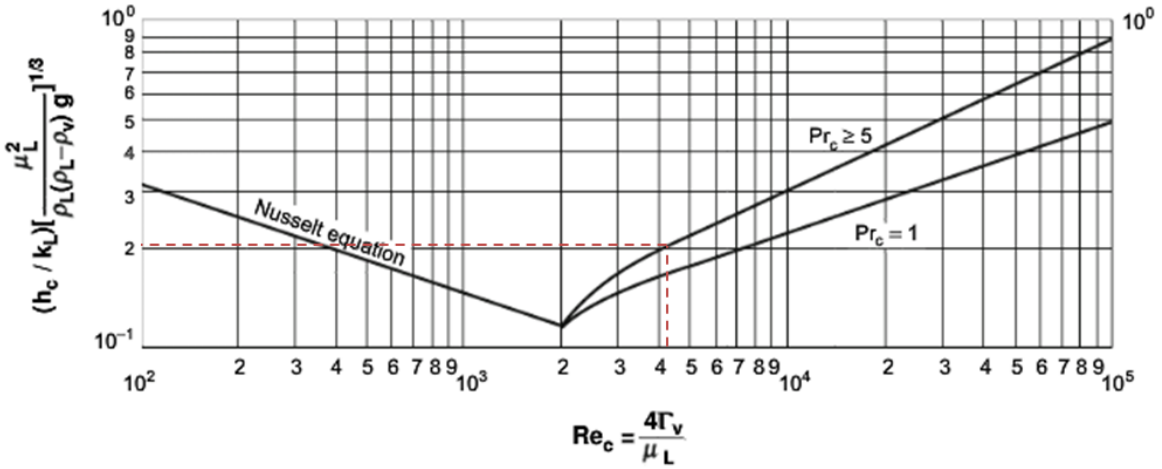

Figure 4.9 Condensation coefficient for vertical tubes [23,24]

The Prandtl number Pr_c for the condensate film shown in Figure 4.9 is given by:

$$Pr_c = \frac{c_{p,L}\,\mu_L}{k_L} \tag{4.26}$$

where $c_{p,L}$, μ_L, and k_L are the heat capacity, dynamic viscosity, and thermal conductivity of the condensate, respectively. Pyrolysis vapors are composed of hundreds of oxygenated compounds, in which phenol is one of the major components. Therefore, phenol was selected to be the representative condensate for the calculation here. The physical properties of phenol are summarized in Table 4.6. With $Re_{D,h} = 4{,}184$ and $Pr_c = 60.2 > 5$, from Figure 4.9, we can obtain:

$$\frac{h_c}{k_L}[\frac{\mu_L^2}{\rho_L(\rho_L-\rho_v)g}]^{1/3} = 2.05 \times 10^{-1} \tag{4.27}$$

and

$$h_i = h_c = 2.05 \times 10^{-1} k_L[\frac{\mu_L^2}{\rho_L(\rho_L-\rho_v)g}]^{-1/3} \tag{4.28}$$

where $\rho_L$and ρ_v ($\rho_v = \rho_h$) are the densities of the condensate and vapors (Table 4.6), and g = 9.8 m/s^2 is the standard acceleration due to gravity. Accordingly, h_i is calculated and $h_i = 216.3\ \mathrm{W/m^2 \cdot K}$.

For the flow of cooling fluid through the annulus, the hydraulic diameter is $D_h = D_o - D_i$, and the Reynolds number is

$$Re_{D,c} = \frac{\rho_c u_c D_h}{\mu_c} = \frac{4\dot{m}_c}{\pi(D_i + D_o)\mu_c} = 63 \tag{4.29}$$

where u_c and μ_c are the linear velocity and dynamic viscosity of cooling fluid (Table 4.7). We calculated that $Re_{D,o}$ is around 63, which is smaller than 2,300 (critical Reynolds number), indicating the annular flow is laminar. Assuming uniform temperature along the inner surface of the annulus and a perfectly insulated outer surface, the convection coefficient at the inner surface may be obtained from Table 4.7 [18]. With $D_i/D_o = 0.681$, linear interpolation provides

$$Nu_{i,c} = \frac{h_o D_h}{k_c} = 4.51 \tag{4.30}$$

and

$$h_o = 4.51\frac{k_c}{D_h} \tag{4.31}$$

where k_c is the thermal conductivity of the cooling fluid (Table 4.6). Hence, h_o is 138.9 W/m2·K.

Table 4.7 Nusselt number for fully developed laminar flow in circular tube annulus with one surface insulated and the other at constant temperature [18]

D_i/D_o	Nu_i	Nu_o
0	--	3.66
0.05	17.46	4.06
0.10	11.56	4.11
0.25	7.37	4.23
0.50	5.74	4.43
1.00	4.86	4.86

With $h_i = 216.3\ \mathrm{W/m^2 \cdot K}$ and $h_o = 138.9\ \mathrm{W/m^2 \cdot K}$, the overall heat transfer coefficient U is equal to 84.6 W/m$^2\cdot$ K using Eq. 4.24. At this point, all the parameters needed for the estimation of L_c are obtained. According to the Eq. 4.17, we calculated that the length of condenser needs to be at least 0.88 m (~ 35”). Considering the assumptions we made in the calculations above, a slightly longer condenser (1.14 m) was constructed and installed in the ablative pyrolysis reactor system, as shown in Figure 4.10. In the preliminary experiments; however, we found that even the condenser with a length of 1.14 m was not sufficient for condensation of all the pyrolysis vapors. This may be due to the simplifying assumption that phenol represents the composition of the pyrolysis vapors. In order to improve the performance of pyrolysis vapors condensation and increase the yield of liquid bio-oil collected, we added an impinger before the condenser, and a Swagelok coalescing filter and a packed quartz wool filter after the condenser (Figure 4.4)

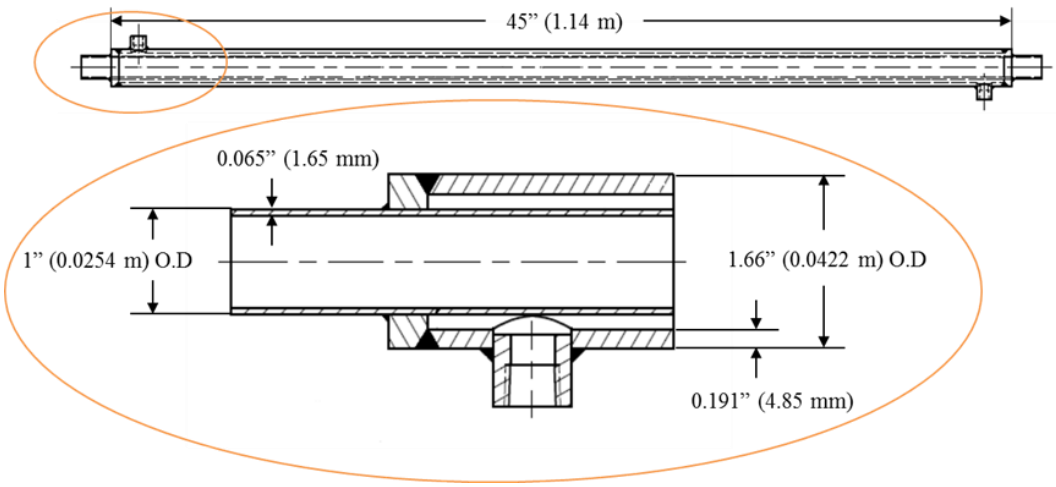

Figure 4.10 Drawing of the concentric tube condenser

4.4 REFERENCES

[1] A.V. Bridgwater, Renewable fuels and chemicals by thermal processing of biomass, Chemical Engineering Journal, 2003; 91: 87-102.

[2] A. Kumar, A conceptual comparison of bioenergy options for using mountain pine beetle infested wood in Western Canada, Bioresource Technology, 2009; 100: 387-399.

[3] Forest Concepts Completes US Department of Energy SBIR Phase I Project to Demonstrate Technical Feasibility of Milling Green and High Moisture Biomass to Biofuel Feedstocks, in, 2014.

[4] J. Lédé, Comparison of contact and radiant ablative pyrolysis of biomass, Journal of analytical and applied pyrolysis, 2003; 70: 601-618.

[5] J. Lede, J. Panagopoulos, J. Villermaux, Experimental Measurement of ablation rate of wood pieces, undergoing fast pyrolysis by contact with a heated wall, Prepr. Pap., Am. Chem. Soc., Div. Fuel Chem.;(United States), 1983; 38.

[6] A. Bridgwater, Principles and practice of biomass fast pyrolysis processes for liquids, Journal of analytical and applied pyrolysis, 1999; 51: 3-22.

[7] A.V. Bridgwater, Review of fast pyrolysis of biomass and product upgrading, Biomass and bioenergy, 2012; 38: 68-94.

[8] J. Lede, J. Panagopoulos, H.Z. Li, J. Villermaux, Fast pyrolysis of wood: direct measurement and study of ablation rate, Fuel, 1985; 64: 1514-1520.

[9] J. Diebold, J. Scahill, Ablative pyrolysis of biomass to olefins and aromatic liquids in a vortex reactor, in: Winter National Meeting of the AIChE, Atlanta, GA, 1984.

[10] J. Diebold, A. Power, Engineering aspects of the vortex pyrolysis reactor to produce primary pyrolysis oil vapors for use in resins and adhesives, in: Research in Thermochemical Biomass Conversion, Springer, 1988, pp. 609-628.

[11] T.B. Reed, Contact Pyrolysis in a "Pyrolysis Mill", in: Research in Thermochemical Biomass Conversion, Springer, 1988, pp. 192-202.

[12] H. Martin, J. Lédé, H. Li, J. Villermaux, C. Moyne, A. Degiovanni, Ablative melting of a solid cylinder perpendicularly pressed against a heated wall, International journal of heat and mass transfer, 1986; 29: 1407-1415.

[13] T.B. Reed, C.D. Cowdery, Heat flux requirements for fast pyrolysis and a new method for generating biomass vapor, in: 193rd National Meeting of the American Chemical Society, American Chemical Society Division of Petroleum Chemistry, 1987, pp. 5-10.

[14] G. Peacocke, A. Bridgwater, Ablative plate pyrolysis of biomass for liquids, Biomass and Bioenergy, 1994; 7: 147-154.

[15] AK Steel, 304/304L Stainless Steel Product Data Bulletin.

[16] C. Kafali, S. Fathali, M. Grigoriu, A.S. Whittaker, Static and kinetic coefficients of friction for rigid blocks, Multidisciplinary Center for Earthquake Engineering Research MCEER, 2007.

[17] J. Meriam, L. Kraige, Engineering Mechanics-Statics-Volume 1, Dynamics, in, John Wiley & Sons, 1993.

[18] T.L. Bergman, F.P. Incropera, A.S. Lavine, Fundamentals of heat and mass transfer, John Wiley & Sons, 2011.

[19] DOWFROSTTM, Engineering and Operating Guide for DOWFROST and DOWFROST HD Inhibited Propylene Glycol-based Heat Transfer Fluids.

[20] A.P. Colburn, O.A. Hougen, Design of cooler condensers for mixtures of vapors with noncondensing gases, Industrial & Engineering Chemistry, 1934; 26: 1178-1182.

[21] R.K. Sinnott, Chemical engineering design,4th ed, Elsevier Butterworth-Heinemann, 2005.

CHAPTER 5. PYROLYSIS OF BEETLE-KILLED WOOD CHIPS IN A NOVEL ABLATIVE REACTOR: DESIGN AND INITIAL RESULTS[3]

5.1 ABSTRACT

We designed and constructed a novel lab-scale ablative reactor for fast pyrolysis of entire wood chips and even wood rods, converting them directly into bio-oil for the first time, at yields of 47-60 wt. %. This novel reactor provides a path that can eliminate grinding costs (~7-9% of overall costs) in pyrolysis. Experimental measurements and modeling work have confirmed that radiation from the hot components does not significantly decompose the wood prior to direct contact with the hot metallic surface in ablative pyrolysis. Wood samples from beetle-killed lodgepole pine (2 × 2 mm wood crumbles, 5 × 15 mm and 10 × 20 mm wood chips, and a 35 dia. × 200 mm wood rod) have been pyrolyzed in the ablative reactor to verify the effect of particle size on the product yield and distribution. The bio-oil yield from fast pyrolysis of wood chips (5 × 15 mm and 10 × 20 mm wood chips) was as high as 60 wt. %, similar to that from 2 × 2 mm wood crumbles. In addition, the yield and composition of bio-oil from ablative pyrolysis were in the same range as those obtained from a fluidized bed reactor with < 1 mm particles, with the small differences (slightly lower yield and HHV, and higher water content) attributed to the longer vapor residence times in the ablative reactor, which promote secondary reactions.

5.2 INTRODUCTION

Lignocellulosic biomass is an abundant and carbon-neutral renewable energy resource, and the chemicals and fuels derived from it have a tremendous potential to reduce the problems caused by our dependence on fossil fuels [1]. Fast pyrolysis is one of the promising technologies to convert lignocellulosic biomass into liquid fuels or chemicals, and it has been developed for over 30 years.

[3] To be submitted.

In this process, biomass is heated up to 400-600 °C at a very high heating rate (~500 °C/s) in the absence of oxygen, whereby it decomposes into organic vapors, solid char, and permanent gases[2, 3]. The organic vapors are rapidly cooled down and condensed to a liquid product, known as bio-oil, which is the main product of fast pyrolysis. Depending on feedstocks, the yield of bio-oil can exceed 70 wt. % on dry feed [2, 3]. Bio-oil can either be combusted in boilers, engines, or turbines to generate heat or power, or be upgraded to produce transportation fuels and commodity chemicals [2-5].

Fast pyrolysis has been extensively studied for different feedstocks including agricultural, woody, and algal biomass [6-9]. In this study, beetle-killed trees were selected as feedstock. To date, about 42 million acres of forests have been attacked by bark beetles in the western United States, and this number is expected to increase in the near future [10]. The high level of tree mortality caused by bark beetle epidemic leads to severe falling of trees, threatening the public safety and increasing the severity of wildfire [10]. Thus, beetle-killed trees should be properly disposed of. However, some undesirable properties (e.g. bluish discoloration and cracking) of beetle-killed trees limit their applications for solid wood and wood panel manufacturing [11]. Nevertheless, low moisture content of these trees makes them an excellent feedstock for fast pyrolysis, because the costs of biomass drying can be reduced or even eliminated. In addition, our previous research using Py-GC/MS-FID showed that the decay stages of beetle-killed trees did not significantly affect the performance of fast pyrolysis, indicating fast pyrolysis is a promising way to convert beetle-killed trees into high-value chemicals and fuels [12].

The reactor is the key component of a fast pyrolysis system. Many types of reactors including fluidized bed reactor, circulating fluidized bed reactor, free-fall reactor, auger reactor, rotating cone reactor, and ablative reactor have been developed. For most pyrolysis reactor configurations,

the biomass feedstock needs to be ground into small particles of around 2 mm, because the process requires maximizing temperature gradients inside the particle [13]. Kumar estimated that the costs of biomass chipping and grinding were about 7-9% of the overall production costs [14]. Forest Concepts also studied the effects of final wood particle size on the total comminution energy cost for the optimized Crumbler® machine, and found out that the comminution energy cost increases from nearly zero to up to $4.5 per US ton as wood particle size is reduced from 12 mm to 1-2 mm [15]. Fortunately, the ablative pyrolysis reactor provides an opportunity to use large pieces of wood instead of only small particles as feedstock, saving on grinding costs. In ablative pyrolysis, biomass undergoes melting and/or sublimation reactions as it directly contacts a hot solid surface. There is a steep temperature gradient at the biomass surface, leading to the formation of a thin superficial layer of reacting solid [16, 17]. The reacting layer moves at constant velocity towards the heart of the cold biomass. Therefore, the reactive process in the ablative reactor takes place only at the superficial layer rather than the entire biomass particle, and reaction rates are not limited by the heat transfer through the entire particle. For this reason, in principle there is no upper limit to the biomass particle size that can be processed. These characteristics have been speculated in the past, but there were no experimental data to back up the claim that fast pyrolysis of large pieces of wood is possible.

To date, only a few ablative pyrolysis reactors have been developed. The first pioneering experiments with ablative pyrolysis were reported by Diebold [18], who used an electrically heated wire to cut pieces of wood. These experiments demonstrated that biomass could be rapidly pyrolyzed via ablation, producing a thin layer of liquid that vaporizes. Lédé et al. did a fundamental study on the ablation heat transfer with specific application to wood pyrolysis [16, 19-21]. However, their experimental setup did not allow the overall product recovery for analytical study

and mass balance calculation. Reed and Cowdery [22] designed and constructed a "pyrolysis mill" based on the principles of a conventional grain mill. Liquid bio-oil yield of up to 48.6% (dry basis) was obtained. However, the particle size of their feedstock, pine sawdust, was only as high as 14 mesh (1.4 mm). The major problem of this system was the slow escape of the pyrolysis vapors from the reactor, lowering the yield of bio-oil. Later, Peacocke et al. [23] designed an ablative reactor system with four rotating blades scrapping a continuous feed of pine wood, and up to 67.7% of bio-oil yield on dry feed has been reported. One limiting factor of this setup was the difficult removal of the char formed on the reactor surface. The char built up below the rotating blades can quickly prevent the incoming particles from being ablated. The particle size of the pine wood feedstock was 4.75-6.25 mm, which was the largest particle size reported for tests in this system. Thus, we herein designed and constructed a novel lab-scale ablative reactor to convert entire wood chips and wood rods into high yield of bio-oil, confirming the characteristic of ablative pyrolysis that reaction rates are not limited by heat transfer through the particle. To the best of our knowledge, our work is the first to report bio-oil production from fast pyrolysis of entire wood chips and wood rods. The results from the ablative reactor were compared to those obtained using a lab-scale fluidized bed reactor. In addition, the effect of pre-heating in this semi-batch reactor on the ablative pyrolysis of wood chips was evaluated prior to the run using both modeling work and experimental measurements.

5.3 ABLATIVE PYROLYSIS REACTOR AND ITS OPERATION

The ablative reactor is composed of a chamber, which contains a spinning bowl where the wood chips can be placed, and a hot plate at the top which can move down and apply pressure against wood chips. Fast pyrolysis initiates as the hot plate contacts the wood chips, and the inert gas at a high flow rate then rapidly sweeps the generated vapors out of the chamber for condensation.

5.3.1 Reactor description

The ablative pyrolysis reactor designed and constructed in the present work is shown in Figure 5.1. This is a semi-batch system with a capacity of 500 g wood chips per run. The reactor chamber is made of A240 304L stainless steel with an internal diameter of 0.30 m and an internal height of 0.42 m. This chamber can be split into an upper chamber and lower chamber, which are connected with flanges. A static seal is created by a graphite gasket placed between the two flanges faces. The wood chip bowl made of A240 304L stainless steel has an internal diameter of 0.21 m and a height of 0.09 m. In order to make the generated pyrolysis vapors escape from the wood chip bowl quickly, 0.05 × 0.01 m rectangular slots were made on the shell of the bowl. To prevent wood chips from dropping out of the bowl from the slots, a 1 mm thick perforated T304 liner with 1.6 mm holes on a 3.2 mm 60° triangular pitch was installed inside the shell. The wood chip bowl is driven by a 3 HP SEW-EURODRIVE gear motor, providing a rotation speed up to 160 rpm. The lower chamber contains a gas inlet and a gas outlet. To minimize the vapor residence time, the product vapors escaped out of the chamber through a perforated tube bent around the circumference of the bowl. The upper plate is driven by a piston connected to a hydraulic system, capable of moving vertically and applying a maximum pressure of 1.5 bar against the wood chips. The lower and upper drive shafts housing on the reactor chamber contain graphalloy bushings to prevent leakages and ingress of air. Three 1 kW Chromalox CIR cartridge heaters were inserted in the upper plate, and are capable of generating a heat flux up to 105 W/m^2 and heating the plate up to 700 °C. Furthermore, two band heaters (Chromalox HBT 120) were used to heat the reactor wall to a minimum temperature of 300 °C, minimizing the condensation of pyrolysis vapors on the inner reactor wall. Each of the band heaters has a power of 2 kW. The temperatures of the cartridge heaters and band heaters are measured and controlled by inbuilt type K thermocouples that are

connected to Chromalox 1/4 DIN temperature controllers. To minimize the heat losses, the entire reactor chamber was insulated using two layers of 1.3 cm thick ceramic sheets and one layer of silica fabric wrap.

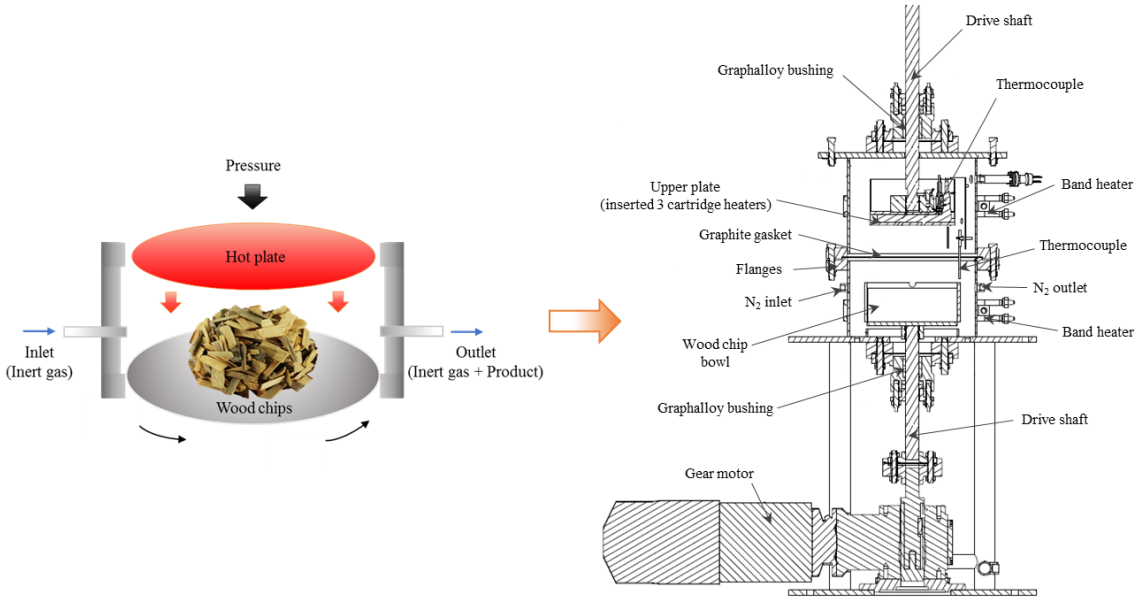

Figure 5.1 Ablative pyrolysis reactor

5.3.2 Reactor operation

Figure 5.2 shows the schematic diagram of the system including reactor, condenser, and gas meter, etc. Prior to the reaction, a specified amount of wood chips is loaded on the wood chip bowl. After sealing the reactor chamber, the upper plate and the reactor wall are pre-heated to the operating temperatures. During the pre-heating time, the upper plate is located at the highest position. The distance between the upper plate and the wood chip bowl bottom is about 0.23 m to minimize the slow pyrolysis of biomass caused by radiation heat transfer during the pre-heating time. At the same time, room temperature N_2 is used as carrier gas being introduced into the system from the gas inlet at the reactor wall. The flow rate of N_2 is controlled by an Aalborg mass flow controller. Once the upper plate and reactor wall reach the operating temperatures, the wood chip bowl driven by the motor starts to rotate, and the upper plate driven by the hydraulic system starts moving

down towards the wood chips. Ablative contact of the hot upper plate with the wood chips initiates fast pyrolysis. The produced pyrolysis vapors then carried by N_2 quickly escape from the reactor chamber through the gas outlet and enter a multi-stage bio-oil collection system. The first stage is an ice-water cooled impinger, which collects the heavy fractions of the bio-oil. The second stage is a counter-current double-pipe condenser, of which 50/50 vol. % propylene glycol/water is used as cooling fluid in the outer pipe, with an inlet temperature of -10 °C. This stage collects the light (aqueous) fraction of bio-oil. The remaining cooled vapors and non-condensable gases flow through a Swagelok coalescing filter and a packed quartz wool fiber which collect any residual aerosols and water vapors. In addition, building vacuum was connected to the system to drive the pyrolysis vapors out of the reactor chamber. However, the non-condensable gases are sent to the retriever and cannot be collected for further analysis with only building vacuum installed. Thus, a parallel GAST vacuum with a gas outlet was installed for a few runs for gas quantification and overall mass balance calculation, though this slightly decreased bio-oil yield (more details are discussed in section 5.5.1). The specifications of both building vacuum and GAST vacuum pump are summarized in Table 5.1. Solid char is left on the wood chip bowl.

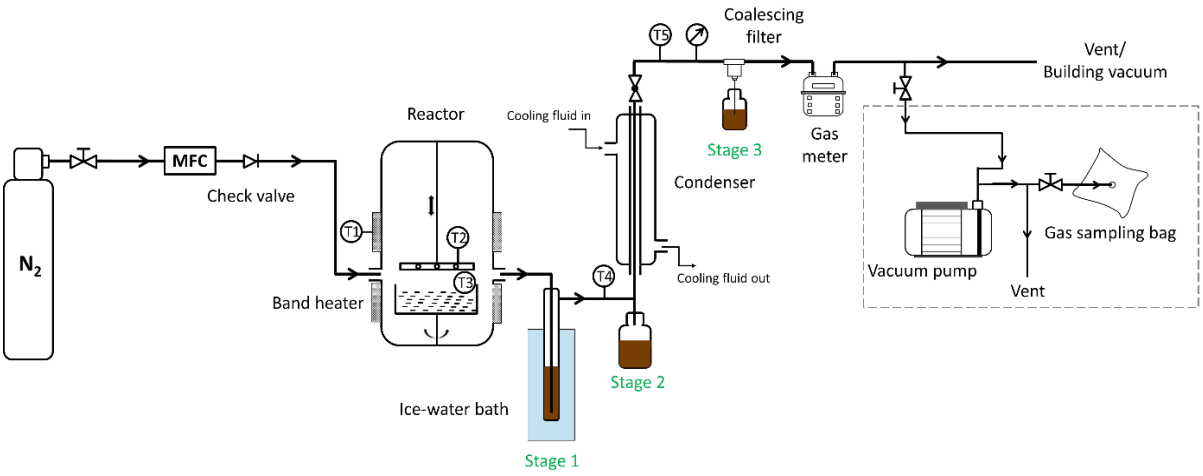

Figure 5.2 Schematic diagram of the system

Table 5.1 Specifications of the building vacuum and GAST vacuum pump

	Building vacuum	Vacuum pump
HP	4.7 HP	0.25 HP
Flow rate	1.7 cfm	1.4 cfm
Vacuum level	22-25” Hg	25” Hg

5.4 MATERIAL AND METHODS

5.4.1 Feedstock

The feedstock used in this study was beetle-killed lodgepole pine (*Pinus contorta)* purchased from Forest Concepts, LLC. These trees were standing dead trees without needles, and 2-4 years after death. Prior to the experiment, the feedstock was chipped, ground, and sieved into three different sizes: 2 × 2 mm, 5 × 15 mm, and 10 × 20 mm. Moreover, a small wood rod sample (35 dia. × 200 mm) was used. All of these samples are shown in Figure 5.3. The composition of the feedstock is given in Table 5.2.

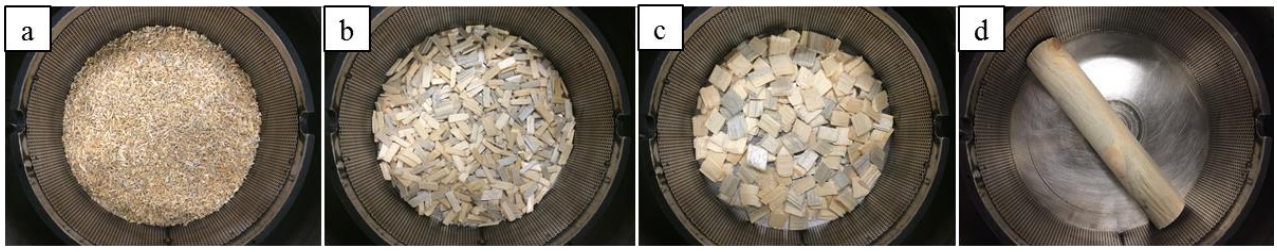

Figure 5.3 Picture of biomass feedstock in the wood chip bowl. a) 2 × 2 mm wood crumbles®; b) 5 × 15 mm wood chips; c) 10 × 20 mm wood chips, and d) 35 dia. × 200 mm wood rod.

Table 5.2 Composition of beetle-killed lodgepole pine feedstock[12, 24]

Proximate analysis (wt. %)			
Moisture	Ash	Volatile	Fixed carbon
7.30	0.26	82.29	10.15
Ultimate analysis (wt. %) [a]			

C	H	O	N
49.62	6.37	43.29	0.44
Chemical composition (wt. %) [a]			
Extractives [a]	Carbohydrates [b]	Lignin [b]	
5.48	61.18	28.84	

a. wt. % of oven dry wood
b. wt. % of oven dry extractive-free wood

5.4.2 Fast pyrolysis in ablative reactor

The ablative pyrolysis reactor system described in section 5.3 was used to carry out the fast pyrolysis of wood chips experiments. Except for the small wood rod (100 g), 50 g wood crumbles or chips were used for each run. All the experiments reported herein were conducted at a pyrolysis temperature (upper plate temperature) of 500 or 550 °C with a reactor wall temperature of 300 °C. The applied pressure against the wood chips was 0.5 bar, the rotation speed of the wood chip bowl was 100 rpm, and the reaction time was 3 min. N_2 was used as carrier gas. The selection of N_2 flow rate and vacuum suction is discussed in section 5.5.1. After reaction, the char left on the wood chip bowl was collected and weighed to determine the yield. Before and after each experiment, the impinger, condenser, and filter were weighed to calculate the total bio-oil yield. Non-condensable gases were quantified when a parallel vacuum pump was installed. The total volume of non-condensable gases was equal to the difference of the final and initial gas meter reading subtracted the total volume of N_2 carrier gas. An average molecular weight was determined by GC/TCD-FID analysis. Assuming the non-condensable gases as an ideal gas, the mass produced was then calculated using the ideal gas law.

5.4.3 Fast pyrolysis in fluidized bed reactor

For comparison purposes, fast pyrolysis of beetle-killed lodgepole pine samples was also carried out in a lab-scale continuous fluidized bed reactor. The schematic diagram of the reactor is shown in Figure 5.4. In this system, the beetle-killed lodgepole pine sample was first ground and sieved to a particle size of < 1 mm to ensure rapid heat transfer rates in the reactor. The biomass was then placed in the hopper. While the system was pre-heated, N_2 was used to purge any oxygen present in the system. When the system reached 500 °C, biomass at a rate of 0.6 kg/h was fed into the reactor by the screw auger. The reactor is a straight tube with an inner diameter 0.038 m and a length of 0.9 m. 500 g alumina sand was used as heating media. N_2 with a flow rate of 30 SLPM was used as carrier gas and the residence time of pyrolysis vapors in the reactor was around 1 s. At the outlet of the reactor, a cyclone was used to separate the char from pyrolysis vapors at a temperature of 325 °C. Vapors then flowed through an impinger, three-stage counter-current double-pipe condensers (at 5 °C), and a coalescing filter for condensation. Non-condensable gases were collected at the end of the system using a gas sampling bag. The char and sand were removed from the reactor and cyclone and weighed when they were cooled to room temperature. The mixture was then burned in a muffle furnace at 600 °C for 6 h, and the residues were weighed after cooling down for determination of char yield. The yield of bio-oil and non-condensable gases were determined in a similar way to what is reported for the ablative unit.

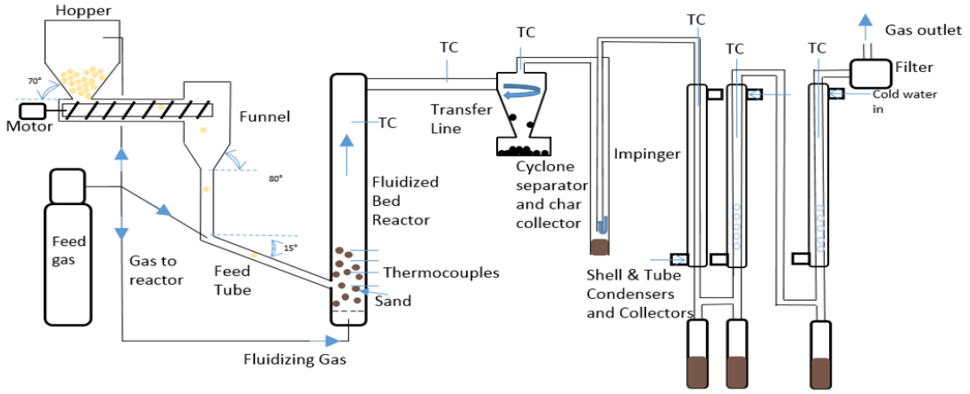

Figure 5.4 Schematic diagram of the fluidized bed reactor system

5.4.4 Product analysis

All bio-oil samples were stored in a refrigerator before analysis. The moisture content of bio-oil was determined using a Karl Fischer titrator (V20, Mettler Toledo). The test method followed the ASTM E203 standard for water using Hydranal-composite 5 K reagent. GC/MS-FID (QP2010, Ultra, Shimadzu) was used to determine the chemical composition of bio-oil using methanol as solvent. The separation of different compounds was achieved by a SHRXI-5MS capillary column (30 m × 0.25 mm I.D. × 0.25 μm film thickness). The GC inlet temperature was 300 °C, and the inlet split ratio was 30: 1. The oven temperature was programmed from 40 °C to 300 °C with a ramp of 10 °C/min. The initial and final temperatures were held for 4 and 5 min, respectively. Compounds in bio-oil were identified by mass spectra comparison with NIST 2010 library, and were quantified by FID using external standards. The elemental composition of bio-oil and biochar were measured using an elemental analyzer (Series II 2400, PerkinElmer). The collected non-condensable gases were analyzed using GC/TCD-FID with a SUPELCO 60/80 Carboxen-1000 packed column (4.6 m × 2.1 mm I.D. × 0.5 μm film thickness). Helium with a flow rate of 35 mL/min was used as carrier gas. The oven temperature was programed from 40 °C (5 min) to 225

°C (10 min) at a heating rate of 20 °C/min. Standard curves were prepared from individual gas (i.e. N_2, CH_4, CO, and CO_2) for quantification.

5.5 RESULTS AND DISCUSSION

5.5.1 Minimizing the vapor residence times

Short vapor residence time is one of the requirements for fast pyrolysis, leading to a high yield of liquid bio-oil. Long vapor residence times promote secondary reactions of pyrolysis vapors, favoring gas and char production [25, 26]. In our ablative pyrolysis reactor, the N_2 flow rate is an important parameter affecting the vapor residence time. Thus, the effect of N_2 flow rate on the product yield has been studied, and the results are shown in Table 5.3. All the experiments were performed using 5 × 15 mm wood chips at 550 °C. As the N_2 flow rate increased from 15 to 40 SLPM, the yield of bio-oil only slightly increased from 41.6 wt. % to 43.0 wt. % and char yield slightly decreased from 26.0 wt. % to 23.7 wt. %. Both conditions showed low yields of bio-oil and high yields of char, indicating the occurrence of secondary reactions to a large extent.

Table 5.3 Product yield at different N_2 flow rates and vacuum conditions

N_2 flow rate (SLPM)	15	40	15	0	15
Vacuum condition	No	No	B	B	B + P
Product yield (wt. %)					
Bio-oil	41.6	43.0	52.8	48.4	47.0
Char	26.0	23.7	19.7	26.1	26.4
Non-condensable gases	NA	NA	NA	NA	15.8

B: building vacuum; P: vacuum pump; NA: not available

The use of vacuum in fast pyrolysis has been investigated by previous works and showed advantages of shortening vapor residence time and reducing occurrence and intensity of secondary reactions, thereby improving bio-oil yield [27, 28]. Thus, building vacuum was used in our reactor

system, of which the specifications were given in Table 5.1. Two experiments were performed using building vacuum with 15 SLPM N_2 flow rate or without N_2 flow rate. Both conditions increased bio-oil yield, and the utilization of building vacuum combined with 15 SLPM N_2 flow rate significantly increased bio-oil yield by more than 10 wt. %, decreasing char yield by 6 wt. %. Therefore, N_2 flow rate of 15 SLPM and building vacuum were selected to use for rest of the experiments in this study. One disadvantage of using building vacuum is that non-condensable gases could not be analyzed and quantified. In order to quantify the gas production and thereby calculate the total mass balance, a vacuum pump with a gas outlet was installed in parallel. From this run, the bio-oil, char, and non-condensable gases yields were 47 wt. %, 26 wt. % and 15.8 wt. %, respectively. The total mass balance was about 90 wt. %. The composition of non-condensable gases was analyzed in GC/TCD-FID, including 38.5 wt. % of CO, 57.3 wt. % of CO_2, and 4.2 wt. % of CH_4. The relatively lower bio-oil yield and higher char yield resulted from the longer residence time caused by weaker suction in the parallel vacuum system.

5.5.2 Wood chips temperature during the pre-heating time

The ablative pyrolysis reactor we designed is a semi-batch reactor. Prior to heating up the system, wood chips are loaded on the wood chip bowl. Due to the radiation from the hot components, the temperature of the wood chips may increase as we pre-heat the upper plate and reactor wall to the operating temperature. However, biomass has been reported to slowly decompose at about 200 °C, which negatively affects bio-oil yield [29]. Thus, prior to ablative pyrolysis, the temperature profile of the wood chips during pre-heating time in our system was evaluated and controlled to minimize the extent of slow pyrolysis before the run.

During the pre-heating time, the wood chips on the bowl exchanged heat with the upper plate, the reactor wall, and the N_2 gas via conduction, convection, and radiation. Since the wood chips

did not directly contact the hot components of the reactor, we are neglecting conduction. Then the total heat rate can be expressed as:

$$q_{total} = q_{conv} + q_{rad} \tag{5.1}$$

where q_{conv} and q_{rad} are convection and radiation heat rates, respectively.

Employing Newton's law of cooling,

$$q_{conv} = \overline{h_{bowl}} A_{bowl}(T_{N_2} - T_{wood}) \tag{5.2}$$

where $\overline{h_{bowl}}$ is the average convection coefficient, A_{bowl} is the area of the wood chip bowl bottom surface, and $T_{N_2}$and T_{wood} are the temperature of N_2 carrier gas and wood chips, respectively. In our ablative system, room temperature N_2 with a volumetric flow rate of 15 SLPM was continuously introduced into the reactor chamber and flowed over the top of wood chips; therefore, $T_{N_2}$was considered as a constant, $T_{N_2} = 20$ ℃. $\bar{h}$ was estimated by correlations for flow over a flat surface [30],

$$\bar{h} = 0.664\, Re_L^{\frac{1}{2}} Pr^{\frac{1}{3}} \frac{k}{L_{bowl}},\ when\ Re_L \le Re_{x,c} \tag{5.3}$$

or

$$\bar{h} = \left[0.664\, Re_{x,c}^{\frac{1}{2}} + 0.037 \left(Re_L^{\frac{4}{5}} - Re_{x,c}^{\frac{4}{5}}\right)\right] Pr^{\frac{1}{3}} \frac{k}{L_{bowl}},\ when\ Re_L > Re_{x,c} \tag{5.4}$$

in which L_{bowl} is the length for the flow, which is equal to the diameter of wood chip bowl. Re_L is the Reynolds number over the entire wood chip surface, and $Re_{x,c} = 5 \times 10^5$ is the critical Reynold number. *k*, *Pr*, and *v* are the thermal conductivity, Prandtl number, and dynamic viscosity of N_2, all of which are functions of temperature.

The radiation heat that reaches the wood chips includes radiation components from the upper plate and reactor wall. Employing the Stefan-Boltzmann law,

$$q_{rad} = q_{plate} + q_{wall}$$

$$= \varepsilon\sigma A_{plate}F_{13}\left(T_{plate}^4 - T_{wood}^4\right) + \varepsilon\sigma A_{wall}F_{23}(T_{wall}^4 - T_{wood}^4) \quad (5.5)$$

where ε is the emissivity of coefficient of A240 304L stainless steel material (ε = 0.67) [30], σ is the Stefan-Boltzmann constant (σ = 5.67 $\times 10^{-8}$ W/m^2 ·K^4), A_{plate} and A_{wall} are the surface area of upper plate and reactor wall, T_{plate} and T_{wall} are the temperatures of the upper plate and reactor wall, and F_{13} and F_{23} are the view factors.

The temperatures of the upper plate and reactor wall, T_{plate} and T_{wall}, are functions of time and were evaluated using energy balances. During the pre-heating time, the upper plate mainly loses heat to N_2 by convection and to the reactor wall by radiation. The reactor wall was well insulated outside, and we assume that the heat loss of the reactor wall inside by convection and the heat absorption by radiation neutralize each other. The energy balances for the top plate and reactor wall are:

$$E_{g,p}\eta_p - \left[\overline{h_{plate}}\left(T_{plate} - T_{N_2}\right)\right] + \varepsilon\sigma F_{12}(T_{plate}^4 - T_{wall}^4)]A_{plate} = \rho_{ss}V_{plate}C_{p,ss}\frac{dT_{plate}}{dt} \quad (5.6)$$

$$E_{g,w}\eta_w = \rho_{ss}V_{wall}C_{p,ss}\frac{dT_{wall}}{dt} \quad (5.7)$$

where $E_{g,p}$ and $E_{g,w}$ are equal to the power of cartridge heaters and band heaters, η_p ($\eta_p = 0.75$) and η_w ($\eta_w = 0.95$) are their efficiencies, V_{plate} and V_{wall} are the volume of the upper plate and reactor wall, A_{plate} is the surface area of upper plate, and ρ_{ss} and $C_{p,ss}$ are the density and heat capacity of stainless steel. $\overline{h_{plate}}$ is the average convection coefficient, which can be calculated similarly to $\overline{h_{bowl}}$ (Eq. 5.3 and 5.4) by replacing L_{bowl} with the length of the upper plate.

A view factor F_{ij} is defined as the fraction of the radiation leaving surface *i* that is intercepted by surface *j* [30]. According to Figure 5.5, F_{13} and F_{23} represent the fraction of radiation leaving the upper plate and reactor wall that is absorbed by the wood chips, and F_{12} represents the fraction

of radiation leaving the upper plate that is absorbed by the reactor wall. The value of the view factor depends on the surface shape, the distance and orientation between the two surfaces.

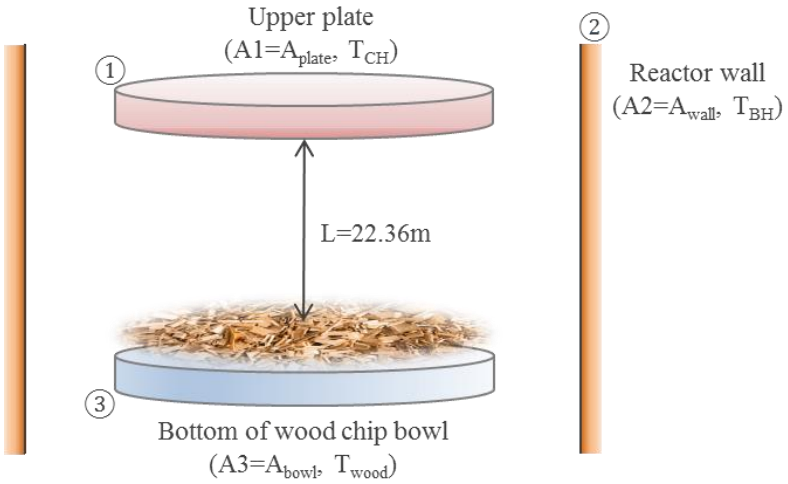

Figure 5.5 Schematic diagram for radiation heat rate calculation

For two coaxial parallel disks, like the upper plate and wood surface in our reactor, the view factor is given as follows [30]:

$$F_{31} = \frac{1}{2}[S - \sqrt{S^2 - 4(\frac{R_1}{R_3})^2}\,] \tag{5.8}$$

in which,

$$S = 1 + \frac{1+{R_1}^2}{{R_3}^2} \tag{5.9}$$

$$R_1 = \frac{r_1}{L} \tag{5.10}$$

$$R_3 = \frac{r_3}{L} \tag{5.11}$$

where r_1 and r_3 are the radius of the wood chip bowl and upper plate, and L (L = 0.2236 m) is the distance between the upper plate and the top of the wood chips during the pre-heating time.

Based on the reciprocity relation [30],

$$F_{13} = \left(\frac{A_3}{A_1}\right) F_{31} = \left(\frac{A_{bowl}}{A_{plate}}\right) F_{31} \tag{5.12}$$

From the summation rule that states all radiation leaving one surface must be intercepted by other surfaces in the enclosure [30], we also obtain:

$$F_{11} + F_{12} + F_{13} = 1 \tag{5.13}$$

$$F_{31} + F_{32} + F_{33} = 1 \tag{5.14}$$

Since radiation travels in a straight line, no radiation can leave a non-concave surface and hit the same surface later. So, $F_{11} = 0$ and $F_{33} = 0$. Then,

$$F_{12} = 1 - F_{13} \tag{5.15}$$

and

$$F_{32} = 1 - F_{31} \tag{5.16}$$

Using the reciprocity relation again,

$$F_{23} = \left(\frac{A_3}{A_2}\right) F_{32} = \left(\frac{A_{bowl}}{A_{wall}}\right) F_{32} \tag{5.17}$$

With this, all the parameters in Eq. 5.1 have been obtained, and the total heat transfer rate to the wood chips is expressed as a function of time and T_{wood}. In order to simulate the temperature profile of wood chips as a function of pre-heating time, a numerical integration has been employed, where the total time can be divided by a small time interval (Δt = 1s). According to the energy balance within the time interval, the temperature of biomass after each time interval is given below:

$$T_{wood}^{i+1} = T_{wood}^{i} + \frac{q_{total}^{i} \Delta t}{m_{wood} C_{p,wood}} \tag{5.18}$$

where T_{wood}^{i} and T_{wood}^{i+1} are the temperatures of wood chips at the beginning and at the end of the time interval, respectively. m_{wood} is the mass of wood chips ($m_{wood} = 50\ g$) and $c_{p,wood}$ is the heat capacity of wood, which is also a function of T_{wood}. Using Matlab, the graphical description of how the temperature of the wood chips varies with the pre-heating time is obtained and compared with the experimental measurements in Figure 5.6. As the temperatures of the upper

plate and the reactor wall increase, the temperature of the wood chips gradually increases. When the upper plate is at 550 °C and the reactor wall is at 300 °C, temperature of the wood chips is around 200 °C. This indicates that the extent of slow pyrolysis of wood chips during the pre-heating time in the semi-batch ablative reactor is small. The results derived from our calculation are in good agreement with the real measurements.

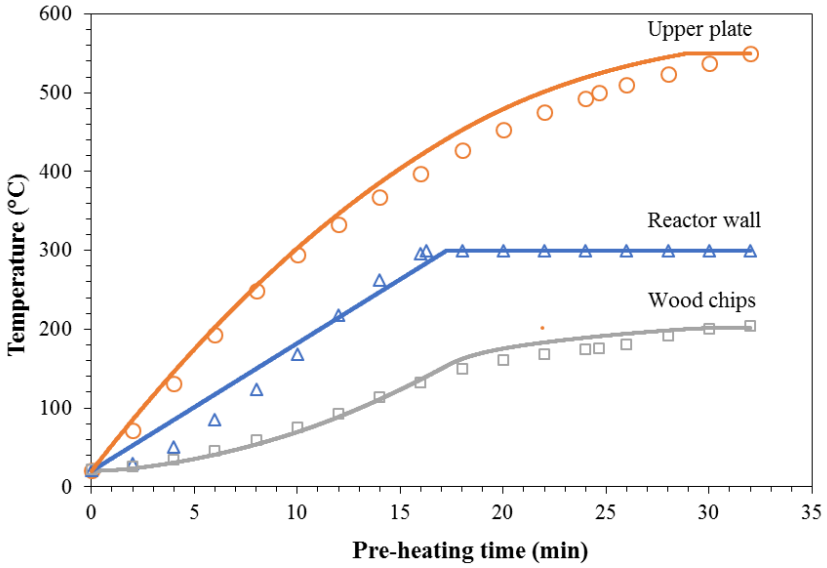

Figure 5.6 Temperature profile of the wood chips during pre-heating time (solid lines represent results from calculation; orange circle, blue triangle, and grey square represent data from measurements)

5.5.3 Ablative pyrolysis of wood crumbles, chips, and rods

Feedstock particle size is one of the important operating parameters in fast pyrolysis, influencing the final product yield and distribution. In most types of pyrolysis reactors, biomass particles are required to be very small (1-2 mm) to provide rapid heating and achieve a high yield of bio-oil [13]. Salehi et al. studied the effect of wood sawdust particle size on the pyrolysis product yield using a fluidized bed reactor [31]. As the particle size increased from < 590 to 1000-1400 μm, the heating rate of the sawdust particle decreased by one order of magnitude and thereby the yield of

bio-oil significantly decreased from 62% to 52% [31]. Shen et al. also investigated the effect of particle size on the fast pyrolysis of oil mallee woody biomass in a fluidized bed reactor, and they found that the bio-oil yield dramatically decreased by 12-14% as biomass particle size increased from 0.3 mm to 1.5 mm [32]. The novel ablative pyrolysis reactor we designed and constructed in this study aims to convert entire wood chips into a high yield of bio-oil. The wood samples with different particle sizes (i.e. 2 × 2 mm wood crumbles, 5 × 15 mm and 10 × 20 mm wood chips, and a 35 dia. × 200 mm wood rod) have been used as feedstocks in our ablative reactor to study the effect of particle size on the product yield and distribution. All these experiments were operated at a pyrolysis temperature of 500 °C, with N_2 carrier gas at a flow rate of 15 SLPM and building vacuum suction as well. Figure 5.7 shows the product yield as a function of particle size, in which the gas yield was calculated by difference assuming 90 wt. % was the total mass balance for each run (section 5.5.1). In addition, replicates were performed using 5 × 15 mm and 10 × 20 mm wood chips to obtain standard deviations for the yield of bio-oil (± 1.4 wt. %), char (± 0.9 wt. %), and non-condensable gases (± 0.6 wt. %), and the standard deviations obtained from 10 × 20 mm were applied to the results from 2 × 2 mm wood crumbles and 35 dia. × 200 mm wood rod. Considering the standard deviations, there was no difference in yields between the 2 mm crumbles and the 5 × 15 mm and 10 × 20 mm wood chips. The yields of bio-oil, char, and non-condensable gases were about 60 wt. %, 18 wt. %, and 13 wt. %, respectively. These results support the hypothesis that the size of the wood chips does not affect the ablative process [16]. The system also successfully pyrolyzed an entire wood rod (35 dia. × 200 mm), though this case shows lower yield of bio-oil (47 wt. %) and higher yield (25 wt. %) of char and non-condensable gases (18 wt. %) than wood chips. 50 g of wood crumbles/chips loading in the wood chip bowl resulted in around 5 mm thickness, whereas the thickness of the wood rod was 35 mm. Using the wood rod as feedstock;

therefore, possibly led to more char due to the poor thermal conductivity of the wood and char, lowering the bio-oil yield.

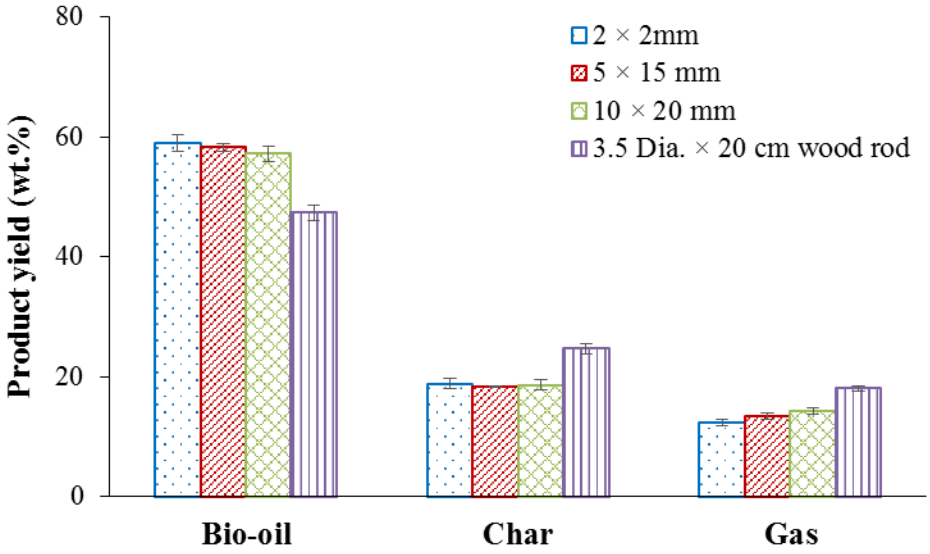

Figure 5.7 Product yield from ablative pyrolysis of wood crumbles, chips, and rods

5.5.4 Comparison with a lab-scale fluidized bed reactor

The fluidized bed reactor is one of the most popular reactor configurations for fast pyrolysis of biomass due to its high bio-oil yield and ready scale-up [2]. Thus, the results from fast pyrolysis of wood chips (10 × 20 mm) in our ablative pyrolysis reactor were compared to those obtained from a lab-scale fluidized bed reactor, using the same feedstock and pyrolysis temperature (500 °C), but a much smaller particle size (<1 mm). In the fluidized bed reactor, 64 wt. % of bio-oil, 10 wt. % of char, and 18 wt. % of non-condensable gases were produced (Figure 8). Similar product yields from fast pyrolysis of pine wood in a fluidized bed reactor were also reported in the literature [33, 34]. Comparing to these results, fast pyrolysis of wood chips in the ablative reactor showed similar product yields, with slightly less bio-oil (~5 wt.%) and gas (~ 4 wt.%), and more char (9 wt. %).

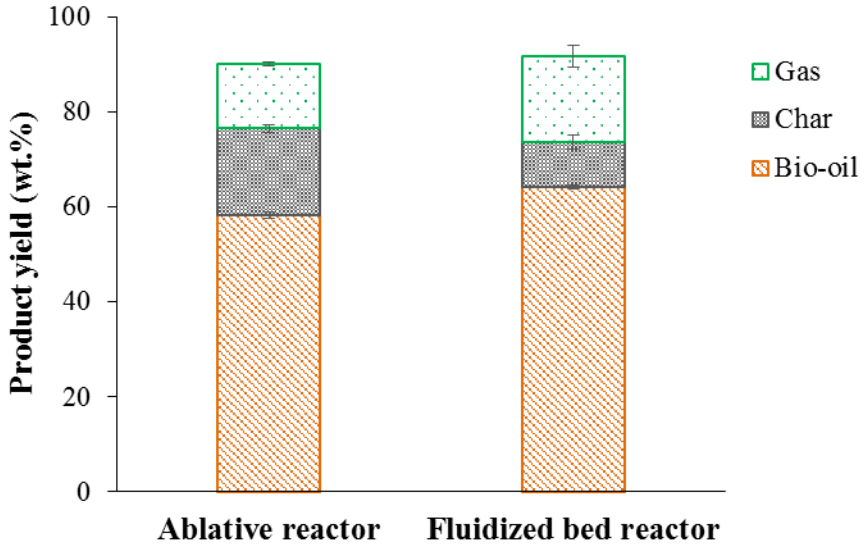

Figure 5.8 Product yield from ablative pyrolysis reactor and fluidized bed reactor

The composition of bio-oil and char from both processes was also analyzed and compared. The water content of bio-oil from ablative pyrolysis reactor and fluidized bed reactor were 34% and 26%, respectively. This water came from both the original moisture in feedstocks and the products of dehydration reactions during pyrolysis process [35]. Since the feedstocks used in these two reactors had similar moisture content (~7%), higher water content of bio-oil from ablative pyrolysis reactor may resulted from the relatively longer vapor residence times, promoting the secondary dehydration reactions and leading to water production [36]. Figure 5.9 shows the organic compound selectivity of bio-oils from ablative pyrolysis reactor and fluidized bed reactor. The bio-oil from both reactors were a mixture of oxygenates, including anhydrosugars (e.g levoglucosan), furans (e.g. furfural, furanmethanol, and 5-hydroxymethylfurfural), guaiacols (e.g. guaiacol, methylguaiacol, and eugenol), phenols (e.g. phenol, cresol, and catechol), esters (e.g. acetonyl acetate and propyl acetate), aldehydes (e.g. glycoaldehyde and succindialdehyde), ketones (e.g. acetol and cyclopentenone), and acids (e.g. formaic acid and acetic acid). Both bio-oils had a higher selectivity to anhydrosugars (20-23%) and guaiacols (16-26%). Compared to the

bio-oil from fluidized bed reactor, the bio-oil from ablative reactor had a relatively higher selectivity to guaiacols, lower selectivity to acids, and similar selectivity to other compounds. Though the vapor residence time in the ablative reactor was speculated to be longer than that in the fluidized bed reactor, the temperature of vapors in the ablative reactor chamber was close to the wall temperature of 300 °C (only metallic surface is at 500 °C), whereas the temperature of vapors in the fluidized bed reactor chamber was much higher (500 °C). The higher vapor temperature in the fluidized bed reactor may be the reason for its higher selectivity to acids and lower selectivity to guaiacols. Patwardhan et al. [37]studied the fast pyrolysis of lignin in the Py-GC/MS and observed increasing selectivity to acetic acid as temperature increased. They also found that the presence of acetic acid promoted the oligomerization of guaiacols. Zhou et al. [38] fast pyrolyzed lignin using Py-GC/MS and also reported that the selectivity of guaiacols decreased with increasing temperature. These previous works are consistent with our experimental results and hypothesis that explain the trends observed. Table 5.4 shows the elemental composition of bio-oil and char from the ablative pyrolysis reactor and fluidized bed reactor, from which the higher heating value (HHV) of bio-oil and char were calculated using an empirical equation. Due to the higher water content, bio-oil from ablative reactor had slightly lower carbon content (37.15% vs. 42. 78%), higher oxygen content (54. 05% vs. 49.27%), and thereby lower HHV (14.31 MJ/kg vs. 16.86 MJ/kg) than that from the fluidized reactor. Similar elemental compositions were observed for the char from both systems. The HHVs of the char from both reactors were around 29 MJ/kg.

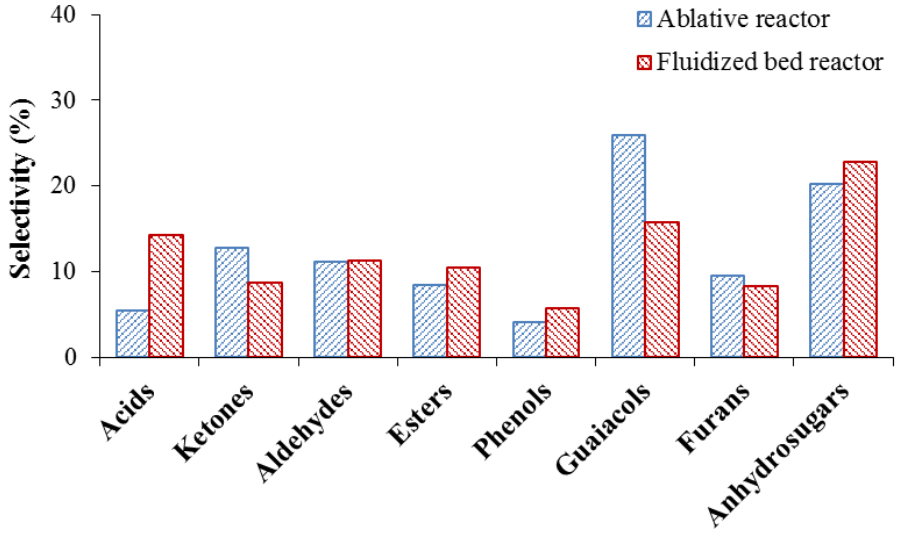

Figure 5.9 Organic compound selectivity of bio-oil from ablative pyrolysis reactor and fluidized bed reactor

Table 5.4 Elemental composition of bio-oil and char from ablative pyrolysis reactor and fluidized bed reactor

Elemental composition (wt. %)	Bio-oil		Char	
	Ablative	Fluidized bed	Ablative	Fluidized bed
C	37.53	42.78	74.68	74.09
H	8.38	7.92	3.41	4.41
O[a]	54.05	49.27	21.45	21.36
N	0.03	0.03	0.17	0.14
HHV(MJ/kg)[b]	14.31	16.86	28.52	29.81

a. calculate by difference
b. HHV (MJ/kg) = $(3.55\ C^2 - 232\ C - 2230\ H + 51.2\ C\ H + 131\ N + 20600) \times 10^{-3}$ [33]

In general, compared to fast pyrolysis of < 1 mm wood particles in a lab-scale fluidized bed reactor, fast pyrolysis of entire wood chips in the ablative reactor showed similar product yield and composition with slightly lower yield, higher water content, and lower HHV of bio-oil. This is mainly caused by the longer vapor residence times in the ablative reactor. The large reactor

chamber volume, which was selected to minimize the slow pyrolysis of wood chips during the pre-heating time in this semi-batch reactor, was the main factor increasing the vapor residence times. However, this problem can be easily solved by modifying the ablative pyrolysis reactor system into a continuous system. It has been proposed many times that it is possible to fast pyrolyze large pieces of wood in the ablative reactor; however, the previously reported largest particle size used in the ablative reactor for bio-oil production was only as high as 4.75-6.25 mm [16, 18-21, 23]. To the best of our knowledge, our study is the first to report bio-oil production from fast pyrolysis of entire wood chips and wood rods, and the yield of bio-oil from wood chips (with a size of up to 20mm) was as high as 60 wt. %. The chopping/grinding costs would be significantly reduced by using wood chips as feedstock, which contribute to 7-9% of overall production costs.

5.6 CONCLUSIONS

A novel lab-scale ablative fast pyrolysis reactor has been designed and constructed in this study, in order to convert entire wood chips and wood rods into bio-oil. Prior to ablative pyrolysis, the temperature profile of wood chips during the pre-heating time in this semi-batch reactor was evaluated and controlled to minimize the extent of slow pyrolysis. The results from our calculations were in good agreement with experimental measurements and verified that the extent of slow pyrolysis of wood chips during the pre-heating time was small in the ablative pyrolysis unit. The beetle-killed lodgepole pine wood samples with different particle sizes (i.e. 2 × 2 mm wood crumbles, 5 × 15 mm and 10 × 20 mm wood chips, and a 3.5 dia × 20 cm wood rod) have been tested in the ablative reactor. Fast pyrolysis of wood chips (5 × 15 mm and 10 × 20 mm wood chips) in the ablative reactor had similar product yield and distribution to that from 2 × 2 mm wood crumbles, and bio-oil yield was as high as 60 wt. %. These results were similar to those from fast pyrolysis of small wood particles (< 1 mm) in a fluidized bed reactor, considering that the ablative

reactor is still in its early stage. Our experiments confirmed that ablative pyrolysis is able to convert entire wood chips and even a wood rod into bio-oil, without significant loss of yield. Further work will focus on the optimization of operating conditions (e.g. temperature, rotation speed, and applied pressure) for maximizing bio-oil yield in the ablative reactor.

5.7 REFERENCES

[1] A.J. Ragauskas, C.K. Williams, B.H. Davison, G. Britovsek, J. Cairney, C.A. Eckert, W.J. Frederick, J.P. Hallett, D.J. Leak, C.L. Liotta, The path forward for biofuels and biomaterials, science, 2006; 311: 484-489.

[2] A. Bridgwater, G. Peacocke, Fast pyrolysis processes for biomass, Renewable and sustainable energy reviews, 2000; 4: 1-73.

[3] A.V. Bridgwater, Review of fast pyrolysis of biomass and product upgrading, Biomass and bioenergy, 2012; 38: 68-94.

[4] T.P. Vispute, H. Zhang, A. Sanna, R. Xiao, G.W. Huber, Renewable chemical commodity feedstocks from integrated catalytic processing of pyrolysis oils, Science, 2010; 330: 1222-1227.

[5] P.M. Mortensen, J.-D. Grunwaldt, P.A. Jensen, K. Knudsen, A.D. Jensen, A review of catalytic upgrading of bio-oil to engine fuels, Applied Catalysis A: General, 2011; 407: 1-19.

[6] Z. Ji-Lu, Bio-oil from fast pyrolysis of rice husk: Yields and related properties and improvement of the pyrolysis system, Journal of Analytical and Applied Pyrolysis, 2007; 80: 30-35.

[7] R.J. Westerhof, D.W.F. Brilman, M. Garcia-Perez, Z. Wang, S.R. Oudenhoven, S.R. Kersten, Stepwise fast pyrolysis of pine wood, Energy & fuels, 2012; 26: 7263-7273.

[8] K.H. Kim, X. Bai, M. Rover, R.C. Brown, The effect of low-concentration oxygen in sweep gas during pyrolysis of red oak using a fluidized bed reactor, Fuel, 2014; 124: 49-56.

[9] K. Wang, R.C. Brown, S. Homsy, L. Martinez, S.S. Sidhu, Fast pyrolysis of microalgae remnants in a fluidized bed reactor for bio-oil and biochar production, Bioresource technology, 2013; 127: 494-499.

[10] U.S.F. Service, Western Bark Beetle Strategy for Human Safety, Recovery and Resiliency, 2011.

[11] L. Safranyik, B. Wilson, The mountain pine beetle: a synthesis of biology, management and impacts on lodgepole pine, Canadian Forest Service, 2007.

[12] G. Luo, F.L. Resende, Fast pyrolysis of beetle-killed trees, Journal of Analytical and Applied Pyrolysis, 2014; 110: 100-107.

[13] A.V. Bridgwater, Renewable fuels and chemicals by thermal processing of biomass, Chemical Engineering Journal, 2003; 91: 87-102.

[14] A. Kumar, A conceptual comparison of bioenergy options for using mountain pine beetle infested wood in Western Canada, Bioresource Technology, 2009; 100: 387-399.

[15] Forest Concepts Completes US Department of Energy SBIR Phase I Project to Demonstrate Technical Feasibility of Milling Green and High Moisture Biomass to Biofuel Feedstocks, 2014.

[16] J. Lede, J. Panagopoulos, J. Villermaux, Experimental Measurement of ablation rate of wood pieces, undergoing fast pyrolysis by contact with a heated wall, Prepr. Pap., Am. Chem. Soc., Div. Fuel Chem.;(United States), 1983; 38.

[17] J. Lédé, Comparison of contact and radiant ablative pyrolysis of biomass, Journal of analytical and applied pyrolysis, 2003; 70: 601-618.

[18] J. Diebold, Ablative pyrolysis of macroparticles of biomass, in: Proceedings of the Specialists Workshop on the Fast Pyrolysis of Biomass, Copper Mountain, Co, 1980, pp. 237.

[19] J. Lede, J. Panagopoulos, H.Z. Li, J. Villermaux, Fast pyrolysis of wood: direct measurement and study of ablation rate, Fuel, 1985; 64: 1514-1520.

[20] H. Martin, J. Lédé, H. Li, J. Villermaux, C. Moyne, A. Degiovanni, Ablative melting of a solid cylinder perpendicularly pressed against a heated wall, International journal of heat and mass transfer, 1986; 29: 1407-1415.

[21] J. Lédé, H.Z. Li, J. Villermaux, H. Martin, Fusion-like behaviour of wood pyrolysis, Journal of analytical and applied pyrolysis, 1987; 10: 291-308.

[22] T.B. Reed, Contact Pyrolysis in a "Pyrolysis Mill", in: Research in Thermochemical Biomass Conversion, Springer, 1988, pp. 192-202.

[23] G. Peacocke, A. Bridgwater, Ablative plate pyrolysis of biomass for liquids, Biomass and Bioenergy, 1994; 7: 147-154.

[24] G. Luo, F.L. Resende, In-situ and ex-situ upgrading of pyrolysis vapors from beetle-killed trees, Fuel, 2016; 166: 367-375.

[25] A. Bridgwater, D. Meier, D. Radlein, An overview of fast pyrolysis of biomass, Organic Geochemistry, 1999; 30: 1479-1493.

[26] A. Bridgwater, Principles and practice of biomass fast pyrolysis processes for liquids, Journal of analytical and applied pyrolysis, 1999; 51: 3-22.

[27] B. Benallal, C. Roy, H. Pakdel, S. Chabot, M. Poirier, Characterization of pyrolytic light naphtha from vacuum pyrolysis of used tyres comparison with petroleum naphtha, Fuel, 1995; 74: 1589-1594.

[28] C. Roy, A. Chaala, H. Darmstadt, The vacuum pyrolysis of used tires: End-uses for oil and carbon black products, Journal of Analytical and Applied Pyrolysis, 1999; 51: 201-221.

[29] H. Yang, R. Yan, H. Chen, D.H. Lee, C. Zheng, Characteristics of hemicellulose, cellulose and lignin pyrolysis, Fuel, 2007; 86: 1781-1788.

[30] T.L. Bergman, F.P. Incropera, A.S. Lavine, Fundamentals of heat and mass transfer, John Wiley & Sons, 2011.

[31] E. Salehi, J. Abedi, T. Harding, Bio-oil from sawdust: effect of operating parameters on the yield and quality of pyrolysis products, Energy & Fuels, 2011; 25: 4145-4154.

[32] J. Shen, X.-S. Wang, M. Garcia-Perez, D. Mourant, M.J. Rhodes, C.-Z. Li, Effects of particle size on the fast pyrolysis of oil mallee woody biomass, Fuel, 2009; 88: 1810-1817.

[33] W.J. DeSisto, N. Hill, S.H. Beis, S. Mukkamala, J. Joseph, C. Baker, T.-H. Ong, E.A. Stemmler, M.C. Wheeler, B.G. Frederick, Fast pyrolysis of pine sawdust in a fluidized-bed reactor, Energy & Fuels, 2010; 24: 2642-2651.

[34] B.-S. Kang, K.H. Lee, H.J. Park, Y.-K. Park, J.-S. Kim, Fast pyrolysis of radiata pine in a bench scale plant with a fluidized bed: Influence of a char separation system and reaction conditions on the production of bio-oil, Journal of analytical and applied pyrolysis, 2006; 76: 32-37.

[35] A. Oasmaa, S. Czernik, Fuel oil quality of biomass pyrolysis oils state of the art for the end users, Energy & Fuels, 1999; 13: 914-921.

[36] H.S. Heo, H.J. Park, Y.-K. Park, C. Ryu, D.J. Suh, Y.-W. Suh, J.-H. Yim, S.-S. Kim, Bio-oil production from fast pyrolysis of waste furniture sawdust in a fluidized bed, Bioresource technology, 2010; 101: S91-S96.

[37] P.R. Patwardhan, R.C. Brown, B.H. Shanks, Understanding the fast pyrolysis of lignin, ChemSusChem, 2011; 4: 1629-1636.

[38] S. Zhou, M. Garcia-Perez, B. Pecha, S.R. Kersten, A.G. McDonald, R.J. Westerhof, Effect of the fast pyrolysis temperature on the primary and secondary products of lignin, Energy & fuels, 2013; 27: 5867-5877.

CHAPTER 6. PYROLYSIS OF BEETLE-KILLED WOOD CHIPS IN A NOVEL ABLATIVE REACTOR: EFFECT OF OPERATING CONDITIONS[4]

6.1 ABSTRACT

We pyrolyzed beetle-killed wood chips (5 × 15 mm) in a novel ablative reactor. The effects of different operating parameters (i.e. pyrolysis temperature, initial thickness of assembled wood chips, rotation speed of wood chip bowl, and applied pressure by the plate on the wood chips) on the product yield and composition were investigated. Our results revealed that bio-oil yield in the ablative reactor was favored at moderate pyrolysis temperature of 500 °C, low initial thickness of wood chips (≤ 5 mm), low applied pressure (≤ 0.5 bar), and high rotation speed (≥ 100 rpm). Simulation of the temperature profile of the wood chips along the depth direction during pyrolysis indicated that ablative pyrolysis of thick layers of wood chips are strongly limited by heat transfer rates. The maximum bio-oil yield obtained in the ablative reactor was about 60 wt. %. The main bio-oil components detected by GC/MS-FID and FTIR were guaiacols, anhydrosugars, ketones and furans. The elemental composition of bio-oil was highly affected by its water content, and the elemental composition of char was primarily affected by the temperature. At higher temperature, char became more carbonaceous in nature. In addition, comparison of the FTIR spectra from raw biomass and char suggests that most components in the original wood chips were decomposed during ablative pyrolysis.

[4] To be submitted.

6.2 INTRODUCTION

In recent decades, billions of coniferous trees across millions of forest acres, ranging from Mexico to northwestern British Columbia, have been attacked by bark beetles [1, 2]. The high levels of tree mortality resulting from the bark beetle outbreak lead to severe falling of trees and fire hazards [3]. This raises an immediate question to forest managers; namely, what to do with these dead trees. The traditional way to dispose of beetle-killed trees is to burn them on site; however, this wastes energy and nutrients and causes air pollution [4]. Moreover, bluish stains and cracks on the beetle-killed trees significantly reduce their commercial value for solid wood manufacturing [3, 5]. Fortunately, these problems may be mitigated by converting beetle-killed trees into liquid fuels or chemicals via fast pyrolysis; in particular, the low moisture content of beetle-killed trees can dramatically reduce or even eliminate the drying costs.

Fast pyrolysis is defined as a rapid thermal decomposition of organic matter in the absence of oxygen, producing primarily liquid bio-oil, char, and non-condensable gases [6, 7]. In our previous work [8], we investigated the degradation stages of beetle-killed trees on the performance of fast pyrolysis, and found that trees that have been attacked and dead for 4 years had similar product yield and distribution to healthy trees. In addition, pyrolysis vapors derived from beetle-killed trees can be successfully upgraded into aromatic hydrocarbons in the presence of HZSM-5, indicating beetle-killed trees are promising feedstocks for biofuel and chemicals production [8, 9]. However, beetle-killed trees are typically located far from urban industrial areas, which means transportation costs may be a key barrier to widespread utilization of this vast resource in fast pyrolysis. Using a mobile pyrolysis unit to convert beetle-killed trees near the harvesting point may significantly reduce the transportation costs, since the energy density of bio-oil is 6-8 times higher than the green wood chips [10, 11]. The techno-economic analyses of biofuel technologies conducted by

Write [12] also pointed out that the transportation costs per mile of bio-oil were only 20% of that for transporting raw biomass. In addition, char that is the byproduct from fast pyrolysis of biomass can be economically used on site as a soil amendment [13, 14]. Mobile pyrolysis units, by definition, are portable and more versatile than conventional centralized biofuel production facilities. The small size enables them to be transported quickly and easily on a tractor trailer to process feedstock at multiple locations [15]. The first mobile system for conversion of biomass into bio-oil and char was developed by a company call Agri-Therm, which had a capacity of processing 5 tons/day of biomass, generating 3 tons/day of bio-oil, and 1.5 tons/day of char [16]. Pyrolysis of biomass in this mobile system was carried out in a fluidized bed reactor. Other companies have also developed mobile units for demonstrations, most of them for the purpose of biochar production.

Recently, we have developed a novel lab-scale ablative pyrolysis unit that simulates the conditions that would be used in the mobile pyrolysis unit in the field, converting beetle-killed trees mainly into bio-oil with char and non-condensable gases as byproducts. In ablative pyrolysis, heat transfer to the wood is carried out via a direct contact with a hot surface. This situation creates a steep temperature gradient within the wood particle, such that pyrolysis takes place within a thin liquid layer contacting the solid rather than the entire wood particle [17-20]. Thus, fast pyrolysis of large pieces of wood is possible in an ablative reactor, which is advantageous over most reactor configurations that can only process small wood particles (1-3 mm). This feature has the potential to save on the grinding costs, which contribute to 7-9% of the overall production costs [21, 22]. This characteristic of ablative pyrolysis has been speculated in the past, and our recent work experimentally supported this claim by converting entire wood chips into bio-oil via ablative pyrolysis, with yields as high as those obtained with 2 mm wood particles [23]. The bio-oil yield

and composition from ablative pyrolysis of wood chips were also in the same range as those obtained from a fluidized reactor with < 1mm wood particles [23]. The scale-up of this novel lab-scale ablative reactor into a mobile pyrolysis unit requires more understanding on the effects of the operating conditions. Thus, in this study, we evaluated the effects of the main operating parameters involved in the ablative pyrolysis of wood chips on the product yield and composition. These operating parameters include the pyrolysis temperature (temperature of the hot plate), the initial thickness of the assembly of wood chips, the relative rotation speed between the wood chips and the hot plate, and the pressure applied by the plate on the wood chips.

6.3 MATERIAL AND METHODS

6.3.1 Feedstock

Beetle-killed lodgepole pine (*Pinus contorta*) in the form of wood chips (5 × 15 mm) was purchased from Forest Concept and used as feedstock in this study. The trees were standing dead trees without needles, and 2-4 years after death. The proximate analysis, ultimate analysis, and chemical composition of the feedstock are shown in Table 6.1 [8, 9, 23]

Table 6.1 Characterization of beetle-killed lodgepole pine feedstock [8, 9, 23]

Proximate analysis (wt. %)			
Moisture	Ash	Volatile	Fixed carbon
7.30	0.26	82.29	10.15
Ultimate analysis (wt. %) [a]			
C	H	O	N
49.62	6.37	43.29	0.44
Chemical composition (wt. %) [a]			
Extractives [a]	Carbohydrates [b]	Lignin [b]	
5.48	61.18	28.84	

a. wt.% of oven dry wood
b. wt.% of oven dry extractive-free wood

6.3.2 Ablative pyrolysis reactor and its operation

The ablative reactor used in this study was designed and constructed to pyrolyze wood chips into bio-oil, and was described in detail in our previous study [23]. Figure 6.1 is the schematic diagram of the ablative pyrolysis system. This is a semi-batch reactor, and the wood chips were placed in the wood chip bowl prior to the reaction. The upper plate and reactor wall were then pre-heated to the set point temperatures. At the same time, room temperature N_2 with a flow rate of 15 L/min was introduced into the system. After pre-heating, the wood chip bowl started rotating, and the upper plate moved down towards the wood chips to initiate fast pyrolysis via direct contact. The reaction time was 3 min. N_2 carrier gas combined with the vacuum suction (straight from the building line) rapidly swept the generated pyrolysis vapors to the multi-stage condensation system, which includes an impinger, a counter-current double pipe condenser, and a coalescing filter, to collect bio-oil. Bio-oil and char were quantified by weighing the system before and after the reaction. The yield of non-condensable gases was calculated by subtraction, assuming 90 wt. % total mass balance as described in [23]. The operating parameters we investigated in this study and their ranges are summarized in Table 6.2. Level "0" shown in Table 2 is the base case, and one of the parameters varied to Level "-1" or "1" each time with others remained unchanged, studying the effects of each parameter. The reactor wall temperature of 300 °C was used for all these experiments.

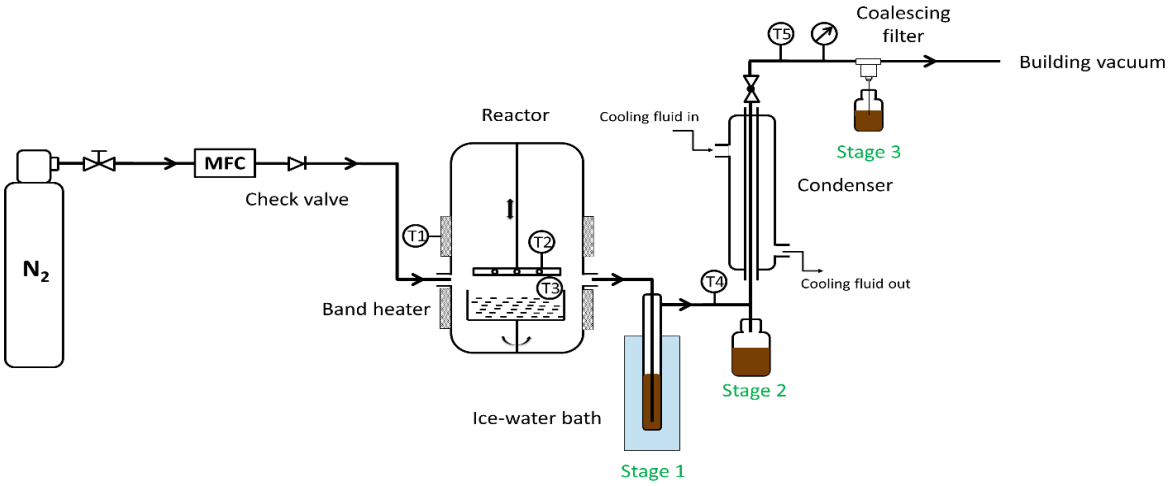

Figure 6.1 Schematic diagram of ablative pyrolysis system

Table 6.2 Ablative pyrolysis system operating parameters [23]

Operating parameters	Level		
	-1	0	1
Pyrolysis temperature (°C)	450	500	550
Initial wood chips mass (g) / thickness (mm)	25 / 2	50 / 5	100 / 10
Rotation speed (rpm)	0	100	160
Applied pressure (bar)	0.3	0.5	1 & 1.5

6.3.3 Product analysis

Bio-oil water content was determined by ASTM E203 standard using a Karl Fischer titrator (V20, Mettler Toledo). Hydranal-composite 5K was used as titrant. The chemical composition of bio-oil was analyzed using GC/MS-FID (QP2010, Ultra, Shimadzu) equipped with a SHRXI-5MS capillary column (30 m × 0.25 mm I.D. × 0.25 μm film thickness) using methanol as solvent. Helium was used as carrier gas. The GC oven temperature was programmed from 40 °C (4 min) to 300 °C at 10 °C/min, and held at 300 °C for 5 min. Identifications of compounds were achieved

by comparing their mass spectra with the NIST 2010 library, and quantifications were obtained using FID with external standards. In total, 40 compounds were quantified using 20 standards.

FTIR (IRPrestige-21, Shimadzu) spectrophotometer in attenuated total reflectance (ATR) mode was used to characterize the functional groups of bio-oil, char, and raw biomass. All spectra were baseline-corrected, and obtained with a wavenumber range of 400-4000 cm^{-1}, resolution of 4 cm^{-1}, and 64 scans.

Elemental composition of bio-oil and char were measured using the PerkinElmer elemental analyzer (2400 Series II). Oxygen content was calculated by difference. Based on the elemental composition, the higher heat values (HHV) of bio-oil and char were calculated using the following empirical equation[24]:

$$HHV\ (MJ/kg) = (1.87C^2 - 114C - 2802H + 63.8H + 129N + 20147)/1000 \quad (6.1)$$

in which the amounts of the elements (C, H, and N) are expressed in mass percentage.

6.4 RESULTS AND DISCUSSION

6.4.1 Product yields

6.4.1.1 Effect of pyrolysis temperature

Pyrolysis temperature, namely the upper plate temperature, is one of the important operating parameters in the ablative reactor, and thereby pyrolysis temperature in a range of 450-550 °C was studied herein. The ablative pyrolysis reactor used here is a semi-batch reactor. Wood chips were loaded in the wood chip bowl prior to the reaction, and therefore the temperature of wood chips increases due to radiation from the hot plate and walls during the pre-heating time. This was discussed in detail in our previous work [23]. According to our calculation and measurements [23], the temperature of the wood chips gradually increased with increasing the upper plate temperature.

As the temperature of upper plate increased from 450 °C to 550 °C, the temperature of wood chips increased from 160 °C to 200 °C (Figure 6.2). Lignocellulosic biomass has been reported to slowly decompose at 200 °C [25]; therefore, our results suggested that the extent of slow pyrolysis of wood chips during the pre-heating time is not significant. We concluded that the radiation emitted by the upper plate and walls did not promote extensive decomposition of the wood chips during pre-heating. This conclusion is supported by the high bio-oil yields obtained in this system, which are typical of fast pyrolysis.

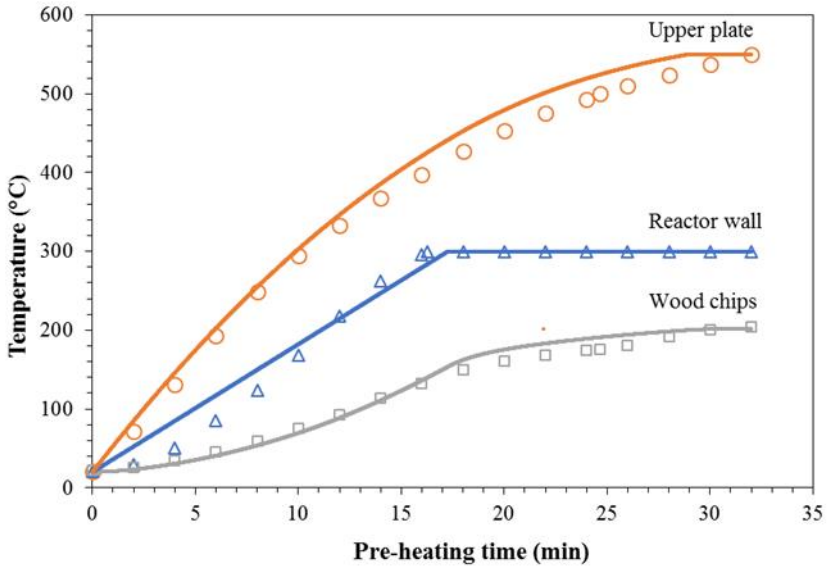

Figure 6.2 Wood chips temperature during pre-heating time (solid lines represent results from calculation; orange circle, blue triangle, and grey square represent data from measurements) [23]

Figure 6.3 shows the product yields and bio-oil water content as a function of pyrolysis temperature. These experiments were carried out using 50 g beetle-killed wood chips, at a rotation speed of 100 rpm and an applied pressure of 0.5 bar. At 500 °C, replicates were performed to verify the reproducibility of the reactor, and the standard deviations obtained for yield of bio-oil, char, and non-condensable gases were ± 0.66 wt. %, ± 0.12 wt. %, and ± 0.54 wt. %, respectively

(included in figure). As the pyrolysis temperature increased from 450 to 500 °C, bio-oil yield increased from 50 wt. % to 60 wt. %, and the yield of char and non-condensable gases decreased from 24 wt. % and 16 wt. % to 18 wt. % and 13 wt. %, respectively. The reason for the higher bio-oil yield and lower char yield at a higher pyrolysis temperature is likely to the greater extent of primary decomposition of biomass [24-27]. However, the bio-oil yield decreased from 60 to 52 wt. % and the non-condensable gases yield slightly increased from 13 to 18 wt. %, when pyrolysis temperature further increased to 550 °C. At higher temperature, secondary cracking reactions of heavier molecular weight compounds in the pyrolysis vapors were promoted, resulting in a lower yield of bio-oil and a higher yield of gas [24, 26-29]. These results are in agreement with those reported in the literature. Salehi et al. [24] pyrolyzed a mixture of sawdust in a fluidized bed reactor over a temperature range of 425-550 °C, and obtained a maximum bio-oil yield of 62 wt. % and a minimum char yield of 15 wt. % at 500 °C, with the yield of non-condensable gases slightly increased with increasing pyrolysis temperature. Garcia-Perez et al. [28] observed a similar tendency with the pyrolysis of oil mallee woody biomass at 350-600 °C in a fluidized bed reactor. The highest yield of bio-oil and the lowest water content were obtained at 450 °C. These trends were also experienced by Heo et al. [30] with the pyrolysis of rice husk. A minimum water content in the bio-oil (~34%) was also observed at 500 °C. Water in bio-oil is from both the original moisture in the wood chips and the product of dehydration during pyrolysis reactions [6, 7]. Since the total amounts of water in the bio-oil samples were the same, the more organics produced at 500 °C is the main reason for its relatively low water content of bio-oil.

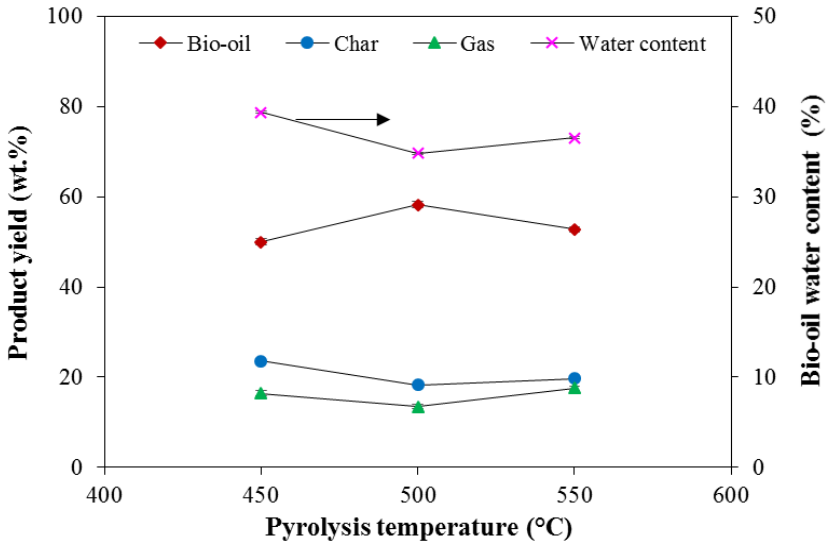

Figure 6.3 Product yield and bio-oil water content at different pyrolysis temperature

6.4.1.2 Effect of initial thickness of wood chips

Beetle-killed wood chips with a mass of 25 g, 50 g, and 100 g were used as feedstock, resulting in an initial thickness of wood chips of around 2 mm, 5 mm, and 10 mm, respectively. Figure 6.4 shows the effect of the initial thickness of the assembly of wood chips on the product yield and bio-oil water content at a pyrolysis temperature of 500 °C, a rotation speed of 100 rpm, and an applied pressure of 0.5 bar. Similar product yields (~ 60 wt. % bio-oil, 18 wt. % char, and 13 wt. % non-condensable gases) were observed at thicknesses of 2 mm and 5 mm. The yield of bio-oil dramatically decreased from 60 wt. % to 50 wt. % as the initial thickness of wood chips increased from 5 mm to 10 mm, while the yield of char and non-condensable gases showed an opposite trend. The water content of bio-oil gradually increased from 32 % to 37 % with increasing initial thickness of wood chips, since less liquid organics were produced with thicker wood layers.

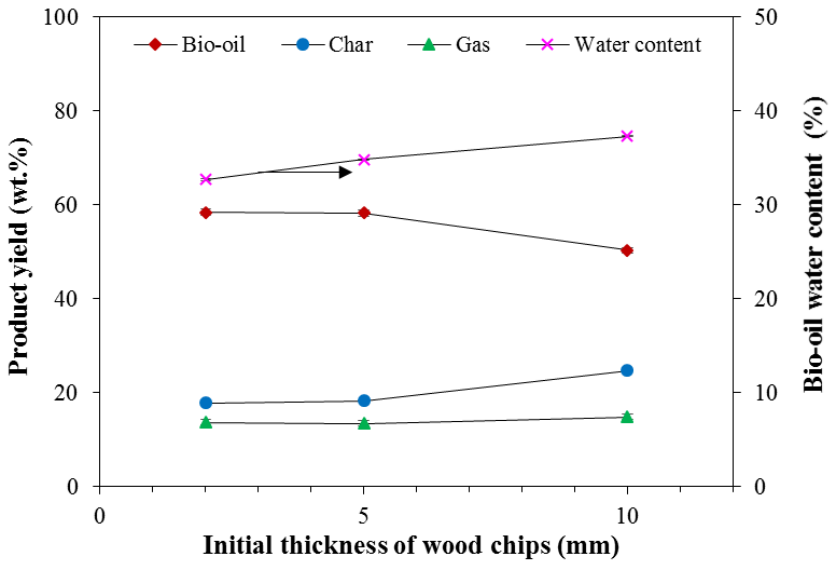

Figure 6.4 Product yield and bio-oil water content at different initial thickness of wood chips

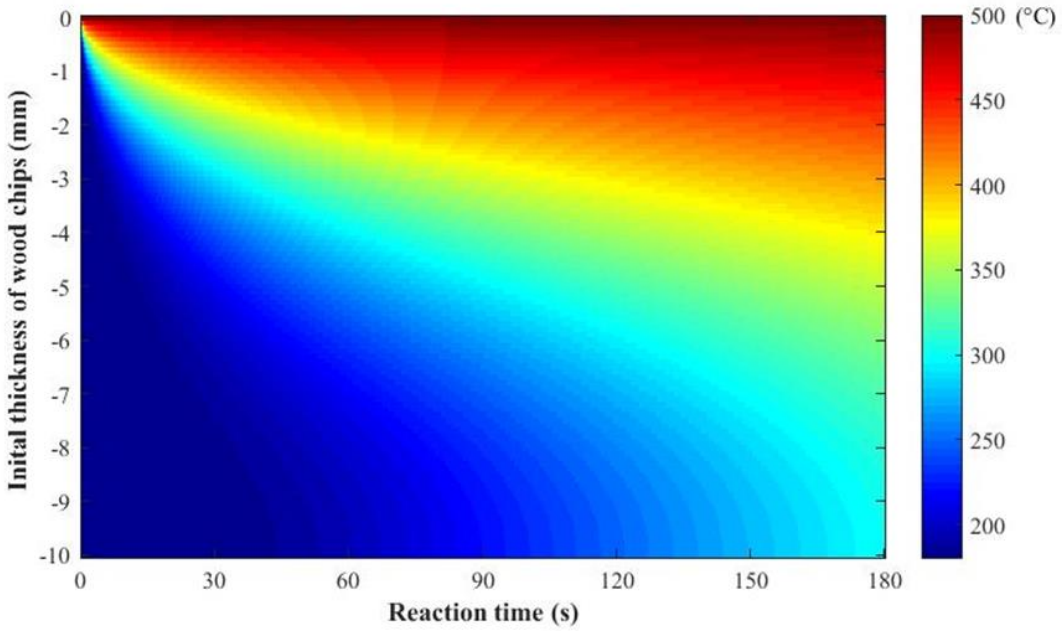

Figure 6.5 Temperature profile of wood chips at different thickness during reaction

To better understand the effect of initial thickness of wood chips on the product yield, the temperature profile of the wood chips as a function of the thickness during pyrolysis was evaluated. In ablative pyrolysis, the surface of wood chips was heated by the hot plate, and the heat diffused

through the wood chips by conduction. The heat conduction through the wood chips was dominant in the vertical direction and was considered negligible in other directions. Thus, the one-dimensional heat conduction equation applies:

$$\frac{\partial^2 T}{\partial z^2} = \frac{k}{\rho c_p} \times \frac{\partial T}{\partial t} \tag{6.2}$$

in which T is the temperature of the wood chips that is a function of time t and thickness z. k, ρ, and c_p are the thermal conductivity, density, and heat capacity of wood. To solve this heat equation, initial and boundary conditions were selected. Initially, the wood chips had a uniform temperature that was equal to the temperature at the end of the pre-heating time. During the reaction, we assumed that the surface temperature of the wood chips was constant and equal to the hot plate temperature. The bowl in contact with the bottom of the wood chips was assumed to be adiabatic herein. Thus,

initial condition: $T(0, z) = T_i$, and $T_i = 180$ ℃ (6.3)

boundary conditions: $T(t, 0) = T_s$, and $T_s = 500$ ℃ (6.4)

$$\frac{\partial T}{\partial z}_{(z=L)} = 0, \text{ and } L = 10\ mm \tag{6.5}$$

In this calculation, the shrinkage of the wood chips thickness due to the compression of hot plate and the char formation was not considered, indicating that the temperature profile obtained from this model represents the worst case scenario for the heat diffusion through the wood chips. Using Matlab, the temperature profile of the wood chips based on the calculation above is shown in Figure 6.5. Temperatures above 400 °C are dominant through a 2 mm wood chips layer, but low temperature regions (200-400 °C) become predominant for a 10 mm wood chips layer. The temperature profile for a 2 mm layer promotes reactions typical of fast pyrolysis, keeping a high bio-oil yield. For the 10 mm thickness, the temperature range through most of the wood is more

characteristic of a slow pyrolysis process, leading to a decrease in bio-oil and increase in char. For the 5 mm wood chips layer, an intermediate situation is observed in the calculation. But it is possible that wood chips compression/shrinking led to a similar temperature profile to the 2 mm case, keeping similar product yields.

6.4.1.3 Effect of rotation speed

In the ablative reactor, the wood chip bowl driven by the motor can rotate with frequency of rotation up to 160 rpm during the reaction, and this rotating speed of wood chip bowl is anticipated to be a critical factor affecting the product yield. Lédé et al. [18, 19] did a fundamental study on the ablation heat transfer with specific application to wood pyrolysis. The experiments were carried out using a cylindrical wood rod applied vertically to the hot surface of a spinning disk. They found that the ablation rate (thickness of wood that was consumed per unit time) of the wood rod increased as the relative velocity of the disk increased, but the ablation rate became constant when the velocity exceeded 1.5 m/s, which is equivalent to a frequency of rotation of 130 rpm in our ablative reactor [18, 19]. Figure 6 shows the product yield and bio-oil water content as a function of the rotation speed. Beetle-killed wood chips with a mass of 50 g were used in these experiments. Pyrolysis temperature and applied pressure were 500 °C and 0.5 bar, respectively. As expected, the lowest bio-oil yield of ~50 wt. % and the highest yield of char (~23 wt. %) and gas (~ 17 wt. %) were obtained at no rotation. As the rotation speed increased to 100 rpm, bio-oil yield significantly increased to 60 wt. %, and the yield of char and gas decreased to 18 wt. % and 13 wt. %, respectively. The water content of bio-oil also decreased from 40 % to 34 %, since more liquid organics were produced at 100 rpm. Similar to the phenomena observed by Lédé et al. [18, 19], when the rotation speed further increased to 160 rpm, product yield and the water content of bio-oil stayed unchanged. The rotation of the bowl may also promote the escape of pyrolysis

vapors out of the hot zone, minimizing secondary reactions like dehydration and favoring the bio-oil production.

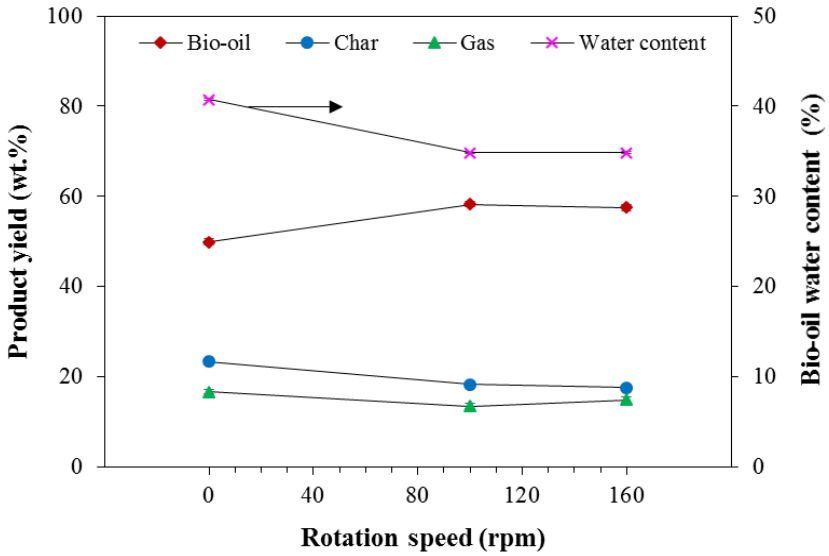

Figure 6.6 Product yield and bio-oil water content at different rotation speed

6.4.1.4 Effect of applied pressure

Fast pyrolysis in the ablative reactor initiated as the hot plate directly contacted the wood chips. At the same time, the hot plate applied pressure against the wood chips. In this study, the effect of applied pressure was studied over a wide range of 0.3-1.5 bar at 500 °C and 100 rpm using 50 g beetle-killed wood chips as feedstock, and the results are shown in Figure 6.7. A higher bio-oil yield (~ 60 wt. %) with a lower water content of 34 % was observed at a lower applied pressure of 0.3 bar and 0.5 bar. As the applied pressure increased to 1 and 1.5 bar, the bio-oil yield significantly decreased to 51-52 wt. % and its water content increased to 37 %. The yield of char and non-condensable gases showed an opposite trend.

Wood is a porous material with poor thermal conductivity. In the ablative reactor, the porosity of wood chips should decrease with increasing applied pressure, which results in an increasing thermal conductivity of wood [31]. Thus, the enhanced heat transfer is believed to favor the

formation of bio-oil. In addition, Lédé et al. [18-20] made a direct measurement of the ablation rate of wood rods undergoing pyrolysis by contact with a hot spinning disk, and found that the ablation rate of wood was directly proportional to the applied pressure. However, the higher applied pressure and increased compression of the wood chips may also reduce the volume available for pyrolysis vapors to escape from the bowl, increasing residence time and thereby significantly increasing secondary reactions, forming more char and non-condensable gases. The counteracting of the positive effect of heat transfer enhancement and negative effect of the mass transfer limitation may explain the relatively lower bio-oil yield observed at higher applied pressure in this study.

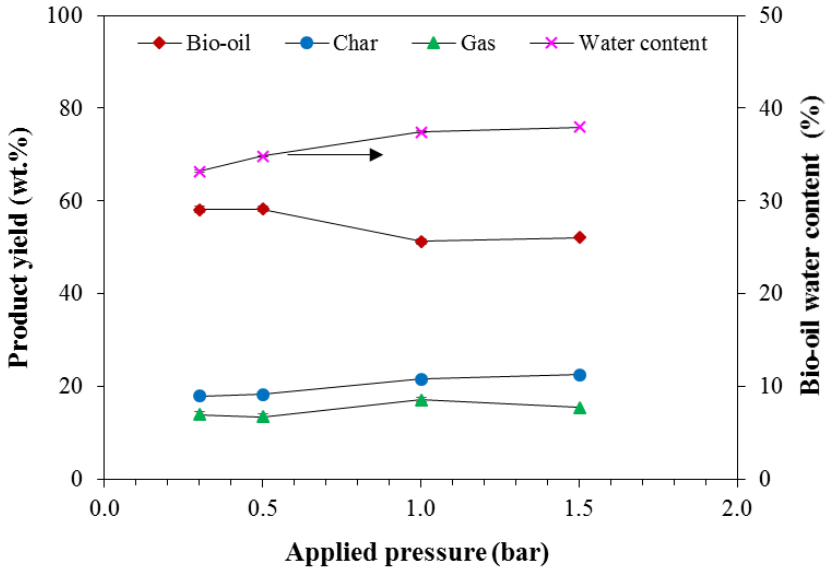

Figure 6.7 Product yield and bio-oil water content at different applied pressure

According to the results above (section 6.4.1.1-6.4.1.4), we found that the bio-oil yield in the ablative reactor was favored at moderate pyrolysis temperature of 500 °C, thin layers of wood chips (≤ 5 mm), low applied pressure (≤ 0.5 bar), and high rotation speed (≥ 100 rpm). The maximum bio-oil yield obtained in this study was of 60 wt. % that is in the same range as other fast pyrolysis studies using pine wood as feedstock. Wang et al. [32] studied fast pyrolysis of pine

wood (3 mm) in a fluidized bed reactor and obtained a maximum bio-oil yield of 63 wt. % with a water content of 33%. About 65 wt. % of bio-oil was obtained by DeSisto et al. [33] when they fast pyrolyzed pine sawdust (0.42 mm) in a fluidized bed reactor. Peacocke and Bridgewater [34] designed and constructed an ablative reactor, in which the ablation was achieved by four rotating asymmetric blades. Fast pyrolysis of pine wood (4.75 – 6.25 mm) produced up to 67.7% with a water content of 20 %. The slightly lower bio-oil yield with higher water content achieved from our ablative reactor may be due to the relatively long vapor residence times.

6.4.2 Product characterization

In addition to the product yield, the bio-oil and char obtained at different operating conditions are also characterized to evaluate their potential utilizations as chemicals or fuels.

6.4.2.1 Bio-oil

The elemental composition of bio-oil from ablative pyrolysis of wood chips as a function of operating parameters is summarized in Table 6.3. The oxygen content ranged from 53-60 wt. %, the carbon content ranged from 32-39 wt. %, the hydrogen content ranged from 7-9 wt. %, and trace nitrogen content was observed in all cases. The oxygen content changes in the same way as the water content with the operating parameters, as depicted in Figure 6.3, 6.4, 6.6, and 6.7. The carbon content changes in a way that is opposite to this trend. The hydrogen and nitrogen contents remained almost constant with the operating parameters. Similar results were also reported in the literature [24, 28, 32]. As expected, higher carbon content and lower oxygen content led to higher HHV. Bio-oil derived from all conditions had HHVs in the range of 11-15 MJ/kg.

Table 6.3 Elemental composition (wt. %) and HHV of bio-oil from different operating parameters

	Pyrolysis temperature (°C)			Initial thickness of wood chips (mm)			Rotation speed (rpm)			Applied pressure (bar)			
	450	500	550	2	5	10	0	100	160	0.3	0.5	1	1.5
C	32.13	37.53	33.67	38.70	37.53	33.29	30.83	37.53	37.32	38.72	37.53	32.58	32.44
H	8.78	8.38	8.54	8.18	8.38	8.93	8.78	8.38	7.98	7.51	8.38	8.12	8.29
N	0.07	0.03	0.02	0.02	0.03	0.02	0.04	0.03	0.03	0.02	0.03	0.02	0.02
O	59.07	54.06	57.32	53.10	54.06	57.75	60.35	54.06	54.67	53.74	54.06	59.28	59.25
HHV (MJ/kg)	11.69	14.31	12.49	14.91	14.31	12.12	11.11	14.31	14.34	15.08	14.31	12.25	12.10

The chemical composition of bio-oil was analyzed using GC/MS-FID, and the selectivity of the organic compounds in bio-oil was not significantly affected by the operating parameters. Table 6.4 shows the organic compounds selectivity of bio-oil obtained at the condition with highest bio-oil yield (500 °C, 5 mm, 100 rpm, and 0.5 bar). Bio-oil was composed of a mixture of oxygenates. It had highest selectivity to levoglucosan (17.99%), followed by glycolaldehyde (10.34%), acetol (8.37%), and 2-methoxy-4-vinylphenol (7.87%). The oxygenates present in the bio-oil can be classified into different chemical groups, including acids, ketones, aldehydes, esters, furans, phenols, guaiacols, and anhydrosugars. Bio-oil had a high selectivity to the group of guaiacols (~ 26%), which are interesting sources for resins production [35, 36], followed by the group of anhydrosugars (~ 20%). Relatively low selectivity of acids and phenols were observed in the bio-oil.

Table 6.4 GC/MS-FID quantified compounds and groups in bio-oil

Group	Selectivity (%)	Compounds	Selectivity (%)
Acids	5.42	Formic acid	2.45
		Acetic acid	2.97
Ketones	12.74	Acetone	0.98
		Acetol	8.37

		2-Cyclopenten-1-one, 2-hydroxy-	2.33
		5,6-Dihydro-2H-pyran-2-one	0.40
		1,2-Cyclopentanedione, 3-methyl-	1.64
Aldehydes	11.16	Glycolaldehyde	10.34
		Succindialdehyde	0.82
Esters	8.40	Isopropyl acetate	0.55
		n-Propyl acetate	3.60
		Methyl pyruvate	3.18
		Acetonyl acetate	1.08
Furans	9.48	2,3-Dihydrofuran	0.10
		Furfural	2.37
		2-Furanmethanol	1.26
		2(5H)-Furanone	2.52
		2(5H)-Furanone, 5-methyl	0.32
		2(5H)-Furanone, 3-methyl-	0.64
		5-Hydroxymethylfurfural	2.28
Phenols	4.11	Phenol	0.36
		o-Cresol	1.21
		m-Cresol	1.12
		Phenol, 2,4-dimethyl-	0.64
		p-Ethylphenol	0.27
		3-Methylcatechol	0.51
Guaiacols	25.90	Phenol, 2-methoxy-	1.59
		2-Methoxy-4-methylphenol	3.93
		p-Ethylguaiacol	0.78
		2-Methoxy-4-vinylphenol	7.89
		p-Eugenol	2.48
		Vanillin	0.49
		trans-Isoeugenol	2.24
		cis-Isoeugenol	3.65
		Coniferyl alcohol	0.79
		Coniferaldehyde	0.70
		Acetovanilone	0.72
		Guaiacylacetone	0.65

Anhydrosugars	20.17	2,3-Anhydro-d-mannosan	2.18
		Levoglucosan	17.99

Figure 6.8 shows the FTIR spectrum of bio-oil at the condition with highest bio-oil yield. The band between 3200 and 3600 cm^{-1} is ascribed to the O-H or N-H stretching vibrations [37-39], indicating the presence of water, alcohols, phenols in bio-oil, since bio-oil contains trace amounts of nitrogen. The bands in the frequency range of 2850-2950 cm^{-1} and 1350-1470 cm^{-1} are related to the C-H stretching vibration and C-H deformation vibration of CH_2 or CH_3 groups, respectively [37-39]. The C=O stretching vibrations between 1650 and 1850 cm^{-1} are compatible with the presence of aldehydes, ketones, or carboxylic acids [37-39]. The O-H bending and C-O stretching vibrations at bands of 950-1300 cm^{-1} are indicative of alcohols or esters in bio-oil [39]. The C=C stretching vibration at the band of 1514 cm^{-1}, together with the C-H bending vibration at the bands of 700-900 cm^{-1}, suggest the presence of aromatics or polycyclic aromatics [38, 39]. The FTIR results are consistent with those from GC/MS-FID.

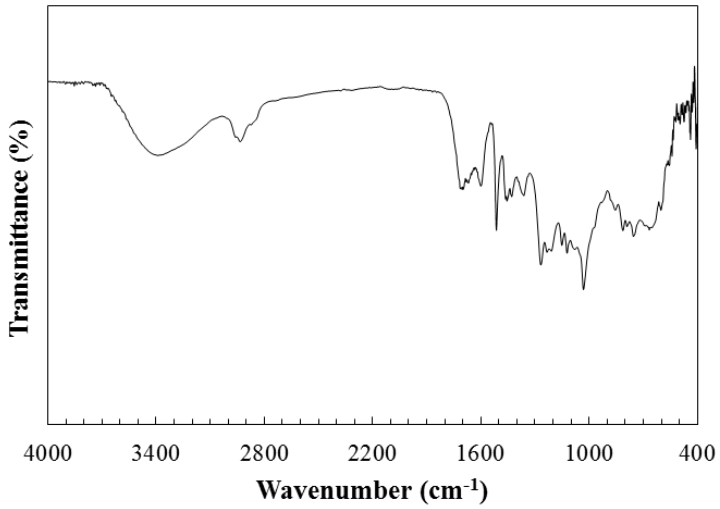

Figure 6.8 FTIR spectrum of bio-oil from optimal conditions

6.4.2.2 Char

Table 6.5 presents the elemental composition and HHVs of char as a function of operating parameters. Char from all the conditions had a high carbon content of 72-75 wt. %, an oxygen content of 21-23 wt. %, a hydrogen content of 3-4 wt. %, and a nitrogen content of about 0.2 wt. %, from which the HHV of char was calculated and was around 28 MJ/kg. These are similar to the values reported in the literature [24, 28, 33]. The trends of elemental composition as well as the mole ratios of H/C and O/C were mainly affected by the pyrolysis temperature and the initial thickness of wood chips. As temperature increased or the initial thickness of wood chips decreased, carbon content slightly increased with a corresponding slight decrease of hydrogen and oxygen contents. As a consequence, H/C and O/C ratios decreased with increasing temperature or decreasing thickness, indicating more carbonaceous polycyclic aromatics and less oxygen-containing aromatic groups were produced [40]. During ablative pyrolysis, high temperature regions are dominant for thinner wood chips layers while low temperature regions become more dominant for thicker wood layers (discussed in section 6.4.1.2). This indicates the elemental composition trends with thickness result from temperature effects. Salehi et al. [24] observed the same tendency when fast pyrolyzed sawdust at a temperature of 425-550 °C in a fluidized bed reactor. Garcia-Perez et al. [28] also reported that the char from fast pyrolysis of mallee woody biomass was more carbonaceous as the temperature increased.

Table 6.5 Elemental composition (wt. %) and HHV of char from different operating parameters

	Pyrolysis temperature (°C)			Initial thickness of wood chips (mm)			Rotation speed (rpm)			Applied pressure (bar)			
	450	500	550	2	5	10	0	100	160	0.3	0.5	1	1.5
C	72.30	74.68	75.57	74.70	74.68	72.8	73.96	74.68	74.96	74.61	74.68	74.41	73.87
H	3.84	3.41	3.07	2.93	3.41	3.9	3.10	3.41	3.17	3.13	3.41	3.26	3.12
N	0.17	0.17	0.17	0.20	0.17	0.2	0.19	0.17	0.19	0.18	0.17	0.21	0.19
O	23.69	21.75	21.19	22.17	21.75	23.0	22.75	21.75	21.69	22.08	21.75	22.12	22.82
H/C[a]	0.64	0.55	0.49	0.47	0.55	0.65	0.50	0.55	0.51	0.50	0.55	0.53	0.51
O/C[a]	0.25	0.22	0.21	0.22	0.22	0.24	0.23	0.22	0.22	0.22	0.22	0.22	0.23
HHV (MJ/kg)	28.06	28.52	28.05	27.77	28.52	27.36	27.70	28.52	28.27	28.05	28.52	28.17	27.71

a. Atomic ratio

The FTIR spectra of raw beetle-killed lodgepole pine (BKLP) and char from the optimal conditions are shown in Figure 6.9. BKLP shows strong bonds in the frequency range of 600-1800 cm^{-1}, which is the fingerprint region of lignocellulosic biomass [25, 41]. The O-H bending and C-O stretching vibrations at bands of 950-1300 cm^{-1} are indicatives of alcohol groups, glycosidic linkage of hemicellulose and cellulose, and aryl-alkyl ethers of lignin [25, 42]. These peaks were found to be flattened in the spectrum of char. In addition, the O-H stretching peak at 3000 and 3600 cm^{-1} and the aliphatic C-H stretching peak at 2800-3000 cm^{-1} presented in the spectrum of BKLP were almost absent in the char spectrum[25]. These suggest the nearly complete decomposition of the original chemical structure of wood in the ablative pyrolysis. In the spectrum of char, the C=C stretching peak at 1600 cm^{-1} combined with the C-H bending bands at 700-900 cm^{-1} are related to the presence of aromatics or polycyclic aromatics, and the C=O stretching peak at 1700 cm^{-1} indicates the presence of carbonyl and carboxyl groups[38].

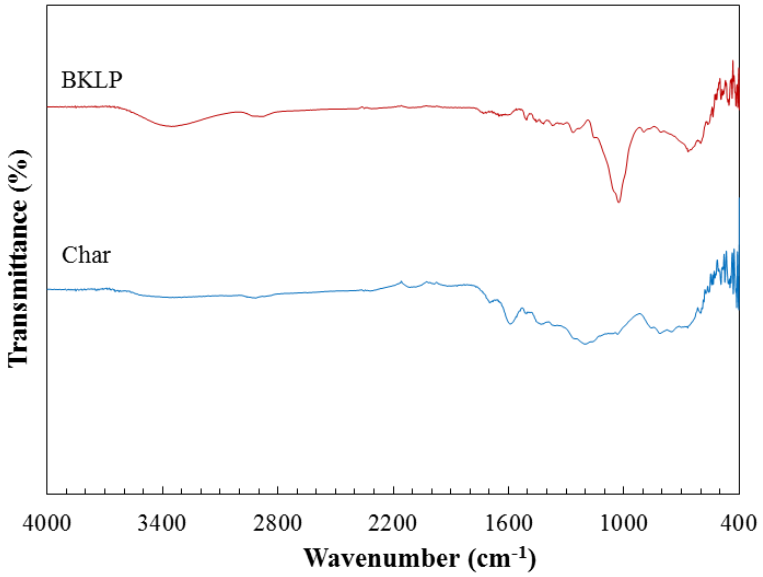

Figure 6.9 FTIR spectra of BKLP and char from optimal conditions

The atomic H/C and atomic O/C ratios of raw BKLP, bio-oil and char from ablative pyrolysis at all operating conditions are depicted in the form of van Krevelen diagram in Figure 6.10, compared with different fossil materials (e.g. coal, heavy oil, and crude oil) and biomass. The raw BKLP has H/C and O/C ratios of 1.55 and 0.66 (dry basis), respectively, which are similar to other woody biomass [43]. In the ablative pyrolysis, 18-25 wt. % of char was formed from raw BKLP. Depending on the operating conditions, char had an atomic H/C ratio ranging from 0.47 to 0.64, and an atomic O/C ratio ranging from 0.21-0.25, which are in the same range as brown coal[43]. The bio-oil from ablative pyrolysis of BKLP had a wide range of O/C ratio of 1.0-1.5 with H/C ratio ranging from 2.3-3.4, depending on the operating conditions. Though bio-oil from fast pyrolysis of biomass in the literature also had a wide range of H/C and O/C ratios (include the range of the bio-oil from the present work) due to different feedstocks, reaction conditions, and reactor configurations, the typical range of H/C and O/C of bio-oil are 1.0-1.4 and 0.6-0.7, respectively [43-45]. The higher H/C and O/C ratios of the bio-oil from ablative pyrolysis are

mainly due to the high water content caused by the long vapor residence time in the ablative reactor. As discussed in our previous work [23], the long vapor residence time in the ablative reactor is mainly resulted from the large reactor chamber volume, which was selected to minimize the extent of slow pyrolysis of wood chips during the pre-heating time in the semi-batch system. However, this issue could be easily solved by modifying this semi-batch reactor into a continuous ablative pyrolysis reactor. In addition, crude oil had a low O/C ratio with an H/C ratio of 1.5-2.1 [43]. This suggests that deoxygenation reactions are essential to upgrade the bio-oil from ablative pyrolysis into transportation fuel.

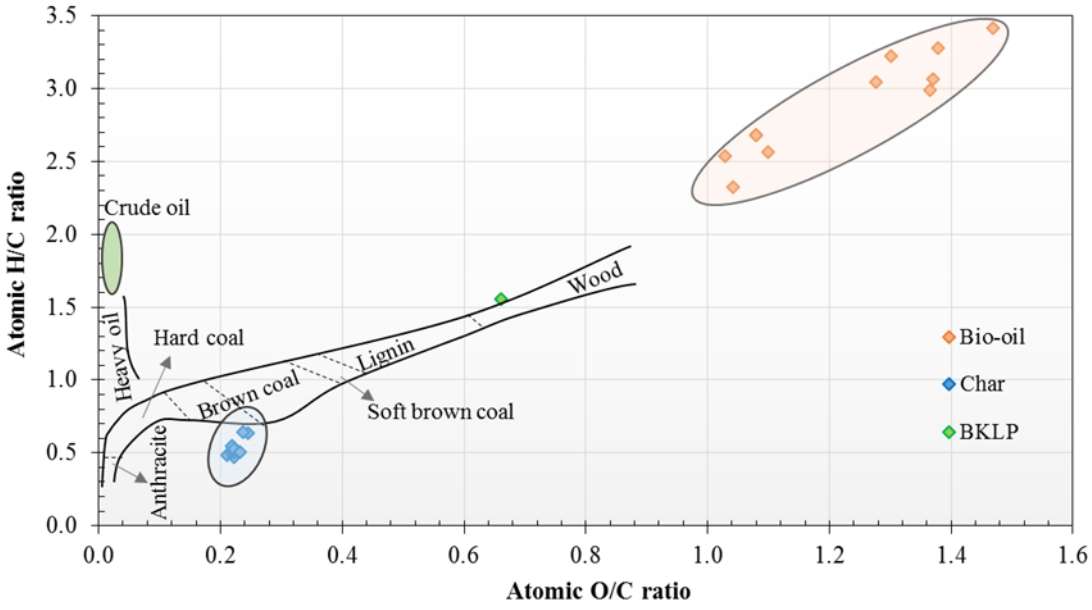

Figure 6.10 Van Krevelen diagram showing the H/C vs O/C of biomass, fossil materials, and bio-oil and char from the ablative pyrolysis (green diamond is raw BKLP, of which the data is on dry basis) [43].

6.5 CONCLUSIONS

Wood chips from beetle-killed trees have been successfully pyrolyzed in a novel ablative reactor, producing high yield of bio-oil. In this study, the effects of the operating parameters in the ablative

reactor on the product yield and composition have been investigated. The operating parameters include the pyrolysis temperature (temperature of the hot plate), the initial thickness of the assembly of wood chips, the relative rotation speed between the wood chips and the hot plate, and the pressure applied by the plate on the wood chips. The maximum yield of bio-oil was 60 wt. % with a water content of 34%, which was achieved at moderate pyrolysis temperature of 500 °C, thin layer of wood chips (≤ 5 mm), low applied pressure (≤ 0.5 bar), and high rotation speed (≥ 100 rpm). The corresponding yields of char and non-condensable gases were 18 wt. % and 13 wt. %, respectively. GC/MS-FID and FTIR were used to characterize the chemical composition of bio-oil. Bio-oil from ablative pyrolysis of beetle-killed wood chips was composed of a mixture of oxygenates with a higher selectivity to guaiacols and anhydrosugars. The elemental composition of bio-oil was mainly affected by its water content; namely, higher water content led to a higher oxygen content while a lower carbon content. Temperature is the critical factor affecting the elemental composition of char. More carbonaceous char was produced at higher temperature. The FTIR spectra of raw biomass and char suggests nearly complete decomposition of wood chips took place in the ablative pyrolysis.

6.6 REFERENCES

[1] U.S.F. Service, Western Bark Beetle Strategy for Human Safety, Recovery and Resiliency, 2011.

[2] B.J. Bentz, J. Régnière, C.J. Fettig, E.M. Hansen, J.L. Hayes, J.A. Hicke, R.G. Kelsey, J.F. Negrón, S.J. Seybold, Climate change and bark beetles of the western United States and Canada: direct and indirect effects, BioScience, 2010; 60: 602-613.

[3] L. Safranyik, B. Wilson, The mountain pine beetle: a synthesis of biology, management and impacts on lodgepole pine, Canadian Forest Service, 2007.

[4] R.D. Perlack, L.L. Wright, A.F. Turhollow, R.L. Graham, B.J. Stokes, D.C. Erbach, Biomass as feedstock for a bioenergy and bioproducts industry: the technical feasibility of a billion-ton annual supply, in, DTIC Document, 2005.

[5] K.L. Woo, P. Watson, S.D. Mansfield, The effects of mountain pine beetle attack on lodgepole pine wood morphology and chemistry: Implications for wood and fiber quality, Wood and Fiber Science, 2005; 37: 112-126.

[6] A. Bridgwater, D. Meier, D. Radlein, An overview of fast pyrolysis of biomass, Organic Geochemistry, 1999; 30: 1479-1493.

[7] A. Bridgwater, Principles and practice of biomass fast pyrolysis processes for liquids, Journal of analytical and applied pyrolysis, 1999; 51: 3-22.

[8] G. Luo, F.L. Resende, Fast pyrolysis of beetle-killed trees, Journal of Analytical and Applied Pyrolysis, 2014; 110: 100-107.

[9] G. Luo, F.L. Resende, In-situ and ex-situ upgrading of pyrolysis vapors from beetle-killed trees, Fuel, 2016; 166: 367-375.

[10] P.C. Badger, P. Fransham, Use of mobile fast pyrolysis plants to densify biomass and reduce biomass handling costs—A preliminary assessment, Biomass and Bioenergy, 2006; 30: 321-325.

[11] K. Raffelt, E. Henrich, A. Koegel, R. Stahl, J. Steinhardt, F. Weirich, The BTL2 process of biomass utilization entrained-flow gasification of pyrolyzed biomass slurries, Applied biochemistry and biotechnology, 2006; 129: 153-164.

[12] M.M. Wright, Techno-economic evaluations of biofuel technologies, ProQuest, 2008.

[13] J.W. Gaskin, A. Speir, L. Morris, L. Ogden, K. Harris, D. Lee, K. Das, Potential for pyrolysis char to affect soil moisture and nutrient status of a loamy sand soil, 2007.

[14] D.A. Laird, The charcoal vision: a win–win–win scenario for simultaneously producing bioenergy, permanently sequestering carbon, while improving soil and water quality, Agronomy Journal, 2008; 100: 178-181.

[15] M. Coleman, D. Page-Dumroese, J. Archuleta, P. Badger, W. Chung, T. Venn, D. Loeffler, G. Jones, K. McElligott, Can portable pyrolysis units make biomass utilization affordable while using bio-char to enhance soil productivity and sequester carbon?, USDA Forest Service Proceedings RMRS-P-61, 2010.

[16] http://agri-therm.com/technology/mps100-agri-therm-mobile-pyrolysis-system/

[17] J. Lede, J. Panagopoulos, J. Villermaux, Experimental Measurement of ablation rate of wood pieces, undergoing fast pyrolysis by contact with a heated wall, Prepr. Pap., Am. Chem. Soc., Div. Fuel Chem.;(United States), 1983; 38.

[18] J. Lede, J. Panagopoulos, H.Z. Li, J. Villermaux, Fast pyrolysis of wood: direct measurement and study of ablation rate, Fuel, 1985; 64: 1514-1520.

[19] H. Martin, J. Lédé, H. Li, J. Villermaux, C. Moyne, A. Degiovanni, Ablative melting of a solid cylinder perpendicularly pressed against a heated wall, International journal of heat and mass transfer, 1986; 29: 1407-1415.

[20] J. Lédé, H.Z. Li, J. Villermaux, H. Martin, Fusion-like behaviour of wood pyrolysis, Journal of analytical and applied pyrolysis, 1987; 10: 291-308.

[21] A.V. Bridgwater, Renewable fuels and chemicals by thermal processing of biomass, Chemical Engineering Journal, 2003; 91: 87-102.

[22] A. Kumar, A conceptual comparison of bioenergy options for using mountain pine beetle infested wood in Western Canada, Bioresource Technology, 2009; 100: 387-399.

[23] G. Luo, D.S. Chandler, L.C.A. Anjos, R.J. Eng, P. Jia, F.L. Resende, Pyrolysis of whole wood chips and rods in a novel ablative reactor (to be submitted), 2016.

[24] E. Salehi, J. Abedi, T. Harding, Bio-oil from sawdust: effect of operating parameters on the yield and quality of pyrolysis products, Energy & Fuels, 2011; 25: 4145-4154.

[25] H. Yang, R. Yan, H. Chen, D.H. Lee, C. Zheng, Characteristics of hemicellulose, cellulose and lignin pyrolysis, Fuel, 2007; 86: 1781-1788.

[26] M. Zhang, F.L. Resende, A. Moutsoglou, D.E. Raynie, Pyrolysis of lignin extracted from prairie cordgrass, aspen, and Kraft lignin by Py-GC/MS and TGA/FTIR, Journal of Analytical and Applied Pyrolysis, 2012; 98: 65-71.

[27] S. Zhou, M. Garcia-Perez, B. Pecha, S.R. Kersten, A.G. McDonald, R.J. Westerhof, Effect of the fast pyrolysis temperature on the primary and secondary products of lignin, Energy & fuels, 2013; 27: 5867-5877.

[28] M. Garcia-Perez, X.S. Wang, J. Shen, M.J. Rhodes, F. Tian, W.-J. Lee, H. Wu, C.-Z. Li, Fast pyrolysis of oil mallee woody biomass: effect of temperature on the yield and quality of pyrolysis products, Industrial & engineering chemistry research, 2008; 47: 1846-1854.

[29] Z. Ji-Lu, Bio-oil from fast pyrolysis of rice husk: Yields and related properties and improvement of the pyrolysis system, Journal of Analytical and Applied Pyrolysis, 2007; 80: 30-35.

[30] H.S. Heo, H.J. Park, J.-I. Dong, S.H. Park, S. Kim, D.J. Suh, Y.-W. Suh, S.-S. Kim, Y.-K. Park, Fast pyrolysis of rice husk under different reaction conditions, Journal of Industrial and Engineering Chemistry, 2010; 16: 27-31.

[31] B. Suleiman, J. Larfeldt, B. Leckner, M. Gustavsson, Thermal conductivity and diffusivity of wood, Wood Science and Technology, 1999; 33: 465-473.

[32] X. Wang, S.R. Kersten, W. Prins, W.P. van Swaaij, Biomass pyrolysis in a fluidized bed reactor. Part 2: Experimental validation of model results, Industrial & engineering chemistry research, 2005; 44: 8786-8795.

[33] W.J. DeSisto, N. Hill, S.H. Beis, S. Mukkamala, J. Joseph, C. Baker, T.-H. Ong, E.A. Stemmler, M.C. Wheeler, B.G. Frederick, Fast pyrolysis of pine sawdust in a fluidized-bed reactor, Energy & Fuels, 2010; 24: 2642-2651.

[34] G. Peacocke, A. Bridgwater, Ablative plate pyrolysis of biomass for liquids, Biomass and Bioenergy, 1994; 7: 147-154.

[35] C. Amen-Chen, B. Riedl, X.-M. Wang, C. Roy, Softwood bark pyrolysis oil-PF resols. Part 1. Resin synthesis and OSB mechanical properties, Holzforschung, 2002; 56: 167-175.

[36] A. Effendi, H. Gerhauser, A.V. Bridgwater, Production of renewable phenolic resins by thermochemical conversion of biomass: a review, Renewable and Sustainable Energy Reviews, 2008; 12: 2092-2116.

[37] D. Zhou, L. Zhang, S. Zhang, H. Fu, J. Chen, Hydrothermal liquefaction of macroalgae Enteromorpha prolifera to bio-oil, Energy & Fuels, 2010; 24: 4054-4061.

[38] D. Özçimen, A. Ersoy-Meriçboyu, Characterization of biochar and bio-oil samples obtained from carbonization of various biomass materials, Renewable Energy, 2010; 35: 1319-1324.

[39] Q. Lu, X.-l. Yang, X.-f. Zhu, Analysis on chemical and physical properties of bio-oil pyrolyzed from rice husk, Journal of Analytical and Applied Pyrolysis, 2008; 82: 191-198.

[40] B.B. Uzun, A.E. Pütün, E. Pütün, Composition of products obtained via fast pyrolysis of olive-oil residue: effect of pyrolysis temperature, Journal of Analytical and Applied Pyrolysis, 2007; 79: 147-153.

[41] G. Bekiaris, J. Lindedam, C. Peltre, S.R. Decker, G.B. Turner, J. Magid, S. Bruun, Rapid estimation of sugar release from winter wheat straw during bioethanol production using FTIR-photoacoustic spectroscopy, Biotechnology for biofuels, 2015; 8: 1.

[42] F. Xu, J. Yu, T. Tesso, F. Dowell, D. Wang, Qualitative and quantitative analysis of lignocellulosic biomass using infrared techniques: a mini-review, Applied Energy, 2013; 104: 801-809.

[43] M. Kleinert, T. Barth, Towards a lignincellulosic biorefinery: direct one-step conversion of lignin to hydrogen-enriched biofuel, Energy & Fuels, 2008; 22: 1371-1379.

[44] I.Y. Mohammed, Y.A. Abakr, F.K. Kazi, S. Yusuf, I. Alshareef, S.A. Chin, Pyrolysis of Napier Grass in a Fixed Bed Reactor: Effect of Operating Conditions on Product Yields and Characteristics, BioResources, 2015; 10: 6457-6478.

[45] D.V. Suriapparao, N. Pradeep, R. Vinu, Bio-Oil Production from Prosopis juliflora via Microwave Pyrolysis, Energy & Fuels, 2015; 29: 2571-2581.

CHAPTER 7. CONCLUSIONS AND FUTURE WORK

7.1 CONCLUSIONS

This research provided a potential pathway to convert beetle-killed trees in the form of wood chips into value-added liquid chemicals and fuels near the harvesting point via ablative pyrolysis, in which the costs of biomass drying, grinding, and transportation could be greatly reduced. The low moisture content of beetle-killed trees makes them an excellent feedstock for fast pyrolysis; however, the effects of their degradation stages on the performance of fast pyrolysis have not been reported in the literature previously. Thus, these effects were investigated for the first time in this research using a micro-pyrolyzer equipped with an online GC/MS (Py-GC/MS). The results revealed that trees that have been attacked and dead for 4 years had similar product yield and distribution to the healthy trees, suggesting that beetle-killed trees are a good feedstock for fast pyrolysis. The volatile compounds from fast pyrolysis of beetle-killed trees were composed of a mixture of oxygenates with a HHV of 26 MJ/kg. In the presence of HZSM-5 catalyst, fortunately most oxygenated compounds in the pyrolysis vapors were successfully upgraded into aromatic hydrocarbons with high selectivity to toluene and xylenes. The HHV of these aromatic volatiles was around 41 MJ/kg, which is close to the HHV of commercial gasoline and diesel (~ 46 MJ/kg), indicating the potential of beetle-killed trees for biofuel and chemical production. Based on a conservative estimation, about 356 million tons of wood from beetle-killed trees in the western US are available for fast pyrolysis. According to our results, around 142 million tons of hydrocarbons, 38 million tons of toluene, and 32 million tons of xylenes could be produced from these beetle-killed trees. If the hydrocarbons were used to produce drop-in fuels, 52 billion gallon fuels would be produced (Density of gasoline = 719.7 kg/m^3), which is about 39% of the annual gasoline

consumption in the U. S. (~133 billion gallons). In addition, the estimated toluene production would be three times more than the current annual production of toluene from fossil fuels worldwide (~10 million tons).

According to the contact method between the catalyst and pyrolysis vapors, the catalytic upgrading can be classified into *in-situ* and *ex-situ* configurations. A systematic study over a wide range of reactions conditions (i.e. pyrolysis temperature, secondary reactor temperature, and catalyst-to-biomass ratios) was performed for both *in-situ* and *ex-situ* upgrading using Py-GC/MS and HZSM-5 as catalyst in this research. The *in-situ* upgrading was highly affected by the catalyst-to-biomass ratio. At the ratio of 10, the highest aromatic yield of 25 % was obtained with the carbonaceous residues yield of 41%. For the *ex-situ* upgrading, the most effective factor is the secondary reactor temperature. The highest aromatic yield of 22% and lowest coke yield of 14% were achieved at the secondary temperature of 600 °C. In addition, the importance of the rates of alkylation and dealkylation reactions of alkyl aromatics on the product selectivity from catalytic upgrading of pyrolysis vapors was extensively discussed in this research for the first time. Because of their exothermicity, alkylation reactions were promoted at lower temperature, and dealkylation reactions were favored at higher temperature. It was also speculated that the alkyl groups involved in the alkylation/dealkylation reactions originate from species other than aromatics, such as ethylene. Due to the lack of research for comparison between *in-situ* and *ex-situ* upgrading, they were directly compared under identical conditions in this research. The *in-situ* and *ex-situ* upgrading showed largely similar yields of aromatic volatiles (21-25%) and carbonaceous residues (34-40%), with differences primarily on species selectivity. As a result of the alkylation/dealkylation reactions, the *in-situ* upgrading had higher selectivity to xylenes and C9 aromatics, and the *ex-situ* upgrading exhibited higher selectivity to benzene and toluene.

Beetle-killed trees are typically located far from urban industrial areas, indicating transportation costs may be a key barrier to widespread utilization of this vast resource in fast pyrolysis. Using a mobile pyrolysis unit to convert beetle-killed trees near the harvesting point may significantly reduce the transportation costs, since the energy density of bio-oil is 6-8 times higher than the green wood chips. Thus, a novel laboratory-scale ablative pyrolysis unit has been developed in our lab to simulate the conditions that would be used in the mobile pyrolysis unit in the field. The ablative reactor provides the opportunity to fast pyrolyze large pieces of wood instead of only small particles into bio-oil, which could significantly reduce the grinding costs (~7-9% of the overall production costs). Though this characteristic of ablative pyrolysis has been proposed in the past, there were no experimental data to back up this claim, until experiments conducted in this research confirmed the possibility of carrying out ablative pyrolysis of entire wood chips (20 mm), with a bio-oil yield as high as 60 wt. %. The yield and composition of bio-oil from ablative pyrolysis were in the same range as those from fast pyrolysis of < 1 mm particles using a fluidized bed reactor, with the small differences (4 wt. % lower yield and HHV, and higher water content) attributed to the longer vapor residence times in ablative reactor. The effects of different operating parameters of the ablative pyrolysis reactor were also investigated. The yield of bio-oil was favored at a moderate pyrolysis temperature of 500 °C, a lower initial thickness of wood chips (≤ 5 mm) and applied pressure (≤ 0.5 bar), and a higher rotation speed (≥ 100 rpm). The elemental composition of bio-oil was highly affected by its water content, and the elemental composition of char was primarily affected by temperature. At higher temperature, char became more carbonaceous in nature. Depending on the operating conditions, bio-oil had a HHV in a range of 11-15 MJ/kg. Char obtained from all the conditions had a similar HHV of 28 MJ/kg.

7.2 FUTURE WORK

The following items are recommended for future work:

- Bio-oil derived from ablative pyrolysis of beetle-killed trees was composed of a mixture of oxygenates with a relatively low HHV. The results from the direct comparison between *in-situ* and *ex-situ* upgrading in this research suggest that a downstream catalytic upgrading unit will be an appropriate option to expand the capabilities of the current ablative pyrolysis system to produce fuel additives and chemicals from beetle-killed trees. In addition, synthesis of novel catalysts, such as bi-functional catalysts, for pyrolysis vapors/bio-oil upgrading will be an interesting topic for future study.
- This research stems from the potential use of mobile pyrolysis unit, converting beetle-killed trees directly into liquid fuel or chemicals near the harvesting point. Further research on developing a continuous ablative reactor system is essential to achieve this long-term goal. Bio-oil yield and quality could be greatly improved in the continuous system by reducing the reactor chamber volume thereby shortening the vapor residence time. Efficient removal of char formed during ablative pyrolysis may significantly reduce the vertical heat transfer limitation observed for the current ablative reactor, enhancing the biomass throughput. So this should also be considered for the reactor design in the future. Additionally, the utilization of non-condensable gases with moderate energy content from fast pyrolysis can also be considered in the design and operation of the continuous reactor. Combustion of those gases, providing heat for the ablative pyrolysis reactor, is one of the potential applications.

VITA

Guanqun Luo was born in China. She got her Bachelor of Engineering majored in Wood Science and Engineering from Beijing Forestry University, China, in 2010. After graduation, she started her Master study in Dr. Armando McDonld's lab at the University of Idaho. She got her Master of Science majored in Natural Resources in 2012, after which time she began her doctoral study in Dr. Fernando Resende's lab at the University of Washington. In June 2016, she received her PhD majored in Environmental and Forest Sciences.